UNITED STATES
EPARTMENT OF
OMMERCE
UBLICATION

NBS MONOGRAPH 118

Photonuclear Reactions

U.S.
ARTMENT
OF
MMERCE
National
Bureau
of
Standards

NBS TECHNICAL PUBLICATIONS

PERIODICALS

JOURNAL OF RESEARCH reports National Bureau of Standards research and development in physics, mathematics, chemistry, and engineering. Comprehensive scientific papers give complete details of the work, including laboratory data, experimental procedures, and theoretical and mathematical analyses. Illustrated with photographs, drawings, and charts.

Published in three sections, available separately:

• Physics and Chemistry

Papers of interest primarily to scientists working in these fields. This section covers a broad range of physical and chemical research, with major emphasis on standards of physical measurement, fundamental constants, and properties of matter. Issued six times a year. Annual subscription: Domestic, $9.50; foreign, $11.75*.

• Mathematical Sciences

Studies and compilations designed mainly for the mathematician and theoretical physicist. Topics in mathematical statistics, theory of experiment design, numerical analysis, theoretical physics and chemistry, logical design and programming of computers and computer systems. Short numerical tables. Issued quarterly. Annual subscription: Domestic, $5.00; foreign, $6.25*.

• Engineering and Instrumentation

Reporting results of interest chiefly to the engineer and the applied scientist. This section includes many of the new developments in instrumentation resulting from the Bureau's work in physical measurement, data processing, and development of test methods. It will also cover some of the work in acoustics, applied mechanics, building research, and cryogenic engineering. Issued quarterly. Annual subscription: Domestic, $5.00; foreign, $6.25*.

TECHNICAL NEWS BULLETIN

The best single source of information concerning the Bureau's research, developmental, cooperative and publication activities, this monthly publication is designed for the industry-oriented individual whose daily work involves intimate contact with science and technology—*for engineers, chemists, physicists, research managers, product-development managers, and company executives.* Annual subscription: Domestic, $3.00; foreign, $4.00*.

* Difference in price is due to extra cost of foreign mailing.

NONPERIODICALS

Applied Mathematics Series. Mathematical tables, manuals, and studies.

Building Science Series. Research results, test methods, and performance criteria of building materials, components, systems, and structures.

Handbooks. Recommended codes of engineering and industrial practice (including safety codes) developed in cooperation with interested industries, professional organizations, and regulatory bodies.

Special Publications. Proceedings of NBS conferences, bibliographies, annual reports, wall charts, pamphlets, etc.

Monographs. Major contributions to the technical literature on various subjects related to the Bureau's scientific and technical activities.

National Standard Reference Data Series. NSRDS provides quantitive data on the physical and chemical properties of materials, compiled from the world's literature and critically evaluated.

Product Standards. Provide requirements for sizes, types, quality and methods for testing various industrial products. These standards are developed cooperatively with interested Government and industry groups and provide the basis for common understanding of product characteristics for both buyers and sellers. Their use is voluntary.

Technical Notes. This series consists of communications and reports (covering both other agency and NBS-sponsored work) of limited or transitory interest.

Federal Information Processing Standards Publications. This series is the official publication within the Federal Government for information on standards adopted and promulgated under the Public Law 89–306, and Bureau of the Budget Circular A–86 entitled, Standardization of Data Elements and Codes in Data Systems.

CLEARINGHOUSE

The Clearinghouse for Federal Scientific and Technical Information, operated by NBS, supplies unclassified information related to Government-generated science and technology in defense, space, atomic energy, and other national programs. For further information on Clearinghouse services, write:

Clearinghouse
U.S. Department of Commerce
Springfield, Virginia 22151

Order NBS publications from:

Superintendent of Documents
Government Printing Office
Washington, D.C. 20402

UNITED STATES DEPARTMENT OF COMMERCE • Maurice H. Stans, *Secretary*

NATIONAL BUREAU OF STANDARDS • Lewis M. Branscomb, *Director*

Photonuclear Reactions

Evans Hayward

Center for Radiation Research
National Bureau of Standards
Washington, D.C. 20234

National Bureau of Standards Monograph 118

Nat. Bur. Stand. U.S. Monogr. 118, 46 pages (August 1970)
CODEN: NBSMA

Issued August 1970

For sale by the Superintendent of Documents, U.S. Government Printing Office, Washington, D.C. 20402
(Order by SD Catalog No. C13.44:118). Price 50 cents.

Library of Congress Catalog Card Number: 70–606490

Contents

Photonuclear Reactions

Evans Hayward

This paper reviews photonuclear reactions in the approximate energy range 10 to 30 MeV. Various sum rules are discussed and applied to experimental data. Several different theories are described and their predictions compared with experiment, and as often as possible open questions and discrepancies are pointed out.

Key words: Nuclear hydrodynamics; particle-hole calculations; photon scattering; photonuclear; sum rules.

I. Fundamentals

1. The Trend of a Photonuclear Cross Section

In order to get a general picture of the photon absorption cross section for an arbitrary nucleus, let us consider the interactions that can occur as a function of increasing photon energy. At the lowest energies only Thomson scattering, the scattering from the whole nuclear charge, can take place. This scattering is an electric dipole phenomenon. For unpolarized incident radiation its differential cross section is:

$$\frac{d\sigma}{d\Omega} = D^2\left[\frac{1+\cos^2\theta}{2}\right], \tag{1.1}$$

where the scattering amplitude $D = -Z^2e^2/AMc^2$.

At slightly higher energies the photon can disrupt the internal nuclear coordinates and excite nuclear energy levels. The first excited state can decay only to the ground state and its ground-state radiation width, γ, is its total width, Γ. Each successive state has the possibility of decaying to all of the states below it. Since the total width, Γ_k, of a state at excitation energy, E_k, is the sum of the partial widths associated with its decay to all lower states, the states at higher excitation become progressively wider and wider. The cross section for the absorption of photons by a single isolated level is

$$\sigma_k(E) = 2\pi\lambda\!\!\!^{-}_k{}^2 \frac{2I_k+1}{2I_0+1}\frac{\gamma_k}{\Gamma_k}\frac{(E\Gamma_k)^2}{(E_k^2-E^2)^2+(E\Gamma_k)^2} \tag{1.2}$$

Here I_k and I_0 refer to the spins of the excited and ground states Through its width, Γ_k, this cross section depends on the properties of all the states between E_k and the ground state. On the other hand, the integrated absorption cross section for a level depends only on the photon energy and the ground-state radiation width. It is:

$$\int \sigma_k(E)\,dE = (\pi\lambda\!\!\!^{-}_k)^2\frac{2I_k+1}{2I_0+1}\gamma_k. \tag{1.3}$$

Above the particle emission thresholds, near eight or ten MeV, for most nuclei, the levels broaden much more rapidly until finally they coalesoe completely.

The giant resonance is the dominant feature of the photon absorption cross section for nuclei. It is a large maximum in the cross section, 3 to 10 MeV in width, located between 13 and 18 MeV for medium and heavy elements and near 20 MeV for the light ones. The giant resonance occurs in all nuclei and may be viewed as a general property of nuclear matter. It results primarily from electric dipole absorption and its integrated absorption cross section is of the order of the dipole sum.

The energy dependence of the giant resonance absorption cross section for medium and heavy nuclei has often been approximated by a Lorentz-shaped resonance line:

$$\sigma(E) = \sigma_0\frac{E^2\Gamma^2}{(E_0^2-E^2)^2+E^2\Gamma^2} \tag{1.4}$$

We now know that this picture is much too simple, since the quadrupole oscillations of the nuclear surface can modify this cross section markedly. For light nuclei, the giant resonance is the envelope of a very detailed structure which depends much more on the individual level properties.

For energies above the giant resonance the most important absorption mechanism is through the quasideuteron effect. This is also primarily an

electric dipole phenomenon that results from the strong two body correlations in the nuclear ground state. The high energy photon, which has low momentum, interacts with a neutron and proton colliding at high velocity and ejects them with the dynamics appropriate to the deuteron photodisintegration.

2. The Interaction Hamiltonian

The nuclear Hamiltonian is usually written as:

$$H = \sum_{ij} \frac{p_i^2}{2M_i} + V_{ij} \tag{1.5}$$

where the sum is over all the particles. When radiation is present its interaction is usually treated as a perturbation to the nuclear Hamiltonian. The nonrelativistic Hamiltonian associated with the electric interactions is:

$$H' = H_1 + H_2 = \sum_i \left[-\frac{e_i}{M_i c} (\mathbf{p}_i \cdot \mathfrak{A}) + \frac{e_i^2}{2M_i c^2} \mathfrak{A}^2 \right] \tag{1.6}$$

where here the sum is over all the charges. The first term, H_1, can describe transitions in which only one photon is absorbed or emitted. It is the term used to calculate the photon absorption cross section and describes the interaction that results in the disruption of internal nuclear coordinates. The second term, H_2, is smaller. First order matrix elements of H_2 are of the same order as the second order matrix elements of H_1. Since H_2 contains two powers of $\mathfrak{A}$, it can describe scattering events in first order.

The second order term may be rewritten as:

$$H_2 = \sum_i \frac{e^2}{2M_i c^2} \mathfrak{A}^2 = \frac{Ze^2}{2Mc^2} \mathfrak{A}^2 = \frac{N+Z}{A} \frac{Ze^2}{2Mc^2} \mathfrak{A}^2$$

$$= \left[\frac{NZ}{A} + \frac{Z^2}{A} \right] \frac{e^2}{2Mc^2} \mathfrak{A}^2 \tag{1.7}$$

where the second term is nuclear Thomson scattering, the scattering from the whole nuclear charge. The first term is scattering that results from the disruption of internal nuclear coordinates and must be combined with second order terms in H_1 to obtain the complete nuclear scattering amplitude, i.e. the Kramers-Heisenberg dispersion relation.

The absorption cross section depends on the matrix elements of H_1. In evaluating these matrix elements we make use of Siegert's theorem which allows us to replace $(\mathbf{p}_i \cdot \mathfrak{A})$ by $(\mathbf{r}_i \cdot \boldsymbol{\mu})$, where $\boldsymbol{\mu}$ is the photon polarization vector and $\mathbf{r}_i$ is the coordinate of the ith proton with respect to the nuclear center of mass. This approximation is valid for electric multipoles when the photon wavelength is large compared to the nuclear radius. At high energies the detailed structure of nucleon and meson currents is important and Siegert's theorem no longer applies.

3. Effective Charges

When a photon interact with a neutron or proton in the nucleus, the rest of the nucleus recoils. The magnitude of the cross section thus depends on the size of the multipole moment set up between the nucleon and the recoiling nucleus. This dynamical effect can be taken into account by making use of the concept of effective charges.

To obtain the effective charges [1] for neutron and proton transitions in electric dipole approximation we need include in H_1 only the first term in the multipole expansion of $\mathfrak{A}$.

$$\mathfrak{A} = \mathfrak{A}_0 \boldsymbol{\mu} e^{-i(\mathbf{k}\cdot\mathbf{r})} = \mathfrak{A}_0 \boldsymbol{\mu} \tag{1.8}$$

$$H_1 = -\sum_i \frac{\mathfrak{A}_0 e_i}{M_i c} (\mathbf{p}_i \cdot \boldsymbol{\mu}) \tag{1.9}$$

Replacing $\mathbf{p}_i$ by $M\mathbf{v}_i$ we have:

$$H_1 = -\sum_{i=1}^{Z} \frac{\mathfrak{A}_0 e_i}{c} (\mathbf{v}_i \cdot \boldsymbol{\mu}) \tag{1.10}$$

The total nuclear current is $Ze\mathbf{V}$, where $\mathbf{V}$ is the velocity of the center of mass:

$$\mathbf{V} = \sum_{k=1}^{A} \frac{\mathbf{v}_k}{A} = \frac{1}{A} \left[\sum_{i=1}^{Z} \mathbf{v}_i + \sum_{j=1}^{N} \mathbf{v}_j \right] \tag{1.11}$$

The energy associated with the center of mass motion is:

$$-\frac{\mathfrak{A}_0}{c} Ze(\mathbf{V} \cdot \boldsymbol{\mu}) = -\frac{\mathfrak{A}_0 Ze}{cA} \left[\sum_{i=1}^{Z} (\mathbf{v}_i \cdot \boldsymbol{\mu}) + \sum_{j=1}^{N} (\mathbf{v}_j \cdot \boldsymbol{\mu}) \right] \tag{1.12}$$

If we add and subtract this from H_1, we have

$$H_1 = -\frac{\mathfrak{A}_0 e}{c} \left[\sum_{i=1}^{Z} (\mathbf{v}_i \cdot \boldsymbol{\mu}) (1 - Z/A) - \frac{Z}{A} \sum_{j=1}^{N} (\mathbf{v}_j \cdot \boldsymbol{\mu}) + Z(\mathbf{V} \cdot \boldsymbol{\mu}) \right]$$

$$= -\frac{\mathfrak{A}_0 e}{c} \left[\frac{N}{A} \sum_{i=1}^{Z} (\mathbf{v}_i \cdot \boldsymbol{\mu}) - \frac{Z}{A} \sum_{j=1}^{N} (\mathbf{v}_j \cdot \boldsymbol{\mu}) + Z(\mathbf{V} \cdot \boldsymbol{\mu}) \right] \tag{1.13}$$

The energy associated with the center of mass motion of the nucleus, $-\mathfrak{A}_0 Ze(\mathbf{V} \cdot \boldsymbol{\mu})/c$, is responsible for Thomson scattering and is not connected with internal nuclear coordinates. The first two terms describe the electric dipole transitions of protons and neutrons having the effective charges N/A and $-Z/A$. The effective charges for transitions in

[1] Figures in brackets indicate the literature references at the end of this monograph.

volving higher electric multipoles are

$$q_p=[(A-1)/A]^L+(-)^L[(Z-1)/A^L]. \quad (1.14)$$

$$q_n=(-)^L Z/A^L \quad (1.15)$$

The magnitudes of these effective charges have some consequences for interactions in which the excited nucleon emerges directly without colliding with the other nucleons. Then for the most important electric dipole case, the ratio of the (γ, n) to the (γ, p) cross section for a given photon energy would be $NZ^2/ZN^2 = Z/N$. In addition, since the effective charges of the deuteron and alpha-particle are respectively $(N-Z)/A$ and $2(N-Z)/A$, their cross sections for direct emission are very small and identically zero for self-conjugate nuclei. Violations of both of these rules have been observed experimentally but they can always be explained away by including a very small Coulomb interaction.

The effective charges for electric quadrupole transitions are:

$$q_p=1-2/A+Z/A^2 \quad (1.16)$$

$$q_n=Z/A^2 \quad (1.17)$$

The direct proton emission is then much more likely. It is also worthwhile to note that for $E2$ transitions the neutron and proton effective charges have the same sign whereas for $E1$ transitions they are opposite. As a consequence, when the absorption process involves a mixture of $E1$ and $E2$ and is followed by direct emission, the proton distributions should be peaked forward and the neutron distributions backward of 90°.

4. The Electric Dipole Sum Rule

The sum rule is a model-independent conservation law which gives for atomic systems the total integrated absorption cross section. This rule is a consequence of the commutation relations and is usually discussed in terms of the oscillator strength. For a transition from the ground state, $|0\rangle$, to an excited state, $\langle k|$, the oscillator strength is defined as

$$f_k=\frac{2ME_k}{\hbar^2}|\langle k|z|0\rangle|^2=\frac{2M\omega_{k0}}{\hbar}\langle 0|z|k\rangle\langle k|z|0\rangle \quad (1.18)$$

where $\langle k|z|0\rangle$ is the matrix element of the dipole operator connecting the two states and M is the mass of the particle undergoing the transition. Since

$$\langle 0|\dot{z}|k\rangle=i\omega_{0k}\langle 0|z|k\rangle \quad \text{and} \quad (1.19)$$

$$\langle k|\dot{z}|0\rangle=i\omega_{k0}\langle k|z|0\rangle \quad (1.20)$$

it is straightforward to show that

$$f_k=-\frac{M}{i\hbar}\langle 0|\dot{z}|k\rangle\langle k|z|0\rangle-\langle 0|z|k\rangle\langle k|\dot{z}|0\rangle$$

$$=-\frac{M}{\hbar}\langle 0|[H,z]|k\rangle\langle k|z|0\rangle$$

$$-\langle 0|z|k\rangle\langle k|[H,z]|0\rangle \quad (1.21)$$

The sum over all the states, k, yields:

$$\sum_k f_k=-\frac{M}{\hbar^2}\langle 0|[[H,z],z]|0\rangle$$

$$=-\frac{M}{\hbar^2}\langle 0|(Hz^2-2zHz+z^2H)|0\rangle \quad (1.22)$$

For an electron in an atom

$$H=p^2/2M+V(r) \quad (1.23)$$

where $V(r)$ is the Coulomb potential. Using the relationship $p=-i\hbar\,\partial/\partial z$, the double commutator becomes $-\hbar^2/M$ so that the summed oscillator strength is 1. For an atom with Z electrons,

$$\sum f_k=Z. \quad (1.24)$$

The integrated absorption cross section into the kth level is proportional to the oscillator strength and is

$$\int \sigma_k(E)\,dE=\frac{2\pi^2e^2\hbar}{Mc}f_k. \quad (1.25)$$

Summed over all the transitions this becomes

$$\int \sigma(E)\,dE=\frac{2\pi^2e^2\hbar}{Mc}Z \quad (1.26)$$

When applied to nuclei this sum rule must undergo two important modifications. The first is a dynamical one that results from the fact that when a photon interacts with a nucleon, the rest of the nucleus recoils; whereas when an electron is excited the recoil of the atom is negligible. The second difference stems from the fact that the nuclear potential is more complicated than the Coulomb potential of the atomic system. The nuclear potential has terms for which the double commutator with z does not vanish.

The first modification can be made by means of the effective charges already discussed. Then the nuclear absorption cross section integrated over all electric dipole transitions becomes

$$\int \sigma(E)\,dE=\frac{2\pi^2e^2\hbar}{Mc}\left[\sum_{i=1}^{Z}(N/A)^2f_i\right.$$

$$\left.+\sum_{j=1}^{N}(-Z/A)^2f_j\right]=\frac{2\pi^2e^2\hbar}{Mc}\cdot\frac{NZ}{A} \quad (1.27)$$

f_i and f_j being just the summed oscillator strength associated respectively with proton and neutron transitions. This result will be referred to as the classical dipole sum. It gives the magnitude of the integrated cross section based simply on the kinetic energy term in the nuclear Hamiltonian.

It is worthwhile to consider how various kinds of nuclear potential affect the dipole sum. It is often stated that velocity dependent or attractive exchange forces act to increase the dipole sum. By considering the expansion of the double commutator it is evident that a potential that contained the nucleon velocities to at least the second power would enhance the dipole sum; it would contribute in the same way as the kinetic energy term.

Next consider the central potential which may be written in terms of the four two-body exchange operators:

$$V_c = V(r_{ij})[wP^W + xP^M + yP^H + zP^B] \quad (1.28)$$

where $w + x + y + z = 1$. The Wigner and Bartlett operators involve no exchange and spin exchange respectively. Therefore their commutators with the coordinate, z, yield nothing. The operators, P^M and P^H, represent space exchange and spin and space exchange; their commutators contribute and contribute in the same way to the dipole sum. Since either operator changes the proton coordinate, z_i, into the neutron coordinate, z_j, the expansion of the double commutator becomes:

$$\begin{aligned}(xP^M + yP^H)z_i^2 - 2z_i(xP^M + yP^H)z_i + z_i^2(xP^M + yP^H) \\ = z_j^2(xP^M + yP^H) - 2z_iz_j(xP^M + yP^H) \\ + z_i^2(xP^M + yP^H) = (z_j - z_i)^2(xP^M + yP^H) \quad (1.29)\end{aligned}$$

The summed oscillator strength resulting from the two-body central potential would be

$$\sum f_k = -\frac{M}{\hbar^2}\sum_{ij}(z_j - z_i)^2 V(r_{ij})\langle 0 \mid xP^M + yP^H \mid 0\rangle$$

$$= -\frac{M}{3\hbar^2}\sum_{ij} r_{ij}^2 V(r_{ij})\langle 0 \mid xP^M + yP^H \mid 0\rangle \quad (1.30)$$

For an attractive potential (V negative) the dipole sum is increased.

The nuclear potential may contain $\ell\cdot s$ or $\ell\cdot\ell$ terms. How do they contribute to the dipole sum? If

$$\begin{aligned}V = C\ell\cdot s = c(\mathbf{r}\times\mathbf{p})\cdot s = C[(xp_y - yp_x)\sigma_z \\ + (yp_z - zp_y)\sigma_x + (zp_x - xp_z)\sigma_y] \quad (1.31)\end{aligned}$$

Since only terms containing $p_z = -i\hbar\,\partial/\partial z$ contribute to the double commutator eq. 1.22 may be written as:

$$\sum f_k = -\frac{MC}{\hbar^2}(yp_z\sigma_x - xp_z\sigma_y)z^2 - 2z(yp_z\sigma_x - xp_z\sigma_y)z$$

$$= -\frac{iMC}{\hbar}[(y\sigma_x - x\sigma_y)2z - 2z(y\sigma_x - x\sigma_y)] = 0 \quad (1.32)$$

Similarly

$$\begin{aligned}V = D\ell\cdot\ell = D(\mathbf{r}\times\mathbf{p})\cdot(\mathbf{r}\times\mathbf{p}) = D[(xp_y - yp_x)^2 \\ + (yp_z - zp_y)^2 + (zp_x - xp_z)^2] \quad (1.33)\end{aligned}$$

Again keeping only terms that involve p_z we have

$$\sum f_k = -\frac{MD}{\hbar^2}(y^2 + x^2)p_z^2 z^2 = 2MD(x^2 + y^2) \quad (1.34)$$

where $\sqrt{x^2 + y^2}$ is the distance of the nucleon from the z-axis.

The integrated electric dipole absorption cross section has then a minimum value resulting from the kinetic energy term in the nuclear Hamiltonian. The sum is augmented further by potential energy terms that do not commute with the dipole operator. In the following, the factor by which the dipole sum exceeds its classical value will be called β so that:

$$\int \sigma\, dE = \frac{2\pi^2 e^2\hbar}{Mc}\frac{NZ\beta}{A} = 0.06\frac{NZ}{A}\beta \text{ MeV barns.} \quad (1.35)$$

The integral in the above expression is over all electric dipole transitions, but since we have neglected all meson currents, a logical upper limit is the meson production threshold. It has been assumed throughout that the photon wavelength is large compared to nuclear dimensions. Violations of this condition will act to decrease the dipole sum.

Because data do not generally extend to the meson production threshold, the integrated cross sections are usually quoted only over the giant resonance, i.e. to 25–30 MeV. Figure 1 summarizes experimental data on the photonuclear cross sections integrated to 30 MeV as a function of Z. It shows that for the lightest elements only about half of a "dipole sum" is in the giant resonance. The magnitude of the integrated cross section increases gradually until for the nuclei heavier than tin the integrated cross section is approximately one dipole sum. The indications are that the amount of

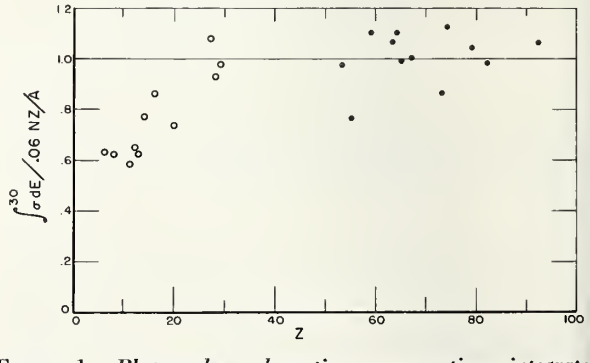

FIGURE 1. *Photonuclear absorption cross sections integrated to 30 MeV.*

The data for the light element come from the total absorption experiment of reference [25]. The data for the heavy elements come from the Livermore neutron yield data [43–52].

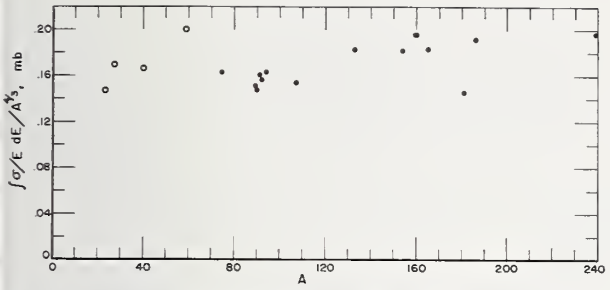

FIGURE 2. *The bremsstrahlung weighted cross section divided by* $A^{1/3}$ *as a function of* A.

The data come from the total absorption experiment [25] and the neutron production experiments [49–52].

integrated cross section above 30 MeV is comparable to that below. When making these comparisons one should remember that higher multipoles undoubtedly contribute especially at the higher energies.

5. The Bremsstrahlung-Weighted Cross Section

Levinger and Bethe [1] have also discussed a second integral, $\int\sigma/E\ dE$, and related it to the mean square radius of the nucleus. Their result:

$$\int \sigma/E\ dE = \sigma_{-1} = \frac{4\pi^2}{3}\frac{e^2}{\hbar c}\frac{NZ}{A}\langle 0 \mid r^2 \mid 0\rangle \qquad (1.36)$$

assumes that there are no nucleon-nucleon correlations in the ground states. It is also independent of the presence of exchange or velocity-dependent forces in the nuclear Hamiltonian.

Subsequently Foldy [2] pointed out that the symmetry properties of the ground-state wave function were more important than correlations between nucleons and specifically that

$$\sigma_{-1} = \frac{4\pi^2}{3}\frac{e^2}{\hbar c}\frac{NZ}{A-1}\langle 0 \mid r^2 \mid 0\rangle. \qquad (1.37)$$

This rule applies even in the presence of correlations for nuclei for which the ground-state wave function is symmetric in the nucleon space coordinates; i.e. the 1s shell nuclei.

Levinger has also combined the classical dipole sum rule, $\int\sigma dE = 60\,NZ/A$ MeV mb, with the harmonic oscillator energy, $E = 42\,A^{-1/3}$, to obtain

$$\sigma_{-1} = 60\frac{NZ}{A}\frac{1}{42A^{-1/3}} = 0.36A^{4/3}\ \text{mb} \qquad (1.38)$$

setting $N = Z = A/2$. This result yields the experimentally observed dependence on A while eq 1.36 does not. See figure 2. The empirical value for the coefficient is better approximated by 0.16 than 0.36. This enormous discrepancy stems largely from the fact that the giant resonance energy is, in nature, nearly twice the harmonic oscillator spacing.

II. The Scattering and Absorption of Photons by Nuclei

1. The Optical Theorem and the Dispersion Relation

Associated with every absorption process there is a higher order coherent scattering process; the total absorption and coherent scattering cross section can both be expressed in terms of the same complex forward scattering amplitude, $R(E,0)$. Familiar examples of this connection are the coherent scattering processes, Rayleigh and Delbruck scattering, which are associated respectively with the absorption processes, the photoelectric effect and pair production. The relationship between the total absorption cross section, $\sigma_t(E)$, and the forward scattering amplitude $R(E,0)$ is called the optical theorem:

$$\sigma_t(E) = 4\pi\lambda\text{-bar}\ \mathrm{Im}\ R(E,0) \tag{2.1}$$

The coherent scattering cross section is

$$\frac{d\sigma}{d\Omega}(E,\theta) = |\,R(E,\theta)\,|^2 \tag{2.2}$$

The dispersion relation gives the connection between the real and imaginary parts of the forward scattering amplitude:

$$\mathrm{Re}\ R(E,0) = \frac{E}{2\pi^2\hbar c} P\int \frac{dE'\sigma_t(E')}{E'^2-E^2} + D \tag{2.3}$$

where $D=-Z^2e^2/AMc^2$, the energy independent Thomson scattering amplitude. This equation permits the evaluation of Re $R(E,0)$ if the cross section, $\sigma_t(E)$, is known at all energies where it is important.

It has already been pointed out that the photonuclear giant resonance may often be adequately represented by a Lorentz-shaped resonance line. Then the forward scattering amplitude is:

$$R(E,0) = \frac{NZ\beta e^2}{AMc^2} E^2 \frac{E_0^2-E^2+i\Gamma E}{(E_0^2-E^2)^2+\Gamma^2E^2} \tag{2.4}$$

where E_0 is the giant resonance energy and Γ its width. Using the optical theorem we find that:

$$\sigma_t(E) = \frac{4\pi e^2\hbar}{Mc}\frac{NZ\beta}{A}\frac{E^2\Gamma}{(E_0^2-E^2)^2+\Gamma^2E^2} \tag{2.5}$$

The amplitude, $R(E,0)$, has been normalized so that the integral of the absorption cross section will yield the dipole sum:

$$\int \sigma_t(E)\,dE = \frac{2\pi^2e^2\hbar}{Mc}\frac{NZ\beta}{A} \tag{2.6}$$

The scattering cross section must include the Thomson scattering amplitude since it interferes with the nuclear scattering amplitude:

$$\frac{d\sigma}{d\Omega}(E,0) = |\,R(E,0)+D\,|^2. \tag{2.7}$$

If the absorption cross section is known but does not fit the Lorentz line, then the real part of the coherent scattering amplitude may be obtained from the dispersion relation.

The shapes of the absorption and coherent scattering cross sections for a hypothetical nucleus with $N=Z=50$ are compared in figure 3. The giant resonance exhausts the dipole sum with $\beta=1.3$ and is represented by a Lorentz line with $E_0=15$ MeV and $\Gamma=5$ MeV. The scattering cross section is asymmetrical because of the interference with

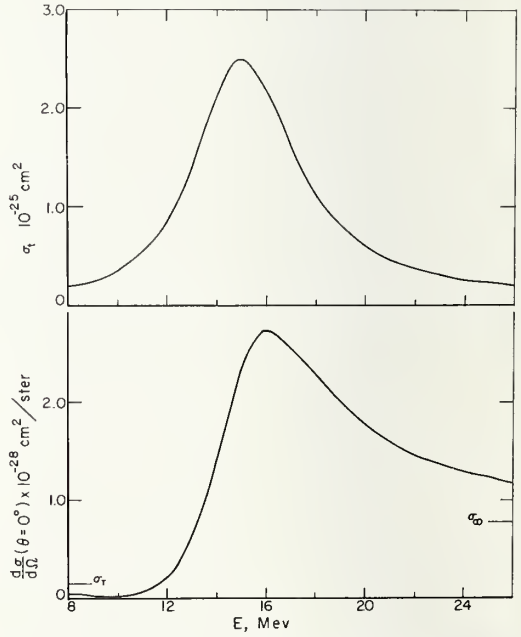

FIGURE 3. *A comparison of the absorption cross section with the forward scattering cross section for a nucleus with* N = Z = 50 *for which the dipole sum is enhanced by a factor* $\beta=1.3$.

The peak in the scattering cross section is shifted to a higher energy as a result of interference with nuclear Thomson scattering. The symbol σ_T stands for the magnitude of the nuclear Thomson scattering cross section which is effective at very low energies. The symbol σ_∞ represents the high energy limit of the scattering at an energy well in excess of all absorption which has been assumed to be entirely of an electric dipole character.

Thomson scattering which interferes destructively on the low and constructively on the high energy side of the giant resonance. The low and high energy limits of the coherent scattering are indicated in the margin. The lower limit is just the Thomson scattering cross section, $(Z^2e^2/AMc^2)^2$. The high energy limit is

$$\frac{d\sigma}{d\Omega}(E\rightarrow\infty)=[(Z^2e^2/AMc^2)(1+N\beta/Z)]^2 \qquad (2.8)$$

This limit is obtained by assuming that the absorption cross section is contained entirely by the Lorentz line and that the latter approaches zero as $E\rightarrow\infty$. Since these conditions are not realized in nature, it is not possible to use the high energy limit of the scattering cross section to evaluate β. Note that for $\beta\rightarrow 1$ this expression reduces to the Thomson scattering cross section for Z free protons.

2. The Kramers-Heisenberg Formula

The preceding discussion relates to the connection between the total absorption cross section and the coherent scattering cross section. By coherent scattering is meant that scattering in which the nuclear system returns exactly to its initial state of energy and angular momentum. No angular momentum is transferred to the nucleus itself. There is, of course, additional elastic scattering in which the nucleus may take up angular momentum but the scattered γ rays lie so close in energy to the incident ones as to be indistinguishable experimentally. These we designate as elastic but incoherent.

In order to absorb angular momentum in the two-step scattering process the nucleus must have some intrinsic asymmetry. This asymmetry is most often provided by its spin but it may also result from the intrinsic deformation for nuclei having large quadrupole moments. The nuclear scattering cross section is obtained by calculating the cross section for one orientation of the nucleus relative to the photon's polarization vector and then averaging over the orientations the nucleus can assume in the laboratory. A final average is then made over the polarizations in the incident photon beam. If the nucleus has no intrinsic asymmetry, the first average need never be performed. The scattered radiation is coherent with the incident radiation and in the dipole case has the familiar $1+\cos^2\theta$ angular distribution.

The usual treatment of angular correlations concerns itself with transition between states of well specified spin and parity. The sequence $I\rightarrow I_k\rightarrow I_f$ is regarded as a two-step process and the spin of the intermediate state, I_k, is an essential parameter. Fano [4] has treated the scattering process by an alternative description in which the angular momentum transfer is the essential parameter.

Considering only electric dipole transitions, Fano has shown that the nuclear scattering cross section can be written as the sum of three independent cross sections each characterized by the angular momentum transferred to the nucleus. The angular momentum transferred, ν, can have the values 0, 1, or 2; the corresponding scattering cross sections are labeled scalar, vector, and tensor. Each of the three cross sections has its own scattering amplitude, A_ν, and angular distribution factor $g_\nu(\theta)$ so that the whole scattering cross section for an unoriented nucleus is:

$$\frac{d\sigma}{d\Omega}=\sum_{\nu=0}^{2}\frac{|A_\nu|^2}{2\nu+1}g_\nu(\theta) \qquad (2.9)$$

The angular distrbution factors, $g_\nu(\theta)$, depend only on the angle between the polarization vectors of the incoming and outgoing photons, λ and μ. Then

$$\begin{aligned} g_0&=\tfrac{1}{3}(\lambda\cdot\mu)^2\\ g_1&=\tfrac{1}{2}[1-(\lambda\cdot\mu)^2]\\ g_2&=\tfrac{1}{2}[1+\tfrac{1}{3}(\lambda\cdot\mu)^2] \end{aligned} \qquad (2.10)$$

For unpolarized incident radiation these become:

$$\begin{aligned} g_0&=\tfrac{1}{6}(1+\cos^2\theta)\\ g_1&=\tfrac{1}{4}(2+\sin^2\theta)\\ g_2&=\tfrac{1}{12}(13+\cos^2\theta) \end{aligned} \qquad (2.11)$$

The scattering amplitude, A_ν, is the Kramers-Heisenberg dispersion formula generalized to include the inchoherent scattering associated with $\nu=1$ and 2.

$$A_\nu=C_\nu\sum_k\langle I_f\,\|\,r\,\|\,I_k\rangle\left[\frac{1}{E_k-\hbar\omega-\frac{1}{2}i\Gamma_k}+\frac{(-1)^\nu}{E_k+\hbar\omega'+\frac{1}{2}i\Gamma_k}\right]\langle I_k\,\|\,r\,\|\,I_0\rangle\begin{Bmatrix} I_0 & I_f & \nu\\ 1 & 1 & I_k\end{Bmatrix}+\sqrt{3}D\delta_{\nu 0}\delta_{0f} \qquad (2.12)$$

and

$$C_\nu=(-1)^{I_0+I_f+\nu}(e/c)^2(\omega'/\omega)^{1/2}\times\omega\omega'[(2\nu+1)/(2I_0+1)]^{1/2}$$

The summation is over all the intermediate states k that can be reached in electric dipole transitions and $\langle I_k\,\|\,r\,\|\,I_0\rangle$ is the reduced matrix element of the dipole operator connecting the states I_0 and I_k. The symbols ω and ω' represent the frequencies of the incoming and outgoing photons and $\begin{Bmatrix} I_0 & I_f & \nu\\ 1 & 1 & I_k\end{Bmatrix}$ is the 6-j coefficient that weights the different components that comprise the total scattering cross section. The delta functions insure that the Thomson scattering amplitude interferes only with the part of the nuclear scattering that is coherent with the incident beam.

3. The Absorption Cross Section

Since the forward scattering amplitude is $A_\nu/3$, it is straightforward to show by the use of the optical

theorem that the absorption cross section into a resonance described by this relation has the Lorentz shape. This manipulation requires setting $I_0=I_f$, $\hbar\omega=\hbar\omega'=E$, and $\nu=0$. Then

$$\sigma_t(E)=\frac{4\pi e^2}{\hbar c}\frac{E^2}{3(2I_0+1)}\sum_k\frac{2E_k\Gamma_k}{(E_k^2-E^2)^2+\Gamma_k^2E^2}\cdot|\langle I_k\|r\|I_0\rangle|^2 \qquad (2.13)$$

since

$$\langle I_0\|r\|I_k\rangle\langle I_k\|r\|I_0\rangle=(-1)^{I_0+1-I_k}|\langle I_k\|r\|I_0\rangle|^2$$

and

$$\begin{Bmatrix}I_0 & I_0 & 0\\ 1 & 1 & I_k\end{Bmatrix}=\frac{(-1)^{I_0+I_k+1}}{[3(2I_0+1)]^{1/2}}$$

In this expression the reduced matrix element may be replaced by either the oscillator strength, f_k, or the ground-state radiation width γ_k.

The oscillator strength of the kth energy level has already been defined as:

$$f_k=\frac{2ME_k}{\hbar^2}|\langle k|r|0\rangle|^2$$

$$=\frac{2ME_k}{\hbar^2}|\langle I_km_k|r_\lambda^1|I_0m_0\rangle|^2 \qquad (2.14)$$

Making use of the Wigner-Eckhart theorem this becomes:

$$f_k=\frac{2ME_k}{\hbar^2}(1\lambda I_0m_0|I_km_k)^2\frac{|\langle I_k\|r\|I_0\rangle|^2}{2I_k+1} \qquad (2.15)$$

Summing over the components, m_k, and averaging over m_0, we obtain:

$$f_k=\frac{2ME_k}{\hbar^2}\frac{|\langle I_k\|r\|I_0\rangle|^2}{(2I_k+1)(2I_0+1)}\sum_{m_k}(1\lambda I_0m_0|I_km_k)^2$$

$$=\frac{2ME_k}{\hbar^2}\frac{|\langle I_k\|r\|I_0\rangle|^2}{3(2I_0+1)} \qquad (2.16)$$

Then:

$$\sigma_t(E)=\frac{4\pi e^2\hbar}{Mc}f_k\frac{E^2\Gamma_k}{(E_k^2-E^2)^2+\Gamma_k^2E^2} \qquad (2.17)$$

Similarly, the ground state radiation width is:

$$\gamma_k=\frac{4e^2}{3}\left[\frac{E_k}{\hbar c}\right]^3\frac{\langle I_k\|r\|I_0\rangle^2}{2I_k+1} \qquad (2.18)$$

So that:

$$\sigma_t(E)=2\pi\lambda_k^2\frac{2I_k+1}{2I_0+1}\frac{\gamma_k}{\Gamma_k}\frac{E^2\Gamma_k^2}{(E_k^2-E^2)^2+\Gamma_k^2E^2} \qquad (2.19)$$

4. The Elastic Scattering Cross Section for Spherical Nuclei

The scattering cross section includes not only the scalar term ($\nu=0$), but the vector ($\nu=1$) and tensor ($\nu=2$) terms as well. The energy dependence associated with the tensor and scalar scattering are the same while that associated with $\nu=1$ is slightly different.

In terms of the oscillator strength, f_k, the elastic scattering amplitude, A_ν, is:

$$A_\nu=C_\nu\sum_k(-1)^{I_0+1-I_k}3(2I_0+1)\frac{\hbar^2}{2ME_k}f_k$$

$$\times\begin{Bmatrix}I_0 & I_0 & \nu\\ 1 & 1 & I_k\end{Bmatrix}\times\left[\frac{1}{E_k-\hbar\omega-\frac{1}{2}i\Gamma_k}+\frac{(-1)^\nu}{E_k+\hbar\omega+\frac{1}{2}i\Gamma_k}\right]+\sqrt{3}D\delta_{0\nu} \qquad (2.20)$$

The electric dipole scattering from discrete energy levels includes contributions from all three of these terms. The radiation pattern is determined by the two spins, I_0 and I_k, and the reduced matrix elements. In the continuum that makes up the giant resonances, at least for the heavy elements, the situation is quite different. Here there are many overlapping energy levels. The sum of their contributions consists of terms of the form:

$$\sum_{I_k=I_0-1}^{I_0+1}(-1)^{I_0+1-I_k}\begin{Bmatrix}I_0 & I_0 & \nu\\ 1 & 1 & I_k\end{Bmatrix}f_k$$

If we make the usual assumption that here f_k is proportional to $2I_k+1$ (or the ground-state radiation widths, γ_k, of these overlapping states are all the same) then since

$$\sum_{I_k=I_0-1}^{I_0+1}(-1)^{I_0+1-I_k}(2I_k+1)\begin{Bmatrix}I_0 & I_0 & \nu\\ 1 & 1 & I_k\end{Bmatrix}=0 \qquad (2.21)$$

for $\nu>0$, the only contribution to the elastic scattering cross section is that resulting from coherent scattering. As a result of this simplification the elastic scattering cross sections for heavy spherical nuclei are related to the giant resonance absorption cross sections through the optical theorem and dispersion relation and have the angular distribution typical of a classical dipole: $1+\cos^2\theta$.

5. The Scattering Cross Sections for Deformed Nuclei

The nuclei having large intrinsic deformations have an important additional component in their scattering cross sections. It is incoherent with the incident radiation and results from the tensor scattering amplitude associated with the transfer of two units of angular momentum to the nucleus.

It is an experimental observation that the giant resonances for the highly deformed nuclei consist of a superposition of two resonances having a 2:1 ratio of areas. These are associated classically with charge oscillations along the one long ($\Delta K=0$) and two short ($\Delta K=\pm1$) axes of the nuclear ellipsoid; in other words the index of refraction of the nucleus depends on its orientation. It is also well established that these nuclei are characterized by rotational

spectra, and that the ground-state is a member of a rotational band. The radial parts of the matrix elements associated with transitions between the giant resonance and all the members of the ground-state, rotational band are the same. The relative intensities of these lines are given by simple angular momentum factors. This scattered radiation is known as Raman scattering.

In the intrinsic nuclear coordinate system the transition matrix elements depend not only on I and m, but also on K, the projection of I on the symmetry axis, and electric dipole transitions are specified by the additional requirement that $\Delta K=\epsilon=0,\pm 1$. The laboratory matrix elements may be expanded in terms of the intrinsic matrix elements, the expansion coefficients being integrals over D functions which may, in turn, be expressed as products of vector coupling coefficients. The scattering amplitude, A_ν, may be written in a compact form [5] if it is assumed that all of the oscillator strength, $NZ\beta/A$, associated with the transition $\Delta K=\epsilon$, is distributed in a resonance located at E_ϵ. The energies of incoming and outgoing photon are set equal, then:

$$A_\nu=\frac{e^2}{Mc^2}\frac{NZ\beta}{A}\frac{E^2}{2}(I_0K_0\nu 0\mid I_0K_f)$$

$$\times\left\{\sum_{\epsilon=-1}^{+1}(1\epsilon 1-\epsilon\mid\nu 0)\frac{(-1)^\epsilon}{E_\epsilon}\left[\frac{1}{E_\epsilon-E-\frac{1}{2}i\Gamma_\epsilon}\right.\right.$$

$$\left.\left.+\frac{(-1)^\nu}{E_\epsilon+E+\frac{1}{2}i\Gamma_\epsilon}\right]\right\}+\sqrt{3}D\delta_{\nu 0}. \qquad (2.22)$$

In the Danos-Okamoto model the transitions that make up the giant resonance of deformed nuclei are associated either with $\Delta K=0$ or $\Delta K=\pm 1$. For a nucleus having positive deformation the former are at the lower energy and the higher energy resonance contains two-thirds of the area. If A and B are the intrinsic scattering amplitudes associated with the major and minor axes of the nuclear ellipsoid and are analogous to eq. (2.4), then the scattering cross sections can be written in a simple form. That associated with $\nu=0$ is:

$$\left.\frac{d\sigma}{d\Omega}\right]_0=\left|\frac{A+2B}{3}+D\right|^2\frac{1+\cos^2\theta}{2} \qquad (2.23)$$

The scattering cross section for $\nu=1$ is identically zero. The Raman scattering cross section is:

$$\left.\frac{d\sigma}{d\Omega}\right]_2=(I_0K_020\mid I_fK_0)^2\mid\tfrac{2}{3}(A-B)\mid^2\frac{13+\cos^2\theta}{40} \qquad (2.24)$$

The weighting factor, $(I_0K_020\mid I_fK_0)^2$, gives the relative intensities of the Raman lines, i.e., the relative contributions to the scattering to those members of the ground-state rotational band that can be reached in dipole-dipole transitions. For a spin zero nucleus all of the transitions involving $\nu=2$ populate the 2^+ state. For odd nuclei there are contributions to the ground-state as well as those having I_0+1 and I_0+2. The total intensity in the Raman spectrum is, however, a constant by virtue of the sum rule:

$$\sum_{I_f=I_0}^{I_0+2}(I_0K_020\mid I_fK_0)^2=1 \qquad (2.25)$$

Since the final states all lie within 200 keV of the ground-state, the Raman lines have not been separated experimentallly. The measured result is independent of the ground-state spin and as large as would be expected for a nucleus with $I_0\rightarrow\infty$ for which the weighting factor approaches 1.

Figure 4 shows the scattering cross section for a deformed nucleus. The lower curve is the coherent scattering associated with the absorption cross section and calculated from eq (2.23). The center curve is that obtained when the elastic scattering for a spin 7/2 (Ta or Ho) nucleus is added to it. The upper curve is the total coherent plus Raman scattering cross section. This is the cross section that is actually measured in a poor resolution experiment. It is independent of the spin of the nuclear ground state and as large as can be obtained for a classical system.

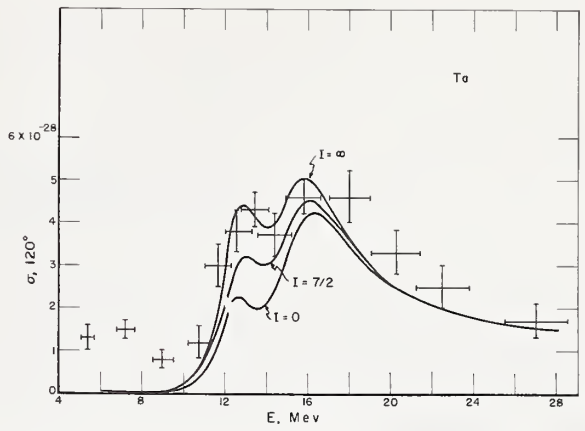

FIGURE 4. *The scattering cross section for a deformed nucleus.*

The lower curve is the coherent scattering associated with the absorption cross section and calculated from eq (2.23). The center curve is that obtained when the elastic scattering for a spin 7/2 (Ta or Ho) nucleus is added to it. The upper curve is the total coherent plus Raman scattering cross section. This is the cross section that is actually measured in a poor resolution experiment. It is independent of the spin of the nuclear ground state and as large as can be obtained for a classical system.

III. Photonuclear Experiments

Photonuclear experiments differ from other experiments in nuclear physics only in that the reactions are initiated by x rays and that the cross sections are generally somewhat smaller. The following paragraphs describe (1) the different kinds of x-ray sources and (2) the different kinds of photonuclear experiments.

1. X-ray Sources

The kind of x-ray source available largely determines the experiments which will be performed. These sources fall into two main classes, x rays produced in nuclear excitation and x rays generated in electromagnetic processes. The former are usually the γ rays that follow neutron or proton capture and as a result they occur at a specific energy with an energy spread that is often determined by Doppler broadening or the target thickness. The latter are produced by bremsstrahlung or positron annihilation in flight and their energy can therefore be controlled at will. The practical energy resolution is, however, no better than a few hundred kilovolts. In general, the nuclear γ rays are continuous in time since they are produced by a Van de Graaff or nuclear reactor; whereas the electromagnetic radiation is pulsed with a duty cycle often as low as 10^{-3}. The latter is a consequence of the pulsed nature of high energy electron accelerators and is a disadvantage except in time-of-flight experiments.

There are three important sources of proton capture γ-rays that have been used to study photonuclear reactions: The $F^{19}(p,\alpha\gamma)$, $Li^7(p,\gamma)$ and the $H^3(p,\gamma)$ reactions. Their properties are compared in table 1. The $F(p,\alpha\gamma)$ reaction has been used by Reibel and Mann [6] in a resonance fluorescence experiment. This reaction produces three γ rays that come from the excited states in O^{16} at 6.14, 6.92, and 7.12 MeV. Their relative intensities can be changed by varying the incident proton energy and as much as 80 percent of the intensity is at 7.12 MeV for proton energies of 2.05 MeV. The energy spread of about 130 keV results from the fact that α particles are also emitted in this reaction.

The $Li^7(p,\gamma)$ reaction is an important source of 17.6 MeV γ rays. Its great disadvantage is that it is contaminated with a broad band of x rays centered near 14.2 MeV. It is however, very useful in experiments where the incident photon energy can be determined from that of an outgoing nucleon.

The $H^3(p,\gamma)$ reaction has been used primarily by Stephens [7–10] and his collaborators. It represents a source of γ rays which may be continuously varied from 20 MeV upward by increasing the bombarding proton energy. The practical upper limit depends on the experiment and results from the serious neutron background generated in the $H^3(p,n)$ reaction. The energy resolution is determined by the thickness of the gas target and can be made as low as 40 keV.

Neutron capture γ rays have been used by Donahue [11–13] and more recently by Ben-David [14–15] to study the (γ,n) and (γ,γ) reactions for excitation energies near 8 MeV. These γ rays occur in a rather restricted energy range but the spread of each line is only a few volts, being determined largely by the Doppler width, $\Delta = E_0(2kT/AMc^2)^{1/2}$ associated with the thermal motions of the target atoms. Table 2 shows a list of useful neutron capture γ rays and their relative intensities.

TABLE 1. *Proton capture γ rays*

Reaction	E_γ(MeV)	ΔE(keV)
$F^{19}(p, \alpha\gamma)$	7.12	130
$Li^7(p, \gamma)$	17.6	12.2
$H^3(p, \gamma)$	>20	40

TABLE 2. *Neutron capture γ rays*

Element	E(MeV)	γ rays/neutron capture*
Hg	5.44	0.038
Cl	6.12	.177
Fe	7.28	.042
Co	7.94	.029
Fe	7.64	.30
Al	7.73	.22
Ni	7.82	.06
Cu	7.91	.20
Cr	8.449	.06
Cl	8.56	.021
Cr	8.881	.14
Ni	8.997	.27
Fe	9.30	.024
Cr	9.72	.06
Fe	10.16	.0006
N	10.83	.13

* The errors on these intensities are of the order of ± 30 percent.

TABLE 3. *Resonance fluorescence γ rays*

Nucleus	E(MeV)	Ground-state radiation width (eV)
Li^6	3.56	7
Mg^{24}	9.92	6
Mg^{24}	10.66	18
Si^{28}	11.4	23
C^{12}	15.1	36

Knowles [16] has described a method for producing monochromatic, partially polarized photons by Compton scattering of neutron capture γ rays. The source is a Ni or Ti target placed in a reactor in a position of high thermal neutron flux. The capture γ-ray beam emerges from the reactor and is scattered from an extensive aluminium plate. The scattering angle determines the photon energy. These monochromatic photons were then scattered from other targets and the resonant radiation studied. In this way an x-ray beam continuous in time and continuously variable in energy from 1 to 10 MeV is produced.

Monochromatic γ rays can also be produced by resonance fluorescene. Here an intense bremsstrahlung beam is incident on a suitable target which picks out the resonant radiation and reradiates it in all directions. Table 3 contains a list of energy levels having large ground-state radiation widths [17]. With the exception of Li^6, for which the 3.56 MeV state is 0^+, the photons scattered from these levels are plane polarized at 90°. The production of such a source suitable for doing experiments is still in the future.

The classical photonuclear experiments have been performed with bremsstrahlung x rays produced by allowing the internal electron beam of a synchrotron or betatron to strike an internal target. The resultant x-ray spectrum is continuous in energy extending up to the kinetic energy of the radiating electron. Figure 5 shows the shape of the bremsstrahlung spectrum according to the formula of Schiff [18] where the spectrum has been integrated over the angles of the outgoing photons. This averaging approximates the multiple scattering of the electrons in practical targets.

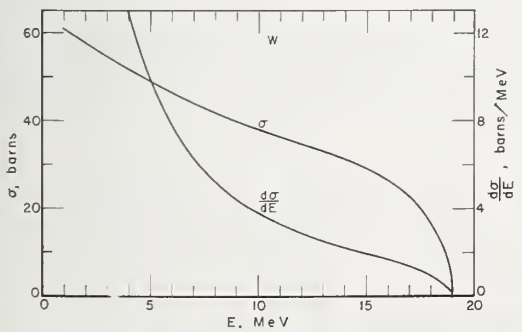

FIGURE 5. *The cross section for the production of X-ray energy (left-hand scale) and photons (right-hand scale) between* E *and* E+dE *when 19 MeV electrons strike a tungsten target.*

In most bremsstrahlung experiments the yield of some reaction is measured as the peak bremsstrahlung energy, E_0, is advanced in small steps. An involved analysis process is then used to obtain the cross section. In such experiments only those photons in the top energy interval, say 0.5 MeV, are used to produce the desired effect while the bulk of the spectrum produces a "background" that must be subtracted off.

The bremsstrahlung monochrometer represents a method for selecting a very small energy interval out of the continuous bremsstrahlung spectrum. This ΔE can be taken several MeV below the peak energy and in this way a reasonable x-ray intensity obtained. This scheme has recently been used in photon scattering [19,20] and photoneutron experiments at the University of Illinois and their arrangement is illustrated in figure 6. The electron beam is deflected from the circular orbit of the betatron and radiates in a thin, external target. The electrons are then analyzed magnetically. The bremsstrahlung photons are allowed to impinge on a target and some product radiation detected in coincidence with the analyzed electron. The energy of the absorbed photon can then be specified by requiring that $\hbar\omega = E_0 - E$. This technique is basically limited by the chance coincidence rate.

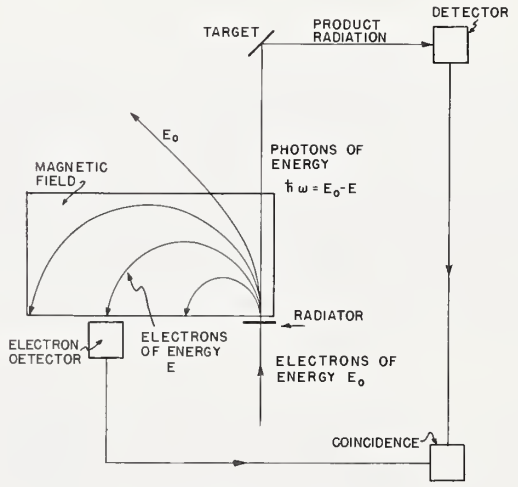

FIGURE 6. *The bremsstrahlung monochromater.*

Monoenergetic electrons are deflected from a circular accelerator and allowed to radiate in a thin foil. The electrons are then analyzed magnetically. The bremsstrahlung photons strike a second target and some product radiation is detected in coincidence with the electron. In this way the photon energy can be specified.

When higher intensities are available, as with the linear accelerator, effectively monochromatic photon beams can be produced by allowing monoenergetic positrons to annihilate with electrons at rest. In the center of mass system two photons each having an energy of mc^2 are emitted isotropically in the anni-

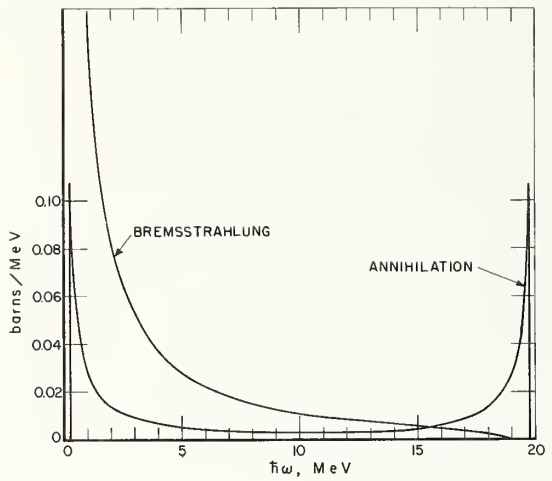

FIGURE 7. *The cross sections for the production of annihilation and bremsstrahlung photons in the energy interval* $d(\hbar\omega)$ *when 19 MeV positions strike a beryllium target.*

hilation of a positron. If the positron has a very high velocity and annihilates in flight then the photons emitted in the forward hemisphere come off within a very small angle in the laboratory system and with a spectrum that increased to a maximum energy of approximately $E^+ + \frac{1}{2}mc^2$. The backward going radiation is concentrated in a similar cone with a lower limit on the laboratory energy of approximately $\frac{1}{2}mc^2$. The relationship between the laboratory photon energy and its angle, θ, relative to the positron direction is:

$$\hbar\omega = mc^2/(1-\beta\cos\theta) \tag{3.1}$$

Here β is the velocity of the center of mass system, $[(E^+-mc^2)/(E^++mc^2)]^{1/2}$. The exact energies of the maximum and minimum photon energies can be obtained by setting θ equal to 0 and π. As the positron energy increases the peaks at either end of the spectrum become sharper and the photon beam is concentrated in a smaller cone.

The cross section for this process differential in the energy of one of the outgoing photons is:

$$\frac{d\sigma}{d(\hbar\omega_1)} = \left(\frac{e^2}{mc^2}\right)^2 \frac{\pi}{mc^2}\frac{1}{(\beta\gamma)^2}\left[\frac{\omega_1}{\omega_2}+\frac{\omega_2}{\omega_1}+\frac{2(mc^2)^2}{(\hbar\omega_1)(\hbar\omega_2)}\right.$$

$$\left.\times(1+\gamma)-\left(\frac{(mc^2)^2(1+\gamma)}{(\hbar\omega_1)(\hbar\omega_2)}\right)^2\right] \tag{3.2}$$

where $\hbar\omega_1+\hbar\omega_2=mc^2(1+\gamma)$ and γ is the positron energy in units of its rest energy E^+/mc^2. The spectrum of photons emitted when a positron of total energy $E^+=mc^2+19$ MeV annihilates in a Be target is shown in figure 7. In a target of practical thickness this spectrum is modified primarily by ionization losses and secondarily by multiple scattering before annihilation in the target.

A second troublesome feature is that the positrons also radiate in the annihilation target. For relativistic particles the ratio of the annihilation to the bremsstrahlung cross sections (per atom) is essentially $137\pi/4\gamma Z$. This shows the importance of using a low Z target to suppress the bremsstrahlung. The energy distribution of the bremsstrahlung photons produced in a Be target by electrons having a kinetic energy of 19 MeV is shown for comparison in figure 7. When annihilation radiation is used as a source of x rays in an experiment, it is obviously necessary to take this bremsstrahlung into account. This is done by measuring the backgrounds with negative electrons striking the annihilation target and assuming that electrons of positive and negative charge produce the same bremsstrahlung spectrum.

The contemporary electron linear accelerators have sufficient intensity to make experiments with positron annihilation radiation practical. Three such systems have been developed. In all, the positrons are created in a shower when the electron beam strikes a high-Z target, but two different locations have been used for this target. In one case [22] the shower is produced at the end of the accelerator and monoenergetic positrons selected and focused by a system of slits and magnets. The lithium annihilation target is located in the field of the final bending magnet and shaped so that the forward radiation is focused on the experimental target while the positrons are bent into a shielded area. In the other case [23] the positrons are created after the first section of the machine and then accelerated up to the desired energy; in this way the positron beam may be carried by the same magnet system that is used to deflect and focus the electron beam. An additional magnet is required for removing the positrons after the annihilation target just as would be used after a bremsstrahlung target. This scheme has the additional advantage that the background generated in the positron-producing shower is at a relatively low energy and far away from the experiment.

Table 4 shows a very rough comparison of the yields and energy spreads for the three x-ray sources just discussed.

The electromagnetic sources always rely on some kind of an energy control device which must be calibrated. The most common calibration points are the thresholds for the production of neutrons (or the resulting radioactivity) when a target is irradiated with x rays. In order to produce an activation curve that begins sharply at the neutron binding energy, it is highly desirable to select a target which can emit s-wave neutrons and leave the residual nucleus

TABLE 4. *Rough comparison of electromagnetic x-ray sources*

Source	photons/electron	ΔE(MeV)
Bremsstrahlung	10^{-5}	0.5
Monochromator	10^{-5}	.1
Positron annihilation	10^{-10}	.5

in its ground-state, since near threshold

$$\sigma(E) = SE^{l+1/2}. \tag{3.3}$$

where E is the energy above threshold. The slope of this curve is then

$$d\sigma/dE = S(\ell+\tfrac{1}{2})E^{l-1/2} \tag{3.4}$$

which is infinite for outgoing s-wave neutrons and varies much more slowly for higher angular momenta. Table 5 lists some targets that have proved useful for this purpose. With the exception of deuterium they are all relatively heavy nuclei from which the s-wave neutrons are simply evaporated. The neutron binding energies in the light elements come at higher energies ($\approx$ 15 MeV) so that it would be highly desirable to use one as a calibration target. For these elements the neutrons are emitted primarily in direct interactions and the matrix elements for the transitions that result in s-wave nucleons are small and consequently the thresholds are less sharp. An extreme example is Al^{27} which cannot absorb electric dipole radiation, emit s-wave neutrons, and leave Al^{26} in its ground state and at the same time conserve parity.

A very excellent alternative is to use the resonance fluorescence of the 15.1 MeV state in C^{12}. This level has a large ground-state radiation width and the scattered photons are easily detected. The disadvantage is, of course, that the dectection apparatus is different from that used to measure the (γ,n) thresholds so that it is often very inconvenient.

2. Photonuclear Experiments

The objective of photonuclear experiments has been first of all to determine the gross features of the photon absorption cross section, such as its magnitude and energy, and then to explore the detailed shape of the cross section with better energy resolution or by examining the spectra of outgoing nucleons. Angular distributions have sometimes been used to infer the multipolarity of the absorbed radiation. In the following we will simply list some different kinds of photonuclear experiments and point out a few of their sailient features.

Table 5. *Calibration Energies**

	Threshold (MeV)
$D(\gamma, n)$	2.22
$Pt^{195}(\gamma, n)$	6.13
$Bi^{209}(\gamma, n)$	7.39
$Au^{197}(\gamma, n)$	8.05
$Cu^{63}(\gamma, n)$	10.8
$C^{12}(\gamma, \gamma)$	15.1

* The neutron binding energies are taken from V. J. Ashby and H. C. Catron, UCRL 5419.

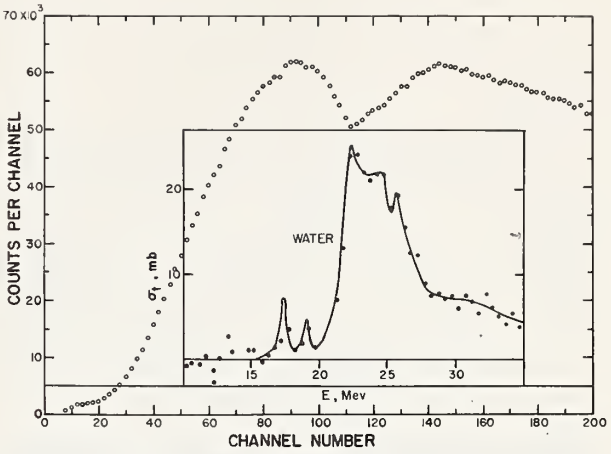

Figure 8. *The spectrum of photons transmitted by 4.5 m of water when 90 Mev bremsstrahlung is incident upon it.*

The insert shows the total photonuclear cross section that has been derived from it (reference [15]).

2.1. Total Absorption Experiments

The continuous bremsstrahlung spectrum is usually used as a source of x rays in these experiments. A well defined beam is filtered through a long absorber of the material under study and the spectrum of transmitted photons recorded. This spectrum is then compared with that which would be expeceted if only the electronic processes, Compton scattering and pair production, were removing photons from the beam and the cross section for nuclear absorption obtained. This analysis requires a detailed knowledge of the electronic absorption coefficients since the nuclear absorption is never more than 10 percent of the total. The results obtained by this method are quantitatively consistent with other measurements.

Figure 8 shows the pulse height distribution produced in a sodium iodide pair spectrometer [24] when a 90 MeV bremsstrahlung spectrum filtered through 4.5. m of water was incident on it. The oxygen cross section [25] derived from it is also shown.

2.2. Elastic Scattering Measurements

Here a sodium iodide spectrometer has been used usually with bremsstrahlung sources to measure the elastic scattering cross section. First the spectrometer is placed in the x-ray beam and compared with the transmission monitor so that N_1 is the number of counts measured in the energy interval, ΔE, near the peak of the bremsstrahlung spectrum when monitor reading is M_1. A second measurement N_2/M_2 is then made with the spectrometer viewing the target from some large angle. The elastic scattering cross section is then:

$$\frac{d\sigma}{d\Omega} = K\frac{N_2}{M_2}\cdot\frac{M_1}{N_1} \tag{3.5}$$

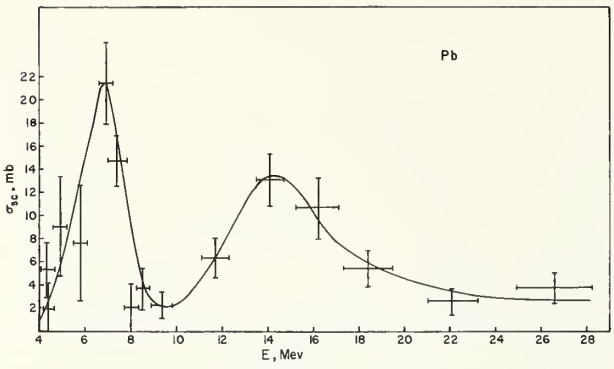

FIGURE 9. *The elastic scattering cross section for lead.*

The broad peak in the scattering cross section in the energy range 10–20 MeV is associated with the giant resonance absorption and is related to it by the optical theorem and the dispersion relation. The peak in the scattering cross section below 10 MeV results from the resonance fluorescence of discrete energy levels.

where K is a constant that depends on the target properties and geometrical factors.

The elastic scattering cross section for lead [26] shown in figure 9 displays two peaks. The higher energy one is the scattering that is related to the giant resonance absorption by the dispersion relation already discussed. The lower energy maximum occurs below the threshold for particle emission where the nuclear energy levels are discrete and well defined. The observed elastic scattering results simply from their resonance fluorescence.

2.3. Partial Cross Sections Obtained by Activation Curve Analysis

In the past, by far the most common photonuclear experiment was one in which the number of outgoing particles or the radioactivity generated in a target was measured as a function of incident bremsstrahlung energy, E_0. Each point on such an activation curve is the ratio of the number of events, $N(E_0)$, counted in some nuclear detector to the reading on an integrating monitor, $M(E_0)$:

$$N(E_0)/M(E_0) = n\int dE\epsilon(E)\sigma(E)I(E, E_0)/E \qquad (3.6)$$

In this expression $I(E,E_0)dE/E$ is the number of photons in dE in a bremsstrahlung spectrum extending to E_0, n is the effective number of atoms/cm^2 in the target and $\epsilon(E)$ is the detector efficiency. The latter must be made independent of E so that it need not be included in the integral. In addition, the monitor must be calibrated so that its reading can be related to the amount of energy incident upon it. Then, the activation curve in the units of events per unit energy incident on the monitor can be converted to a cross section by means of the inverse matrix of the bremsstrahlung spectrum which has been tabulated by Penfold and Leiss [27]. These tables are now almost universally used in the reduction of photonuclear data.

Since this reduction process is essentially one of differentiation, great care must be taken not to introduce artificial wiggles in the activation curve nor to destroy those that result from structure in the true cross section. The monitor response function must be smoothed but the details in the activation curve should not be removed since they contain the interesting nuclear information.

The most important limitation on this kind of experiment is the statistical inaccuracy resulting from the finite number of counts acquired. The statistical errors in the cross section may be evaluated by propagating those on the activation curve through the inverse matrix used to reduce the data. Figure 10 shows an activation curve obtained by counting the total number of neutrons emitted by a gold sample [28]. Approximately 5×10^5 counts per point have been obtained. The cross section resulting from this analysis is also shown along with the statistical errors. The latter are as large as 25 percent on the high energy side of the resonance.

In a heavy element such as gold, photon absorption is followed almost exclusively by neutron emission, since the Coulomb barrier essentially eliminates proton emission. The total absorption cross section may then be obtained by correcting for the multiplicity of neutrons emitted in the $(\gamma,2n)$ process. The lower set of points in figure 10 shows the importance of this effect. This correction is usually quite uncertain. In a few cases the $(\gamma,2n)$ cross section has actually been measured and these data can be used. More often the magnitude of the effect is estimated from the statistical theory with an appropriate contribution for direct emission.

2.4. Radiative Capture Cross Sections

The giant resonance of nucleus, A, can be excited by nucleon capture into the nucleus, A–1. If the ground-state gamma radiation is observed,

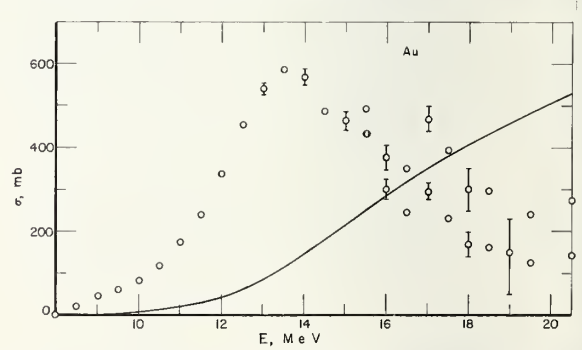

FIGURE 10. *The activation curve or number of neutrons generated as a function of bremsstrahlung energy incident on a gold target.*

The neutron production cross section derived from it is also shown. On the high energy side of the giant resonance there are two sets of points. The lower ones represent the photon absorption cross section and were obtained from the upper ones by correcting for the emission of two neutrons in the $(\gamma, 2n)$ process where it is energetically possible. The errors indicated are statistical.

TABLE 6. *Ground-state, proton capture experiments*

Target	Excited nucleus	T(MeV)	Reference
H^3	He^4	19.80	29
Li^7	Be^8	17.25	30
B^{11}	C^{12}	15.95	31, 32
C^{12}	N^{13}	1.94	33
N^{15}	O^{16}	12.11	34
F^{19}	Ne^{20}	12.87	35, 30
Na^{23}	Mg^{24}	11.69	36
Al^{27}	Si^{28}	11.59	31, 37
P^{31}	S^{32}	8.86	38, 39
K^{39}	Ca^{40}	8.33	30, 40

then the principle of detailed balance can be applied to infer the inverse photo-nuclear cross section.

The advent of the tandem accelerator has made possible the exploration of the giant resonance with an energy resolution of a few tens of kilovolts by studying the ground-state, proton capture cross sections. Sufficient energy is available here to excite the giant resonances of the light nuclei where the Coulomb barriers are still low enough to make the measurements practical. This is accomplished by measuring the (p,γ_0) cross section as a function of incident proton energy, the γ ray being selected with a sodium iodide spectrometer. Often this is made difficult by the proximity of the first excited state to the ground state of the final nucleus.

In order to make comparison with photonuclear reactions it is necessary for the two adjacent nuclei to exist in nature. A list of those that have been explored is given in table 6 along with the binding energies, T, and references to contemporary experiments.

The cross sections for two reactions the exact inverse of one another are related through the principle of detailed balance. This rule, which is a consequence of general S-matrix theory, states that

$$\sigma_1 g_1 p_1^2 = \sigma_2 g_2 p_2^2 \tag{3.7}$$

where σ_1 and σ_2 are the cross sections for the two processes referred to the same excitation energy E_e. The quantities, g_1 and g_2, are the statistical weights associated with the two interacting particles, and p stands for the momentum of their relative motion. This equality is only valid for unpolarized beams and unoriented targets.

Consider $\sigma(\gamma, p_0)$ for the nucleus A. Then $g=g_\gamma g_A=2(2I_A+1)$ and $p=\hbar\omega/c$. For the inverse $\sigma(p,\gamma_0)$ reaction $g=2(2I_{A-1}+1)$ and $p=\mu v_{\text{rel}}=\sqrt{2ME_p}(A-1)/A$. Substituting in the above expression we have:

$$(2I_A+1)(\hbar\omega/c)^2\sigma(\gamma,p_0)=(2I_{A-1}+1)$$
$$\times(A-1/A)^2(2ME_p)\sigma(p,\gamma_0) \tag{3.8}$$

The excitation energy in a (p,γ_0) reaction is:

$$E_e=\frac{A-1}{A}E_p+T \tag{3.9}$$

where T stands for the proton binding energy. In the (γ,p_0) reaction the excitation energy is:

$$\rightarrow E_e=\hbar\omega(1-\hbar\omega/2AMc^2) \tag{3.10}$$

Substituting for $\hbar\omega$ and E_p in the above expression we obtain:

$$\sigma(\gamma,p_0)=\frac{(2I_{A-1}+1)}{(2I_A+1)}\frac{A-1}{A}\frac{(E_e-T)}{E_e^2}2Mc^2\sigma(p,\gamma_0) \tag{3.11}$$

Thus the proton-capture experiments yield the cross section for populating the ground state of the residual nucleus in a (γ,p) reaction and sets a lower limit on the total (γ,p) cross section.

More than anything else these experiments have demonstrated the detailed structure that exists in the giant resonances of the light nuclei and shown that its character changes drastically as we progress from C^{12} to Ca^{40}. Figure 11 shows a comparison of the cross sections [33, 37] for C^{12} and Si^{28} and is

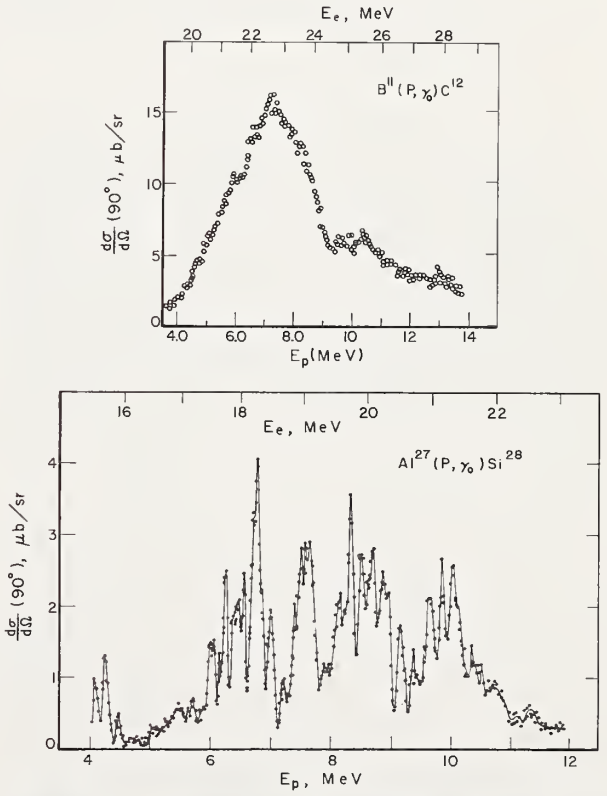

FIGURE 11. *A comparison of the ground-state, proton-capture cross sections [32] for* B^{11} *and* Al^{27}.

There is an important qualitative difference between the amount of structure seen for these two nuclei.

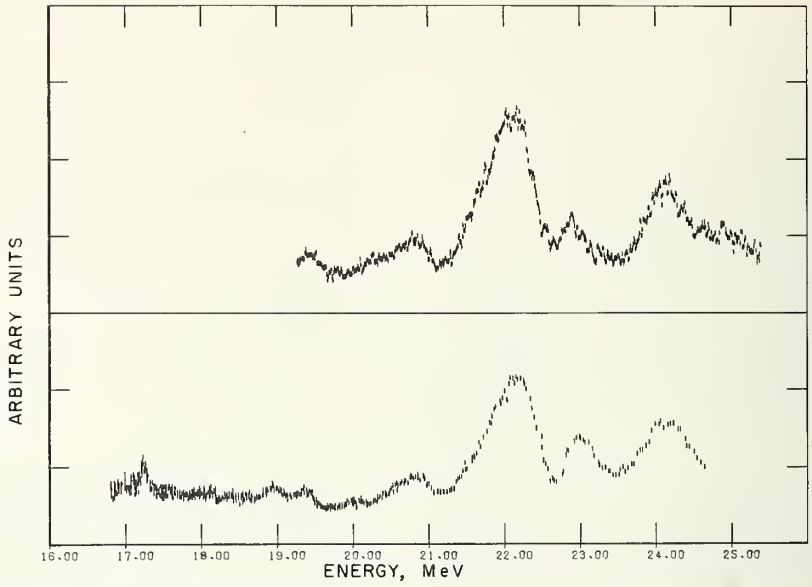

FIGURE 12. *A comparison of the photoproton* [42] *(upper) and photoneutron* [41] *(lower) spectra obtained when oxygen targets are irradiated with bremsstrahlung x rays.*

The bremsstrahlung spectra extended to 25 MeV and in both cases it has been assumed that only the ground state of the residual nucleus is populated.

meant to illustrate the large qualitative difference between these two nuclei.

2.5. Spectroscopy

A vast amount of data exists and is still being accumulated on the energy distributions of photonucleons. The classical spectroscopy experiments were those in which a target was irradiated with bremsstrahlung from a betatron and the outgoing nucleons detected in nuclear emulsions. Other more tractable detectors are now coming into use especially with the higher intensities available from linear accelerators. Nevertheless, even now very few spectra have been measured at more than one bremsstrahlung energy. We can look forward in the next few years to a great deal of exciting new data obtained using either positron annihilation radiation or with varying bremsstrahlung energies.

Experiments that make use of high resolution detectors have been complementary to the radiative proton capture experiments in revealing a large amount of structure in the giant resonances of the light nuclei. When irradiated by the continuous bremsstrahlung spectrum the nucleus absorbs out narrow bands of x rays corresponding to its excited states and emits particle groups to the available states in the residual nucleus. Figure 12 shows a comparison of the neutron [41] and proton [42] spectra from O^{16} where the level density in the residual nuclei is exceptionally low and a great deal of structure is observed. In both cases it has been assumed that the outgoing nucleon leaves the final nucleus in its ground state; it is evident that the same giant resonance structure is reproduced in both.

2.6. Angular Distributions

The angular distribution measurements suffer from the same criticisms as the spectroscopy experiments; namely, that the precise energy of the absorbed photons is not always known In fact, these two kinds of data are often obtained in the same experiment. Sometines fast neutron angular distributions are measured with threshold detectors, the $Al^{27}(n,p)Mg^{27}$ and $Si^{28}(n,p)Al^{28}$ reactions being favorites. The latter, for example, samples neutrons essentially in the energy range 5 to 10 MeV. The qualitative result of these experiments is that near the peak of the giant resonance the photonucleon angular distributions peak at 90° as would be expected for an electric dipole interaction. As the excitation energy increases these distributions begin to peak slightly forward as a result of interference with radiation of opposite parity, presumably $E2$.

The most accurate angular distributions, yielding the most detailed information, are those obtained from the ground-state, proton capture experiments. These are found to be almost energy independent throughout the giant resonance.

IV. Heavy Nuclei and the Hydrodynamic Model

1. Survey of Experimental Data

Three gross quantities can be determined from the photonuclear cross section measurements, the cross section magnitude, the giant resonance energy, and its width.

Some data on the photonuclear cross sections ntegrated to 30 MeV have already been presented n figure 1. The data on the light elements came rom the total absorption experiment of Wyckoff t al. [25]. These results are consistent with the alues obtained by summing the separately mea- ured (γ,n) and (γ,p) cross sections. For the heavy lements only the neutron producing cross sections re important and the data presented here come rom the Livermore neutron yield measurements 43–52]. The neutron yield data for nuclei having $A<100$ are excluded, because for them the (γ,p) cross ections are appreciable. The general conclusion rom these and other data is that the integrated ross sections for nuclei as light as carbon and oxygen s approximately half of the dipole sum. This value ncreases gradually with atomic number and finally bove $Z=50$ levels off at a constant value. These articular data show the constant to be 1.0 but it ıay be somewhat larger. The reason for this large ncertainty has to do with the systematic errors ssociated with bremsstrahlung beam monitoring nd the determination of the neutron detector fficiency. In any case, the heavy element cross ctions integrated over the giant resonance are t least as large as the dipole sum.

Figure 13 shows a plot of $E_0A^{1/3}$ vs A. The data r $A\leq 40$ are taken from reference [25] and those for the heavy elements from the Livermore experiments. The horizontal line corresponds to the dependence

$$E_0=80A^{-1/3}\ \text{MeV},$$

the prediction of the hydrodynamic model. The resonance energies lie fairly close to this line for the heavy elements but begin to fall lower for $A<100$.

Figure 14 shows a plot of the giant resonance width vs A. The data have been taken from the same experiments as for figure 13. These data show that the average giant resonance width is about five MeV and that the dependence on A proceeds through several maxima. These are associated with the three major regions of large intrinsic nuclear deformation, near $A=25$ 160, and 240. Closed-shell nuclei have the narrowest giant resonances.

2. The Hydrodynamic Model

Many of the features of the giant resonances of the heavy elements may be described in terms of the hydrodynamic model. In this model these many particle systems are assumed to consist of interpenetrating neutron and proton fluids of constant total density confined within a rigid boundary. The giant resonance is then associated with the lowest mode of the electric dipole counter-oscillation of these two fluids. The attraction between the two fluids produces a restoring force the magnitude of which is related to the symmetry energy, $K(N-Z)^2/A$, of the semiempirical mass formula.

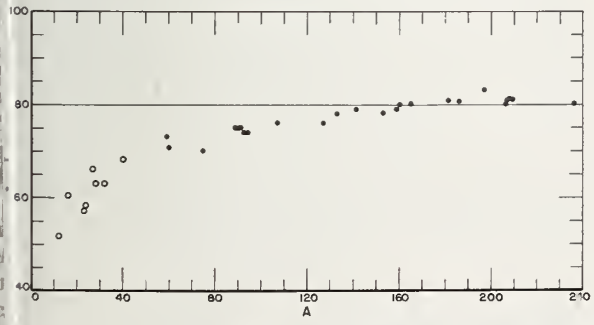

GURE 13. *The giant resonance energy times* $A^{1/3}$ *as a function of* A.

The data for the light elements come from reference [25] and those for dium and heavy elements from many recent neutron yield measurements -52].

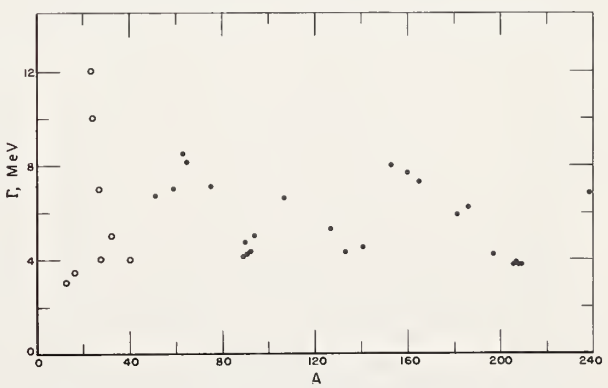

FIGURE 14. *The giant resoance width as a function of* A.

The data come from the same experiments as those used for figure 12.

The model [53] establishes a connection between the resonance energy and the integrated absorption cross section associated with this lowest dipole mode. The resonance energy obtained on the assumption that the fluids are contained within a rigid boundary is

$$E_0 = \frac{2.08\hbar}{R}\left[\frac{8KNZ}{MA^2}\right]^{1/2} \tag{4.1}$$

where 2.08 is the solution of the eigenvalue equation for a sphere of radius R. These assumptions also lead to the conclusion that only 86 percent of the oscillator strength is contained in the lowest mode, the rest being at higher energies.

Therefore

$$\int \sigma\, dE = \frac{2\pi^2 e^2 \hbar}{Mc}\frac{NZ}{A}(0.86). \tag{4.2}$$

This classical description has no mechanism for the inclusion of the exchange forces that are responsible for the enhancement of the dipole sum. This effect may be artificially inserted by replacing the nucleon mass by an effective mass that is somewhat smaller, i.e., $M^* = M/\beta$ where $\beta > 1$. Then eqs (4.1) and (4.2) become:

$$E_0 = \frac{2.08\hbar}{R}\left[\frac{8KNZ\beta}{MA^2}\right]^{1/2}, \tag{4.3}$$

$$\int \sigma\, dE = \frac{2\pi^2 e^2 \hbar}{Mc}(0.86)\frac{NZ\beta}{A}. \tag{4.4}$$

The softness of the nuclear surface tends to increase the nuclear radius, $R = 1.2A^{1/3}$ Fermi, by ≈ 10 percent and perhaps to increase the fraction of the oscillator strength in the lowest mode. There is thus some arbitrariness in the choice of parameters to be used. One selection might be $K = 23$ MeV, $R = 1.2A^{1/3}$, and $\beta = 1.1$. Then

$$E_0 = 80A^{-1/3}\ \text{MeV}. \tag{4.5}$$

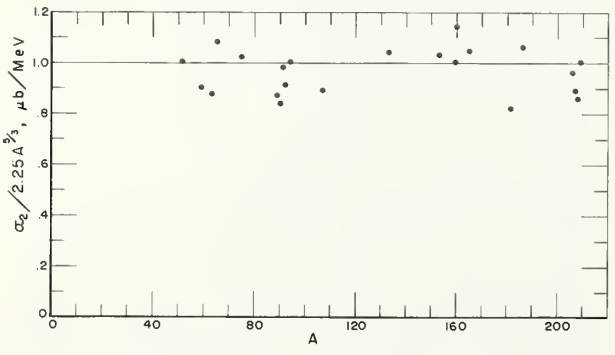

FIGURE 15. *The integral, σ_{-2}, in units of .00225 $A^{5/3}$ as a function of Z.*

The data come from the Livermore neutron yield experiments [43–52].

Using the same model Migdal [3] has shown that the static polarizability of the nuclear ground state is:

$$\epsilon_0 = e^2R^2A/40K. \tag{4.6}$$

The polarizability is proportional to the forward scattering amplitude and is simply

$$\epsilon = \lambda\!\!\!^{-2}R(E, 0) \tag{4.7}$$

In order to obtain the static polarizability we need only consider Re $R(E,0)$, since Im$R(E,0) = 0$ at zero frequency. Taking the limit of Re $R(E,0)$ as the energy approaches zero, we have from eq (2.3):

$$\epsilon_0 = \lim_{E\to 0}\frac{\hbar c}{2\pi^2}\int \frac{\sigma(E')\, dE'}{E'^2 - E^2} = \frac{\hbar c}{2\pi^2}\int \frac{\sigma(E)\, dE}{E^2} \tag{4.8}$$

or

$$\int \frac{\sigma\, dE}{E^2} = \frac{2\pi^2}{\hbar^2}\epsilon_0 = \frac{2\pi^2}{\hbar^2}\frac{e^2R^2A}{40K} = 2.25\ 10^{-6}A^{5/3}\frac{\text{barns}}{\text{MeV}} \tag{4.9}$$

Figure 15 shows a plot of this experimental integral in units of 0.00225 $A^{5/3}$ mb/MeV for the heavy elements that can be described by the hydrodynamic model.

3. Deformed Nuclei

The hydrodynamic model predicts that the giant resonance energy varies inversely as the nuclear radius or as $A^{-1/3}$. A natural consequence of this prediction is that for deformed nuclei having two characteristic dimensions, the giant resonance should be a superposition of two resonances. Most deformed nuclei are prolate ellipsoids. The higher energy resonance corresponding to charge oscillations along the two short axes would then comprise two-thirds of the integrated cross section. The separation of the two resonance energies is a measure of the quadrupole moment of the ground state.

For deformed nuclei, the eigenvalues for excitation for the lowest $E1$ mode differ by only a few percent from the value $KR = 2.08$ obtained for the spherical case. Danos [54] has shown that the connection between the resonance energies, E_a and E_b, and the lengths of the long and short axes a and b, is

$$E_b/E_a = 0.911a/b + 0.089 \tag{4.10}$$

In terms of $d = a/b$ and the mean nuclear radius R, the intrinsic quadrupole moment is:

$$Q_0 = \tfrac{2}{5}R^2ZA^{2/3}\frac{d^2-1}{d^{2/3}} \tag{4.11}$$

Careful measurements of neutron yield cross sections have shown that the giant resonances for the rare earth nuclei do indeed have two maxima and these cross sections can be fit by the sum of two

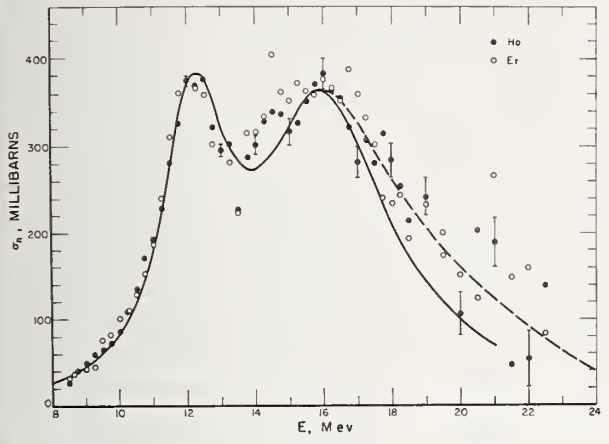

FIGURE 16. *The neutron yield data for holmium and erbium.*

The solid curve is the sum of two Lorentz lines having the parameters $\sigma^0{}_a = 318$ mb, $E_a = 2.2$ MeV, $\Gamma_a = 2.33$ MeV, $\sigma^0{}_b = 328$ mb, $E_b = 16$ MeV, and $\Gamma_b = 4.5$ MeV. The dashed curve is a smooth line drawn through the data. A better fit [56] is obtained with the data if the coupling [66] with the surface vibrations is taken into account.

resonance lines having approximately a 2:1 ratio of areas.

$$\sigma(E) = \sigma_a{}^0 \frac{(E\Gamma_a)^2}{(E_a{}^2 - E^2)^2 + E^2\Gamma_a{}^2} + \sigma_b{}^0 \frac{(E\Gamma_b)^2}{(E_b{}^2 - E^2)^2 + E^2\Gamma_b{}^2} \qquad (4.12)$$

where $\sigma_b{}^0\Gamma_b = 2\sigma_a{}^0\Gamma_a$. As an example figure 16 shows the results of such an analysis for holmium and erbium [55]. The solid curve is the sum of two Lorentz lines having the parameters $\sigma_a{}^0 = 318$ mb, $E_a = 2.2$ MeV, $\Gamma_a = 2.33$ MeV, $\sigma_b{}^0 = 328$ mb, $E_b = 16$ MeV, and $\Gamma_b = 4.5$ MeV. The dashed line is a smooth curve through the data points.

In the region of large nuclear deformation beyond the closed shell at Pb^{208} only the giant resonance of U^{235} has been studied in detail [46]. The total photon absorption cross section was obtained by summing the (γ,n), $(\gamma,2n)$ and (γ,F) cross sections. All were obtained using positron annihilation radiation as a source. The fission cross section was measured in a multipleplate ionization chamber and the neutron-producing cross section with BF_3 counters embedded in paraffin. The (γ,n) and $\gamma,2n)$ cross sections have been obtained from a statistical analysis of the time distribution of the neutron counts relative to the accelerator burst. The result is shown in figure 17. This total cross section has also been fit with the sum of two resonance lines.

In the region of large deformation between the closed shells at O^{16} and Ca^{40}, the hydrodynamic model is certainly not applicable. Nevertheless, the vestiges of the double-humped absorption cross section are still apparent.

The determination of the giant resonance energies for a deformed nucleus is one of the most accurate ways to obtain its intrinsic quadrupole moment. This method measures the intrinsic rather than the spectroscopic quadrupole moment because the measurement takes place in a time determined by the giant resonance width, $\hbar/6$ MeV. This is very small compared to the time required for the nucleus to roll over in the laboratory system, a measure of which is the spacing of the levels in the ground-state rotational band, $\hbar/100$ keV.

Table 7 summarizes the data on the giant resonances of the deformed nuclei. It contains the resonance parameters used to fit the data in the various experiments as well as the intrinsic quadrupole moments, Q_0, derived by means of eq. (4.11).

The experimental results just discussed in no way establish the spatial correlation assumed to exist between the nuclear axes in the intrinsic system. There are two ways to demonstrate this correlation experimentally. The first is to show that the photonuclear cross section depends on the nuclear orientation relative to the direction of the incident photon beam. The second is to demonstrate that the nuclear polarizability is a tensor through the observation of the nuclear Raman effect. Both of these experiments have now been performed.

The yield of photoneutrons from an aligned holmium target has been measured [56] as a function of bremsstrahlung energy and as a function of the angle between the alignment axis and the photon beam direction.

The scattering cross sections from holmium ($I_0 = 7/2$) and erbium (mostly $I_0 = 0$) have been measured with poor energy resolution so that they include all the Raman components. These data are shown in figure 18. The coincidence of the two measured cross sections demonstrates the validity of the sum rule of eq. 2.25. The lower curve is the coherent scattering cross section obtained from the measured absorption cross section (dashed curve of figure 16) through the optical theorem and the dispersion relation. The upper one includes the tensor scattering cross section calculated using the resonance parameters that fit the neutron yield cross section.

The results of the alignment experiment as well as the measurement of the Raman scattering definitely show that the nuclear polarizability is a

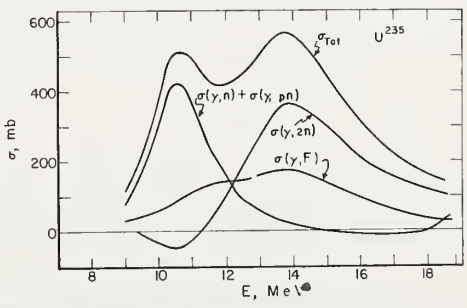

FIGURE 17. *The photon absorption cross section for* U^{235}.

The measured partial cross sections [46] that make up the total are shown. The resonance parameters that fit the data are given in table 7.

TABLE 7. *Giant resonance parameters for deformed nuclei*

Nucleus	E_a MeV	E_b MeV	Γ_a MeV	Γ_b MeV	$\frac{\sigma_b \Gamma_b}{\sigma_a \Gamma_a}$	Q_0 barns	Q_0 (Coul. Ex.) barns	Ref.
Eu^{153}	12.33	15.79	2.75	5.83	3.05	6.8±0.3	7	[52]
Tb^{159}	12.5	16.3	2.4	4.0	2.0	6.8±0.6	6.9	[28]
	12.5	16.4	3.4	3.4	1.19	6.6±0.6		[57]
	12.1	16.0	3.3	4.9	1.77	8.0±0.6		[61]
	12.22	15.67	2.64	4.97	2.3	7.2±0.3		[52]
Gd^{160}	12.23	15.96	2.77	5.28	2.07	7.7±0.3	7.6	[52]
Ho^{165}	12.2	16.0	2.3	4.5	2.0	7.7±0.6	7.8	[58]
	12.1	15.75	2.65	4.4	2.07	7.4±0.9		[44]
	12.1	15.6	2.7	4.8	2.03	7.1±0.6		[61]
	12.28	15.78	2.57	5.0	2.23	7.7±0.3		[52]
Er	12.2	16.0	2.3	4.5	2.0	7.7±0.6		[58]
Ta^{181}	12.5	15.5	2.3	4.4	2.15	6.9±0.3	6.8	[28]
	12.5	15.5	2.3	3.6	2.19	6.9±1.6		[59]
	12.6	15.3	2.0	4.0	1.8	6.1		[60]
	12.75	15.5	3.0	5	1.9	6.7±0.7		[44]
	12.4	15.5	2.4	3.8	1.8	7.1±0.8		[57]
	12.4	15.3	2.6	4.5	2.1	6.8±0.6		[61]
	12.59	15.13	1.94	4.98	3.96	6.4±0.3		[52]
W^{186}	12.59	14.88	2.29	5.18	3.58	6.0±0.2		[52]
U^{235}	10.85	14.1	2.45	4.00		12.8±1.3	~10	[46]

tensor. These experiments also indicate that the absorption cross section has a component that is not associated with the tensor polarizability and is not sensitive to alignment. In the results presented here it is most clearly seen as the difference between the actual data points between 14 and 16 MeV in figure 16 and the sum of the two Lorentz lines used to fit the data.

4. The Dynamic Collective Model

In recent years there has been an enormous flurry of activity that stemmed from the simultaneous recognition by several theorists that the quadrupole oscillation of the nuclear surface could couple with the giant resonance and perhaps produce observable effects. Calculations and estimates of these effects on both the photonuclear absorption and scattering cross sections have been made by Semenko [62, 63], Le Tourneux [64, 65] and Danos and Greiner and their collaborators [66–73]. Their magnitudes depend on the softness of the nuclear surface, the parameters entering the calculations being the transition rates and energies of the low-lying, collective states.

This theory makes use of the adiabatic approximation which assumes that the nucleus changes its shape in a time $\approx \hbar/1$ MeV long compared to the giant resonance oscillation time, $\approx \hbar/15$ MeV.

For the deformed nuclei the coupling of the giant resonance with the oscillations of the nuclear surface has two effects. First the higher energy, $\Delta K = 1$ mode is split in two; i.e., the nucleus acquires a dynamic triaxiality. Secondly, each of the three modes is divided up so that the main line shares approximately 10 percent of the strength with a satellite. The predicted absorption cross sections based on this redistribution of strength is qualitatively very similar to that obtained in the simpler model; perhaps it provides a better fit to the existing data.

The coupling of the giant resonance with the surface vibrations, of course, implies that the giant resonance decays through the low-lying vibrational states that can be reached in dipole-dipole transitions. Consider only even-even nuclei for simplicity. Then the most important such contribution comes from the scattering to the 2^+-state of the γ-vibra-

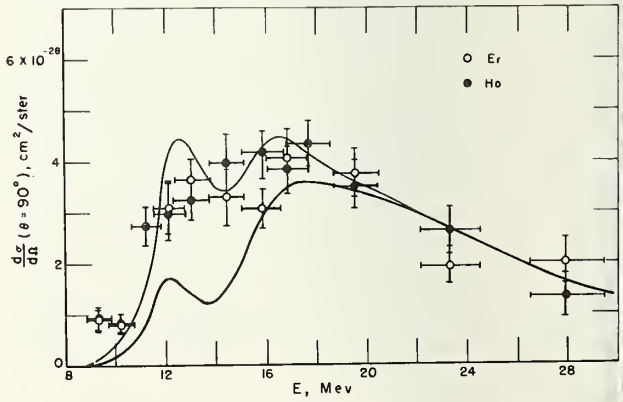

FIGURE 18. *The scattering cross sections for holmium and erbium.*

The lower curve is the coherent scattering cross section calculated from the measured absorption cross section of figure 16. The upper one includes the contribution from Raman scattering calculated from the two-resonance fit to the neutron yield data. The experimental result shows that the total scattering cross section is independent of the spin of the ground state according to the sum rule of eq 2.25.

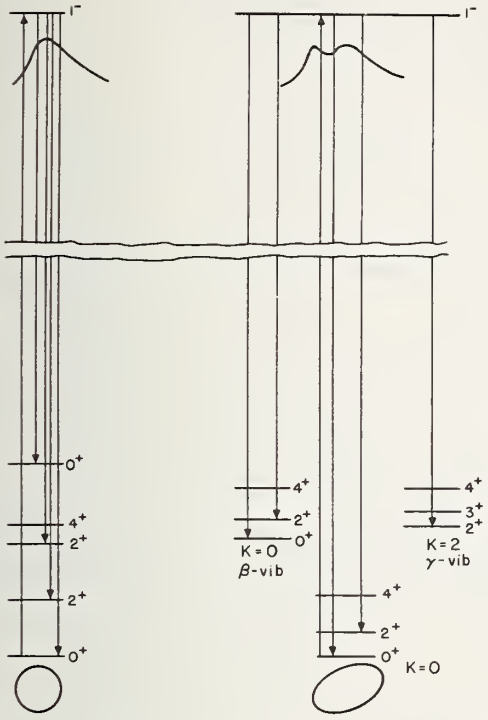

FIGURE 19. *A comparison of the energy level diagrams for even-even, spherical and deformed nuclei.*

tional band. These ideas are illustrated in figure 19. This can be as much as 30 percent of the total scattering cross section. The latter consists of the coherent scattering plus that which populates the ground-state rotational band. Figure 20 shows the scattering cross sections predicted by Arenhövel and Greiner [68] for Er^{166}. The main component is the coherent scattering associated with the absorption cross section; it is augmented on the high energy side owing to constructive interference with nuclear Thomson scattering. Also shown is the cross section for populating the 1st 2^+ state of the ground-states rotational band and the cross section for populating the 2^+ state of the γ-vibrational band ($K=2$). The latter two components are not coherent with the incident radiation and result from two-step scattering processes in which two units of angular momentum are absorbed by the nucleus.

It is worthwhile to point out that the scattering to the 2nd 2^+ state is associated only with the upper ($\Delta K=\pm 1$) resonance. This is required by the selection rule for electric dipole transitions $\Delta K=\pm 1$ since the γ-vibrational band has $K=2$. It might be interesting to demonstrate this in an experiment by injecting monochromatic photons at the energies of the two peaks in the absorption cross section (12 and 16 MeV) and measuring the spectra of the deexcitation γ rays.

The softness of the nuclear surface produces much more dramatic effects on the giant resonances of the spherical vibrational nuclei. These nuclei have a dynamic deformation. The effect of the coupling is

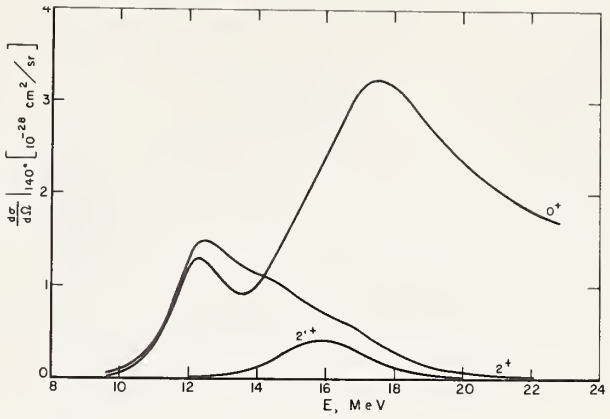

FIGURE 20. *The predicted scattering cross sections [68] for* Er^{166}, *showing the different energy dependence for the coherent scattering cross section, the Raman scattering to the* 2^+ *state of the ground-state, rotational band, and the scattering that populates the* 2^+ *state of the* γ*-vibrational* (K = 2) *band.*

to produce bumps on the giant resonance, the number and amplitude of which depend on the nuclear (lack of) rigidity. The theory of this effect, explored by Le Tourneux and Greiner and his collaborators, is based on the hydrodynamic model and assumes that the surface vibrations are harmonic.

As an illustration the (γ,n) cross section of Pr^{141} is shown [74] in figure 21. It displays a striking amount of structure, a far cry from the single Lorentz line of the simple model. At least part of this structure can be explained by the dynamic collective model. The heights of the vertical lines are proportional to the strengths of the transitions found using the low energy spectrum of the nearby even-even nucleus Nd^{146}. The theory still does not explain the large amount of structured oscillator strength on the rising side of the experimental cross section. This may represent the vestiges of the in-

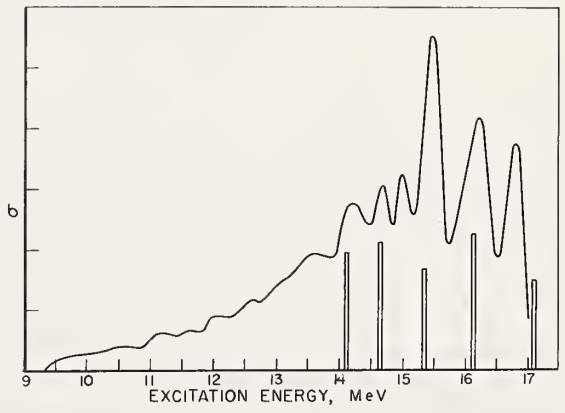

FIGURE 21. *The* (γ, n) *cross section for* Pr^{141}.

The heights of the vertical lines are proportional to transition strengths obtained using the dynamic collective model. The unexplained structure of the rising side of the cross section may result from single particle transitions.

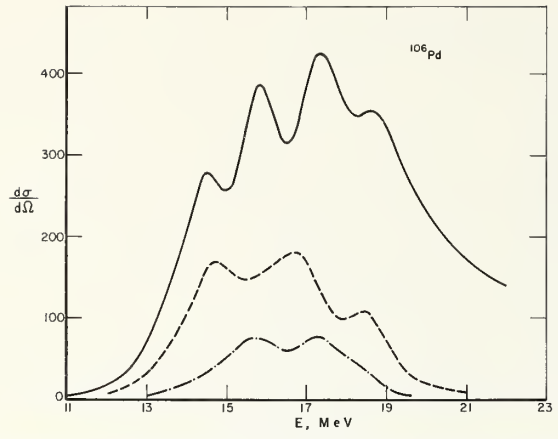

FIGURE 22. *The predicted* [72] *scattering cross sections for* Pd^{106} *showing the coherent scattering cross section and those for transitions to the 1st and 2nd* 2^+ *states.*

dependent particle model transitions that are so important for light nuclei.

Very careful work is required to see the structure demonstrated here. In addition to the difficulties associated with the analysis of bremsstrahlung-induced cross sections there is often a fundamental lack of information concerning how to correct for the emission of two neutrons above the $(\gamma,2n)$ threshold or how to include the $(\gamma,2n)$ cross section if it is not measured. In this instance the data were obtained by measuring the residual radioacitivty so that the $(\gamma,2n)$ cross section is not included.

Figure 22 shows the prediction of Arenhövel and Weber [72] for the different components that make up the scattering cross section for the spherical vibrator, Pd^{106}. The upper curve is the coherent scattering cross section and the two lower ones the cross sections for populating the 1st and 2nd 2^+ states (see also fig. 19).

5. Photon Scattering Experiments

The calculations in the dynamic collective model are so far available for even-even targets which occur in nature only in isotopic mixtures. The experiments, on the other hand, are usually performed using odd-A, monoisotopic targets. The data for the odd target are then compared with the calculations performed for its even-even neighbor, the justification being that the dipole excitations of the core are by far the most important and that the softness of the nuclear surface is a slowly varying function of A. In the following we show that it is also legitimate to make the same comparison for photon scattering cross sections provided the measurement is made with poor energy resolution (NaI(Tl) spectroscopy) such that the transitions to all the final states are recorded. In so doing we assume that the addition of an extra nucleon to the even-even core serves only to produce a multiplicity of states, separated somewhat in energy. These become the final states populated in photon scattering by the odd-A nucleus.

The electric dipole scattering amplitude, A_ν, of eq. (2.12), can be rewritten as:

$$A_\nu=(-1)^{I_0+I_f+\nu}[(2\nu+1)/(2I_0+1)]^{1/2}\times\sum_k\langle I_f\,||\,r\,||\,I_k\rangle\langle I_k\,||\,r\,||\,I_0\rangle F_{\nu k}\times\begin{Bmatrix}I_0 I_f\,\nu\\1\;1\;I_k\end{Bmatrix}+\sqrt{3D}\delta_{\nu 0}\delta_{0f}\quad(4.13)$$

where

$$F_{\nu k}=(e/c)^2\omega^2\left[\frac{1}{E_k-\hbar\omega-\frac{1}{2}i\Gamma_k}+\frac{(-1)^\nu}{E_k+\hbar\omega+\frac{1}{2}i\Gamma_k}\right],$$

and $D=-Z^2e^2/AMc^2$. Here the incoming and outgoing photon energies, $\hbar\omega$, have been set equal; i.e., they are unresolved experimentally. The summation is over all the intermediate states, k, that can be reached in electric dipole transitions. The second term is the nuclear Thomson scattering amplitude.

For an even–even nucleus $I_0=0$, $I_k=1$, $I_f=\nu$, and

$$A_\nu=(2\nu+1)^{1/2}\sum_k\langle\nu\,||\,r\,||\,1\rangle\langle 1\,||\,r\,||\,0\rangle F_{\nu k}\begin{Bmatrix}0\;\nu\;\nu\\1\;1\;1\end{Bmatrix}+\sqrt{3}D\delta_{\nu 0}\delta_{0f}$$

$$=\frac{(-1)^\nu}{\sqrt{3}}\sum_k\langle\nu\,||\,r\,||\,1\rangle\langle 1\,||\,r\,||\,0\rangle F_{\nu k}+\sqrt{3}D\delta_{\nu 0}\delta_{0f}\quad(4.14)$$

The odd-A nucleus is formed by the addition of an exterior nucleon, having spin j, to the even–even core, having collective states I. We assume that the only consequence of adding this single nucleon is that it couples with the states of the core to produce a multiplicity of states, separated somewhat in energy and characterized by the angular momenta, J. The ground-state spin $J_0=j$. The low-lying collective states have the wave functions $|\,Ij;J\rangle$ and the states formed by the electric dipole excitations of the core have the wave functions $|\,I_k j;J_k\rangle$. Neglecting core-particle interactions the reduced electric dipole matrix elements for the odd-A nucleus can be expressed in terms of those for the adjacent even–even nucleus through the use of the projection formula of tensor algebra [75].

$$\langle I_k j;J_k\,||\,r\,||\,I_0 j;J\rangle=(-1)^{I_k+j+J_0+1}\sqrt{(2J_k+1)(2J_0+1)}\times\begin{Bmatrix}J_k\;J_0\;I\\I_0\;I_k\;j\end{Bmatrix}\langle I_k\,||\,r\,||\,I_0\rangle\quad(4.15)$$

Since $I_0=0$ and $I_k=1$, the reduced matrix element connecting the ground-state, $J_0=j$, of the odd-A

system with the dipole states, J_k, is:

$$\langle 1j; J_k \| r \| 0j; j\rangle = (-1)^{2j}\sqrt{(2J_k+1)(2j+1)} \times \begin{Bmatrix} J_k & j & 1 \\ 0 & 1 & j \end{Bmatrix} \langle 1 \| r \| 0\rangle = (-1)^{J_k+3j+1}\sqrt{(2J_k+1)/3} \times \langle 1 \| r \| 0\rangle. \quad (4.16)$$

Similarly, the reduced matrix element connecting J_k with the final state, J_f, is:

$$\langle \nu j; J_f \| r \| 1j; J_k\rangle = (-1)^{\nu+j+J_k+1}\sqrt{(2J_f+1)(2J_k+1)} \times \begin{Bmatrix} J_f & J_k & 1 \\ 1 & \nu & j \end{Bmatrix} \langle \nu \| r \| 1\rangle \quad (4.17)$$

Combining eqs (4.13), (4.16), and (4.17), we obtain for the scattering amplitude of the odd-A nucleus:

$$A_\nu = (-1)^{j+J_f+1}\sqrt{\frac{(2\nu+1)(2J_f+1)}{3(2j+1)}} \times \sum_k \langle \nu \| r \| 1\rangle\langle 1 \| r \| 0\rangle F_{\nu k}(2J_k+1) \times \begin{Bmatrix} J_f & 1 & J_k \\ 1 & j & \nu \end{Bmatrix} \begin{Bmatrix} 1 & 1 & \nu \\ J_f & j & J_k \end{Bmatrix} + \sqrt{3}D\delta_{\nu 0}\delta_{jJ_f} \quad (4.18)$$

Summing over J_k and making use of the orthogonality relation of the $6j$-symbols, we obtain:

$$A_\nu(\text{odd-}A) = (-1)^{j+J_f+1}\sqrt{\frac{(2J_f+1)}{3(2j+1)(2\nu+1)}} \times \sum_k \langle \nu \| r \| 1\rangle\langle 1 \| r \| 0\rangle F_{\nu k} + \sqrt{3}D\delta_{\nu 0}\delta_{jJ_f} \quad (4.19)$$

A comparison of eq (4.14) and eq (4.19) reveals that

$$A_\nu(\text{odd-}A) = (-1)^{j+J_f+\nu+1}\sqrt{\frac{(2J_f+1)}{(2j+1)(2\nu+1)}}\, A\ (\text{even–even}) \quad (4.20)$$

The scattering cross section is proportional to $|A_\nu|^2$. In a poor resolution experiment one would detect the scattered photons without distinguishing between the final states, J_f; one would sum over J_f. And since

$$\sum_{J_f} \frac{(2J_f+1)}{(2\nu+1)(2j+1)} = 1, \quad (4.21)$$

the scattering cross sections for the even–even and odd-A targets are identical in this model. This result permits the comparison of measurements made on an odd-A target with a calculation made for an even nucleus.

It is, of course, important to measure the branching ratios to the various final states throughout the giant resonance. Since the giant resonance absorption cross section is a continuous function of energy, monochromatic photons are required to attack this problem at all. The sources already mentioned, positron annihilation radiation, the bremsstrahlung monochrometer, or the 17.6 MeV radiation from the $Li^7(p, \gamma)$ reaction, are all candidates, provided the energy spread of the source can be made small compared to the differences in the energies of the γ rays being examined. Shimizu [76] has already made an attempt in this direction using the Li γ rays on Ta.

Another approach is not to try to separate the deexcitation γ rays according to their energy, but to separate them according to their angular momentum [77]. This can be done by using a plane polarized photon source such as is obtained by fluorescing the 1^+ state in C^{12} at 15.1 MeV. Fortunately, this energy occurs in the giant resonances of many nuclei. The experiment simply consists in measuring the ratio of the number of $\approx$15 MeV photons scattered in the plane and perpendicular to the plane of the polarization vector, $\boldsymbol{\lambda}$. If we use sodium iodide detectors having poor energy resolution then we are integrating over all the final states and can apply an even-even nucleus theory to an odd-A target.

Rewriting eq (2.9) which gives the scattering cross section in terms of the angular momentum, ν, absorbed by the nucleus in the two-step scattering process, we have

$$\frac{d\sigma}{d\Omega} = \sum_{\nu=0}^{2} \frac{|A_\nu|^2}{2\nu+1} g_\nu(\theta) \quad (4.22)$$

The scattering associated with $\nu = 1$ is unimportant so we need consider only $\nu = 0, 2$.

If $\boldsymbol{\lambda}$ and $\boldsymbol{\mu}$ are the polarization vectors associated with the incoming and outgoing photons, then the factors $g_\nu(\theta)$ are:

$$g_0 = \tfrac{1}{3}(\boldsymbol{\lambda}\cdot\boldsymbol{\mu})^2,$$
$$g_1 = \tfrac{1}{2}[1-(\boldsymbol{\lambda}\cdot\boldsymbol{\mu})^2],$$
$$g_2 = \tfrac{1}{2}[1+\tfrac{1}{3}(\boldsymbol{\lambda}\cdot\boldsymbol{\mu})^2]. \quad (4.23)$$

If we have plane polarized incident radiation with λ perpendicular to the plane of scattering,

$$g_0^{\perp} = \tfrac{1}{3} \quad (4.24)$$

For λ in the plane of scattering,

$$g_0^{\parallel} = \tfrac{1}{3}\cos^2\theta \quad (4.25)$$

The average is the familiar distribution for unpolarized radiation:

$$g_0 = \tfrac{1}{6}(1+\cos^2\theta) \quad (4.26)$$

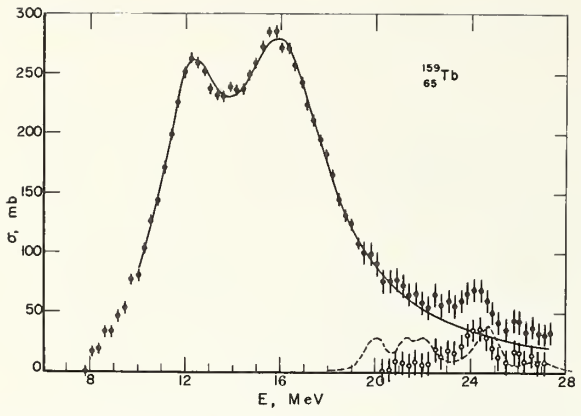

FIGURE 23. *The sum of the cross sections* [61] (γ, n), (γ, 2n) *and* (γ, 3n) *for* Tb^{159}.

The smooth curve is the sum of two Lorentz lines that fit the data. This curve has been subtracted from the data for energies above 20 MeV. These data are then compared with the predicted [78] E2 cross section.

Similarly,

$$g_2^{\perp}=\tfrac{7}{6},$$

$$g_2^{\parallel}=1+\tfrac{1}{6}\cos^2\theta, \text{ and}$$

$$g_2=\tfrac{1}{12}(13+\cos^2\theta). \tag{4.27}$$

The total scattering cross section is:

$$\frac{d\sigma}{d\Omega}=|A_0|^2 g_0+\frac{|A_2|^2 g_2}{5} \tag{4.28}$$

For plane polarized incident radiation,

$$\frac{d\sigma^{\perp}}{d\Omega}=\frac{|A_0|^2}{3}+\frac{7|A_2|^2}{30} \tag{4.29}$$

$$\frac{d\sigma^{\parallel}}{d\Omega}=\frac{|A_0|^2\cos^2\theta}{3}+\frac{|A_2|^2}{5}(1+\tfrac{1}{6}\cos^2\theta). \tag{4.30}$$

At $\theta=\pi$, the latter becomes

$$\frac{d\sigma^{\parallel}}{d\Omega}\left(\frac{\pi}{2}\right)=\frac{|A_2|^2}{5}. \tag{4.31}$$

Thus a measurement of the 90° scattering cross sections using photons polarized perpendicular and parallel to the plane of scattering yields the relative intensities of the scalar ($\nu=0$) and tensor ($\nu=2$) components. Unfortunately, there are very few potential sources of plane polarized radiation. Besides the carbon line, the level in Si^{28} at 11.4 MeV is the most promising.

6. The E2 Giant Resonance

In a further treatment Ligensa et al. [78] have extended the quantum hydrodynamics of deformed nuclei to quadrupole multipolarity. This theory includes rotations, β and γ vibrations, the odd particle, giant dipole phonons, and giant quadrupole phonons and yields for the giant quadrupole absorption cross section:

$$\sigma(E)=\frac{2\pi}{5}\frac{NZ}{A}\frac{e^2}{\hbar c}\frac{R^2}{Mc^2}$$

$$\times(1+\alpha)\sum_k \frac{E_k^2 f_k/\Gamma_k}{[(E^2-E_k^2)/E\Gamma_k]^2+1} \tag{4.32}$$

where

$$f_k=\frac{2\pi}{3}\frac{A}{NZ}\frac{2M}{\hbar^2}\frac{E_k}{5(2I_0+1)}\frac{|\langle k\,||\,Q\,||\,0\rangle|^2}{R^2(1+\alpha)}$$

are the quadrupole strengths and Q is the quadrupole operator.

There are five main $E2$ giant resonances. The surface oscillations cause some of the modes to split. The parameters in the problem are fixed by the position of the lower giant dipole peak and the low energy spectrum of the nucleus with no free parameters.

Figure 23 compares the prediction for Tb^{159} with the results of Begère et al. [61]. The smooth curve is the sum of two Lorentz lines that fit the data. This has been subtracted from the data points of energies in excess of 20 MeV to obtain the experimental $E2$ cross section. The latter resembles remarkably well the theoretical curve shown dotted.

V. Light Nuclei and the Independent Particle Model

1. Survey of Experimental Data

The data for the nuclei with $A<40$ can be contrasted with those for the nuclei with $A>100$ already presented. We assume that nature knows how to make a smooth transition between the two. For the light nuclei the (γ, n) and (γ, p) cross sections are of comparable magnitude in the energy region of the giant resonance. The total absorption cross section can be obtained directly or by summing the separately measured (γ, n) and (γ, p) cross sections. When this is done, it is found that the total absorption cross section integrated to 30 MeV may contain as little as 50 percent of a dipole sum.

Since the electric dipole sum rule is a conservation law that sets a lower limit on the integrated absorption cross section, it is necessary to look elsewhere for the remainder of the dipole strength. An important contribution can be found in the quasideuteron cross section which is important at high energies and results from the high momentum components in the nuclear ground state which are associated with strong two-body forces.

A selection of data on the integrated partial cross section is given in table 8. The second and third columns contain the separately measured (γ, n) and (γ, p) cross sections and the fourth column their sum. The fifth column contains the integral of the total absorption cross section measured at the Lebedev Institute and the sixth those measured at NBS [25].

The giant resonances for the light nuclei between carbon and calcium are all located near 20 MeV; there is apparently no systematic dependence on A. The width of these giant resonances increases in the middle of the $s-d$ shell where the nuclei are known to be deformed:

The giant resonances of the light nuclei display different kinds of structure. If it is fair to make any generalization at all, we might say that the nuclei in the 1s shell have perfectly smooth giant resonances owing to their low level densities and general simplicity; the nuclei in the $1p$ shell have giant resonances usually consisting of several peaks about 1 MeV wide suggestive of single particle transitions; in the $2s-1d$ shell the giant resonances retain the ≈ 1 MeV structure, the latter being fractured into many sharp states.

2. The Independent Particle Model

The independent particle model description of the nuclear photo-effect has been emphasized by Wilkinson [92, 93] and is quite fundamental to many calculations currently in vogue. In this formulation the giant resonance was ascribed to the electric dipole absorption of photons by the valence nucleons and those in the uppermost filled shell. These particles make transitions upward to the next unfilled shell of opposite parity according to the selection rule $\Delta l = \pm 1$. The transition energies are all nearly the same and are thus grouped together to form the giant resonance. Furthermore, their summed oscillator strength is just equal to the dipole sum.

Let us consider the simplest case in which we have pure shell-model states and for convenience introduce a harmonic oscillator potential. Then the electric dipole transition probability for a single particle to

TABLE 8. *Integrated cross sections for light nuclei in units of* $(2\pi^2e^2\hbar/\mathrm{Mc})\times(\mathrm{NZ/A})$

The exponents represent the upper limits of the integration in MeV.

	(γ, n)	(γ, p)	$\sum$	σ_T Leb	σ_T NBS	$\frac{\gamma, p}{\gamma, n}$	Reference
Li	0.47^{30}	0.14^{30}	0.61^{30}	----------	----------	----------	[79, 80]
C	$.22^{28}$	.29	.51	0.78^{30}	0.63^{30}	1.3	[81, 32]
O	$.19^{31}$	$.37^{40}$	$.56^{36}$	$.71^{30}$	$.62^{30}$	1.95	[82, 83, 84]
Mg	$.23^{29}$	$.50^{32}$	$.73^{30}$	1.02	$.65^{30}$	2.2	[81, 85, 86]
Si	$.19^{28}$	$.68^{28}$	$.87^{28}$	----------	$.78^{30}$	3.6	[87, 88]
P	$.27^{28}$	$.75^{32}$	1.02^{30}	----------	----------	----------	[89, 85]
S	$.17^{28}$	$.77^{32}$	0.95^{30}	1.19^{30}	$.83^{30}$	5.2	[89, 85]
Ca	$.12^{28}$	$.73^{28}$	$.85^{28}$	1.54^{30}	$.73^{30}$	6.1	[91, 88, 90]

TABLE 9. *Radial integrals for the harmonic oscillator*

Transition	$\int dr\, r^3 R_{1\ell} R_{2\ell'}$
$1s \rightarrow 1p$	$1/\alpha\sqrt{3/2}$
$1p \rightarrow 1d$	$1/\alpha\sqrt{5/2}$
$1p \rightarrow 2s$	$1/\alpha$
$1d \rightarrow 1f$	$1/\alpha\sqrt{7/2}$
$1d \rightarrow 2p$	$-1/\alpha$
$2s \rightarrow 2p$	$-1/\alpha\sqrt{5/2}$

proceed from state 1 to state 2 is:

$$D^2 = q^2 \left| \int \psi_2^* z \psi_1 \, dr \right|^2 \tag{5.1}$$

where q is the effective charge, Ne/A for protons and $-Ze/A$ for neutrons. The radial and angular parts of the matrix element may be separated by replacing z by $\sqrt{4\pi/3}\, rY_{10}$, then:

$$D^2 = \left(\frac{4\pi}{3}\right) q^2 \sum_m \langle j_2 m_2 \mid Y_{10} \mid j_1 m_1 \rangle^2 \left| \int dr\, r^3 R_1 R_2 \right|^2 \tag{5.2}$$

where $j = \ell \pm \frac{1}{2}$.

We can dispose of the dependence on m by making use of the Wigner-Eckart theorem and summing the Clebsch-Gordan coefficients:

$$D^2 = \left(\frac{4\pi}{3}\right) q^2 \sum_{m_2} (j_1 m_1 10 \mid j_2 m_2)^2 \times \frac{\langle j_2 \| Y_1 \| j_1 \rangle^2}{2j_2+1} \left| \int dr\, r^3 R_1 R_2 \right|^2$$

$$= \frac{4\pi}{3} q^2 \frac{\langle j_2 \| Y_1 \| j_1 \rangle^2}{3} \left| \int dr\, r^3 R_1 R_2 \right|^2 \tag{5.3}$$

Making use of the relationship [94]:

$$\langle j_2 \| Y_1 \| j_1 \rangle^2 = (2j_1+1)(j_1 \tfrac{1}{2} 10 \mid j_2 \tfrac{1}{2})^2 (3/4\pi), \tag{5.4}$$

we have the fairly simple expression:

$$D^2 = \frac{q^2}{3} (2j_1+1)(j_1 \tfrac{1}{2} 10 \mid j_2 \tfrac{1}{2}) \left| \int dr\, r^3 R_1 R_2 \right|^2 \tag{5.5}$$

The radial functions, R_1 and R_2, depend of course on the nuclear potential. Those associated with the harmonic oscillator are very frequently used since they can be expressed analytically. For the first two shells they are [95]:

$$R_{1\ell} = \frac{\alpha^{3/2}}{\pi^{1/4}} \left[\frac{2^{\ell+2}}{(2\ell+1)!!} \right]^{1/2} (\alpha r)^\ell e^{-1/2(\alpha r)^2} \tag{5.6}$$

$$R_{2\ell} = \frac{\alpha^{3/2}}{\pi^{1/4}} \left[\frac{2^{\ell+3}}{(2\ell+3)!!} \right]^{1/2} (\alpha r)^\ell \left[\frac{2\ell+3}{2} - (\alpha r)^2 \right] e^{-1/2(\alpha r)^2}: \tag{5.7}$$

where ℓ is the orbital angular momentum of the nucleon and $\alpha = [M\omega_0/\hbar]^{1/2}$. The values of the integrals,

$$\int dr\, r^3 R_{1\ell} R_{2\ell'}, \tag{5.8}$$

are given in table 9 for the electric dipole transitions from the $1s$, $1p$, $1d$, and $2s$ shells. These are the elementary transitions that must be included for the elements up to Ca^{40}.

The nucleus, O^{16}, has received more attention than any other from both the theorists and experimentalists. The structure is simple enough to be tractable. In the independent particle model its electric dipole absorption cross section consists of the five transitions from the filled p-shell to the $2s$ and $1d$ shells (see fig. 24). These are listed in table 10 along with the transition probabilities, D^2, evaluated by means of eq (5.5). The radial integrals of table 9 have been used. For the harmonic oscillator, of course, all the transitions take place at the energy $\hbar\omega_0 = 41A^{-1/3}$ MeV, 15 MeV in O^{16}.

The electric dipole absorption cross section integrated over all the transitions yields the unenhanced dipole sum. For a single transition at energy E_k the integrated absorption cross section is:

$$\int \sigma_k \, dE = \frac{4\pi^2 E_k}{\hbar c} D_k^2 \tag{5.9}$$

By summing the transition probabilities, D_k^2, such as those given in table 10, it is straightforward to show for simple nuclei that:

$$\sum_k D_k^2 = \frac{e^2}{2} \frac{NZ}{A} \frac{\hbar}{M\omega_0} \tag{5.10}$$

In so doing it is necessary to weight the transitions from partially-filled shells by the ratio of the number

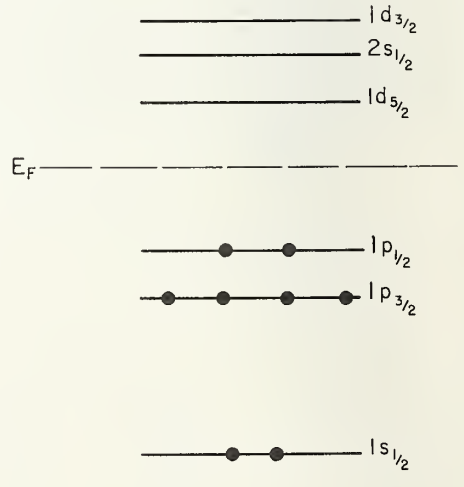

FIGURE 24. *Shell-model levels for* O^{16}.

Table 10. *Transitions in* O^{16}

Transition	$3D^2/q^2$	$D^2(\%)$	E(MeV)	E'(MeV)	$D'^2(\%)$	F
$1p_{3/2}\rightarrow 2s_{1/2}$	4/3	11	18.53	19.6	2	0.951
$1p_{3/2}\rightarrow 1d_{5/2}$	6	50	17.65	22.2	73	.898
$1p_{1/2}\rightarrow 1d_{3/2}$	10/3	28	16.58	18.1	1	.903
$1p_{1/2}\rightarrow 2s_{1/2}$	2/3	5.5	12.38	13.5	4	.996
$1p_{3/2}\rightarrow 1d_{3/2}$	2/3	5.5	22.73	25.2	20	.963

of particles, n, to the number of nucleons the shell can contain, $(2j_1+1)$. Since eq (5.5) represents the transition probability from a filled shell, that from a partially filled shell would be

$$D^2 = nq^2/3(j_1\tfrac{1}{2}10 \mid j_2\tfrac{1}{2})^2 \left| \int dr\, r^3 R_1 R_2 \right|^2 \qquad (5.11)$$

The integrated absorption cross section is then:

$$\int \sigma\, dE = \frac{2\pi^2 e^2 \hbar}{Mc} \frac{NZ}{A} \qquad (5.12)$$

More realistic choices for the nuclear potential alter the radial integrals and change the transition energies, E_k, by splitting the basic shell-model states into their various components. The effect of the spin-orbit force, for example, is to remove the degeneracy between the two possible j-values for a given ℓ, i.e., $=\ell\pm\frac{1}{2}$.

In the extreme, when we consider nuclei having large intrinsic deformations, each value of j is further split into components labelled by the quantum number Ω, the projection of j on the nuclear symmetry axis. Here the transition strength is divided up among the many single-particle transitions that can occur, and for electric dipole transitions we have the additional selection rule $\Delta K = 0, \pm 1$ (K is the projection of I_0 on the nuclear symmetry axis). The transition energies then fall quite naturally into two groups, corresponding to $\Delta K = 0$ and $\Delta K = \pm 1$. These may be associated with particle motion along and perpendicular to the symmetry axis. In fact, Wilkinson [96] has used the Nilsson wave functions to predict the giant resonance shapes for the rare earth nuclei and obtained results quite analogous to those already presented in the hydrodynamic model.

The independent particle description of the nuclear photoeffect as outlined above has a very important qualitative shortcoming, namely that it gives the giant resonance energy as essentially $41A^{-1/3}$ MeV, the harmonic oscillator spacing. We have already seen that the expression, $E_0 = 80A^{-1/3}$, applies well to the heavy elements, and the light elements all have their giant resonances near 20 MeV. The latter is still appreciably higher than the oscillator spacing.

3. The Particle-Hole Model and Its Extensions

The particle-hole calculations, introduced by Elliott and Flowers [97] and pursued by Brown and his followers, made substantial improvements in the situation. These improvements take place in two independent steps. The first is to take for the basic transition energies not the harmonic oscillator spacing but energies based on experimentally observed spectra. The states that make up the giant resonance differ from the ground state in that one particle has been elevated to the next open shell of opposite parity. The energy of such a state is given by the sum of the hole energy and the particle energy. When considering nucleus A, the energies of the hole states manifest themselves in the levels of nucleus $A-1$, the energies of the particle states in those of nucleus $A+1$. These states can usually be identified by their spins and parities. In this way the harmonic oscillator energies are replaced by those prescribed by nature. They are not exactly right because the hole-core interactions in the $(A-1)$-particle system and the particle-core interactions of the $(A+1)$-particle system are not precisely the same as those in the A-particle system. Nevertheless, the single particle energies obtained in this way are (for light elements) several MeV greater than the oscillator spacing and a much closer approximation to the true transition energies. The second step is to take into account the particle-hole interaction by diagonalizing the matrix elements for all of the elementary transitions with an appropriate force. In this process the amplitudes of the basic transitions add coherently in such a way that nearly all of the dipole strength is concentrated in one or two transitions which are those most elevated in energy.

Returning once more to the example of O^{16}, the elementary, unperturbed transition energies are taken from the known energy levels of O^{15} and O^{17}. These are illustrated in figure 25 and the transition energies tabulated in table 10. At this stage it was assumed that there is complete charge symmetry and that the proton transition energies are the same as those for neutrons. The transition probabilities for the unperturbed situation are those given by eq (5.5) and evaluated for O^{16} in table 10.

Several different particle-hole calculations [97–101] have been performed for O^{16} and they show that the position and strength of the electric dipole states are not critical to the choice of interaction. In all cases most of the dipole strength becomes concentrated in two states that have been pushed up in energy to 22 and 25 MeV. Gillet's transition energies and relative transition probability, D'^2, are given in table 10 for his approximation II which includes some ground-state correlations.

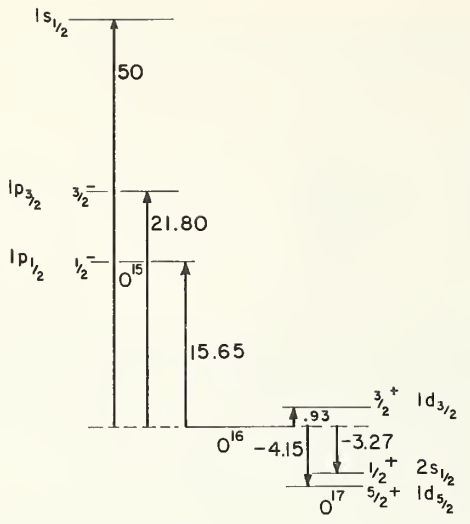

FIGURE 25. *The energy levels in* O^{15} *and* O^{17} *from which the unperturbed transition energies are obtained.*

Each of the dipole states is a mixture of the five basic shell model transitions. Nevertheless, each one consists primarily of the one indicated in the first column in table 10. The final column gives the fraction, F, of the amplitude resulting from this basic transition. Notice that the two important transitions are primarily of the $p \rightarrow d$ type and that the less intense is the one in which the nucleon spin is flipped. In general, the most important shell-model transition is the one involving the largest angular momentum. After diagonalization this transition collects an even greater fraction of the transition strength and locates it at a higher energy.

It has already been pointed out that for the harmonic oscillator all of the transitions take place at the same energy and that the sum $\sum E_k D_k^2$ has its classical value. In the particle-hole calculations the degeneracy in the E_k is removed. If correlations in the nuclear ground-state are neglected, $\sum D_k^2$ is the same both before and after the diagonalization process and one is led to the inconsistency that $\sum E_k D_k^2$ exceeds the classical dipole sum even for forces that commute with the dipole operator.

This difficulty stems from an inconsistency in the calculations as they are performed. The single-particle transition energies are closely related to the true nuclear Hamiltonian yet the transition matrix elements used, D_k, are those appropriate to the harmonic oscillator. The strong two-body forces which spread the nuclear energy levels also modify the ground-state wave function in such a way that the matrix elements are decreased. The inclusion of ground-state correlations, as has been done by Gillet and others, represents an attempt to alter these wave functions appropriately. Drastic changes will, however, be required to decrease the predicted summed oscillator strength, $\sum E_k D_k^2$, for the light elements to the point where the experimentally observed magnitude of approximately one-half the dipole sum is obtained.

Even though the particle-hole calculations succee in placing the electric dipole oscillator strength at it experimentally observed energy, it fails in severa respects because of omissions from the theory. Firs the calculations assume (and therefore predict) tha all of the electric dipole oscillator strength is in th giant resonance. Neglected are the important tw body correlations that rob the giant resonance of a least half of its strength and place it at higher energie Secondly, the $2p-2h$, $3p-3h$ etc. excitations ar usually neglected; these can produce structure in th cross sections. Thirdly, the nuclear ground state not the pure Hartree-Fock state; it contains co relations which can influence the mode of deca and some of which look like a deformation. Finall most calculations treat the neutrons and proto as though they are the same and therefore they d not include the effect of the Coulomb interactio

The theories [102–104] have now developed i such a way that the neutron and proton excitatio are considered separately and their continua ar treated more or less correctly. Though these calcul tions certainly involve vastly different technique they should all yield the same result. As an examp we show the result of Raynal, Melkanoff and Sawad [102], the dashed curve of figure 26a. They hav used a real realistic Saxon-Woods potential and th widths of the states emerge as a result of the of diagonal two-body matrix elements. The exper mental data shown in the lower plot are from th

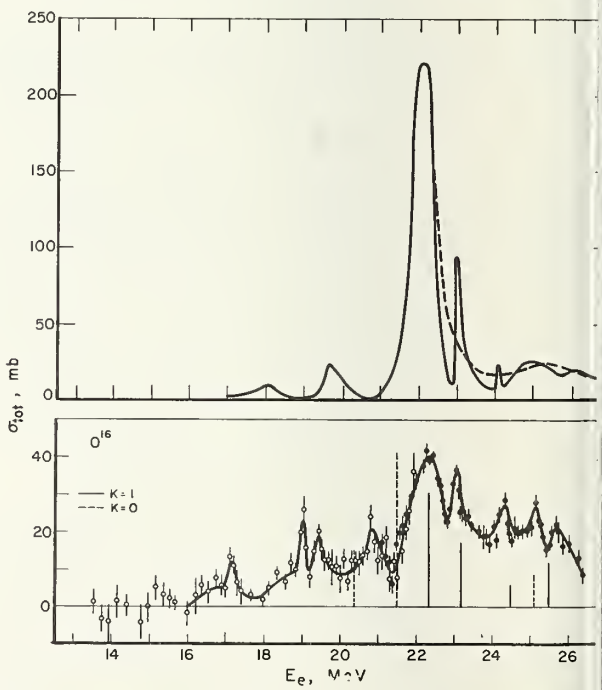

FIGURE 26. *The upper dashed curve is the result of the continuu calculation of reference 102.*

The solid curve is the result [111] of including the interference with t $2p-2h$ quasibound states listed in table 11 as well as the $4p-4h$ states 21.05 MeV. The lower curve shows the experimental total absorption cr section [84] as well as the result of Kluge [105] who assumed the O^{16} grou state to have a slight positive deformation.

total absorption experiment [84] done at the Lebedev Institute. The details of this experimental cross section are, after all, what the theories are trying to emulate; its magnitude is just a little too large, however, to be consistent with other measurements (see table 8). A comparison of the dashed curve with the experimental result shows that the theoretical cross section magnitude is too big and that the experimental data show much more structure.

These structures in the experimental cross section have been explained in part by two apparently different ideas, both suggested by experiment. First, Kluge [105] has taken the ground state of O^{16} to have a slight ($\approx 10\%$) positive deformation. This means that the 6 MeV 0^+ state, which supports a rotation band, is partly mixed into the ground state. His result is reproduced in figure 26b where the positions of the $K=0$ and $K=1$ transitions are indicated with heights proportional to their intensities.

The hypothesis of Kluge is bolstered by the experimental fact that the giant resonance state does not decay exclusively through the $\frac{1}{2}^-$ and $\frac{3}{2}^-$ ground and third excited states of O^{15} and N^{15}. Approximately 7 percent of the time it decays through the $\frac{1}{2}^+$ and $\frac{5}{2}^+$ first and second excited states in these nuclei [106–110]. In all the theories, based on the simple model described above, O^{16} emits only s and d-wave particles. In order to emit p-wave particles and populate the positive parity states, the O^{16} ground state must be contaminated by more complicated configurations.

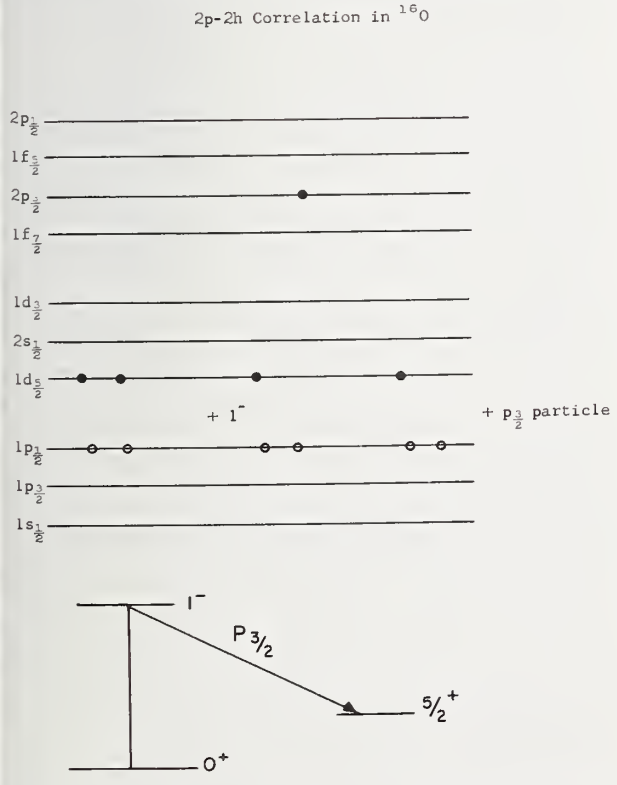

FIGURE 27. *This diagram illustrates how a* 2p−2h *fluctuation in the* O^{16} *ground state on interacting with an electric dipole photon can leave the residual nucleus in its* $5/2^+$ *state.*

This ground state is momentarily deformed.

As an example, we now show how a simple 2 particle-2 hole correlation in the O^{16} ground state permits the $\frac{5}{2}^+$ state to be populated and at the same time look like a deformation. Since the nuclei in the middle of the $s-d$ shell have large intrinsic deformations, a ground-state correlation in O^{16} that resembles a deformation is one in which two particles are promoted from the $1p_{1/2}$ to the $1d_{5/2}$ shells leaving the ground state with 0^+. When the electric dipole photon interacts with this system it can promote one of the nucleons momentarily situated in the $1d_{5/2}$ orbit to the $2p_{3/2}$ shell. The latter then emerges leaving the residual nucleus in its $\frac{5}{2}^+$ state (see fig. 27). An analogous scheme exists for populating the $\frac{1}{2}^+$ state. It is straightforward to concoct more elaborate fluctuations involving $3p-3h$, $4p-4h$, etc. which surely exist in nature.

Gillet, Melkanoff, and Raynal [111] have noticed, on the other hand, that at least two of the minima in the O^{16} absorption cross section occur at just the energies where there are peaks in the N^{14} (d, γ_0) O^{16} and C^{12} (α, γ_0) O^{16} cross sections [112, 113]. In both cases the angular distribution of the outgoing γ-ray labels the excited state as 1^-. Because these states are excited by deuterons and alpha particles they must have $T=0$ unlike the main giant resonance which has $T=1$; furthermore they must represent $2p-2h$ and $4p-4h$ configurations respectively. The dominant 22 MeV state is then broken into three parts by destructive interference with the $4p-4h$, $T=0$ state at 21.05 MeV and the $2p-2h$, $T=0$ state at 22.7 MeV. Gillet et al. point out that there are, in fact, exactly four $2p-2h$ quasi-bound states in the energy region of the giant resonance. These are made by coupling two $1p-1h$ states to $T=1$ and 1^-. This requires one ph state to be $T=0$ with positive parity and the other $T=1$ with negative parity. Table 11 lists the four possible $2p-2h$ quasi-bound states and their excitation energies. There is a remarkable correspondence between these energies and the dips in the cross section of Dolbilkin et al. [84] (see fig. 26).

TABLE 11. *The* 2p2h *quasi-bound states in* O^{16}

$T=0$, + parity	$T=1$, − parity	Energy (MeV)
0^+	1^-	23.0
2^+	1^-	26.0
2^+	2^-	24.2
2^+	3^-	23.9

4. Caldwell's Experiment

Using the annihilation radiation as a source Caldwell [110] has measured the cross sections for the

TABLE 12. *Integrated cross sections* [110] *for* O^{16} *photoreactions*

Reaction	Final state (MeV)	$\int_{Th}^{28.6} \sigma dE$(MeV-mb)	Fractional $\int_{Th}^{2.87} \sigma dE$
(γ, p)	Ground state	34.42	0.287
	5.3 (1, 2^+, 5, 2^+)	[a]4.94	.041
	6.33 (3, 2^-)	22.30	.185
	7.30 (3, 2^+)	5.47	.047
	9.1	2.03	.017
	9.22	1.50	.013
	9.9	2.36	.020
	10.8	[b]2.34	.020
(γ, n)	Ground state	26.67	.223
	5.2(1, 2^+, 5, 2^+)	3.49	.029
	6.18 (3, 2^-)	9.43	.079
	6.79 (3, 2^+)	4.50	.038
(γ, α)	15.11 (1^+, $T=1$)	0.23	.002

[a] The 9.22 MeV cascade transition cross section has been subtracted from the 5.3 (1, 2^+, 5, 2^+) values.

[b] Observed 10.8 MeV yields multiplied by $\frac{\Gamma_{tot}}{\Gamma_{\gamma 0}} = 3.0 \pm 0.5$ from Ref. 114.

photodisintegration of O^{16} leaving O^{15} in its ground state and three excited states and N^{15} in seven excited states. This was accomplished by embedding NaI(Tl) detectors in the 4π neutron detector and measuring photon spectra in coincidence with neutrons and in anticoincidence with neutrons (to obtain the (γ, p) partial cross sections). Using the ground-state cross section obtained by others [42, 34], the total photonuclear cross section has been constructed and found to agree with the total absorption cross section of Wyckoff et al. (see fig. 28). Caldwell's integrated partial cross sections are listed in table 12.

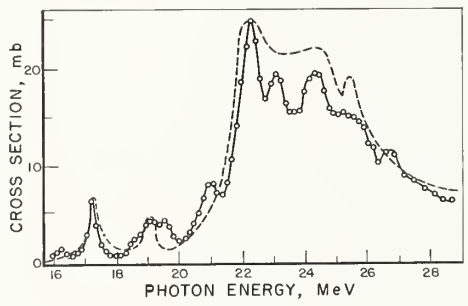

FIGURE 28. *The total photonuclear cross section for* O^{16} *as synthesized by Caldwell* [110] *compared with the directly measured cross section (dashed curve) of reference* [25].

Caldwell's resulting partial cross sections are compared with the predictions of the calculation of Buck and Hill [103]. The latter is one of a number of rather sophisticated treatments of the O^{16} problem that take into account the continuum and recognize the difference between neutrons and protons. The calculation succeeds, really for the first time, in obtaining some correct cross section magnitudes and the gross shape of all the partial cross sections. The theory, however, overestimates by 40 percent the magnitude of the decay through the $\frac{3}{2}^-$ states. Part of this strength is siphoned off through the positive parity states and the rest is located above 30 MeV; neither of these possibilities are, of course, included in the theory.

Using his experimental data and the penetrability factors given by Buck and Hill, Caldwell has estimated the amplitude of the $T=0$ contamination of the $T=1$ giant resonance to be ≈ 0.08.

VI. The Decay of the Dipole State

1. Introduction

We have just seen that the nuclear absorption of x rays in the giant resonance region takes place through the excitation of a single particle. The excited nucleons may emerge directly without further interaction, and under these circumstances their energy and angular distributions reflect the absorption process. Alternatively the excited nucleon may undergo one, two, or many interactions before it escapes the nuclear surface. In this way it loses all memory of the absorption process.

In light nuclei ($A \leq 40$) the nucleon emerges with only a few interactions. For heavier nuclei evaporation is the dominant decay mode. At Ca^{40} the $1d_{3/2}$ shell is filled for both neutrons and protons. New nuclei are built by filling the higher angular momentum f and g shells. When these nucleons are excited by giant resonance photons, they are unable to penetrate the angular momentum barrier and hence remain in the nucleus making collisions and sharing their energy with the other nuclear particles. Eventually sufficient energy is concentrated on a neutron having low angular momentum and it is evaporated from the nucleus; protons belonging to this distribution have insufficient energy to surmount the Coulomb barrier. As a result, neutron emission becomes the dominant mode of decay, and for heavy nuclei photon absorption results almost exclusively in neutron emission. How the transition is made between the dominance of direct emission for $A < 40$ to that of the evaporation process for $A > 100$ has not yet been established in detail.

The relative magnitudes of the (γ, p) and (γ, n) cross sections for the nuclei in these two extreme ranges of atomic number provide an interesting contrast. For the special case of the self-conjugate nuclei nature has conspired to make the neutron and proton escape probabilities equal by adjusting the depth of the nuclear potential felt by the protons to compensate almost exactly for the Coulomb barrier. The proton binding energies are thus lower than those for neutrons. The (γ, n) and (γ, p) cross sections for these nuclei should therefore be identical in both magnitude and shape. The experimental fact is that the ratio $\int \sigma(\gamma, p)\, dE / \int \sigma(\gamma, n)\, dE$ increases from one for He^4 to about six for Ca^{40} (see fig. 29). This rather striking effect must result from the mixing of states of different isotopic spin both in the ground and excited states.

For heavy nuclei, on the other hand, the (γ, p) cross sections are almost insignificant and are located near 25 MeV, an energy where both $E1$ and $E2$ absorption participate. The protons are emitted with high energies in direct interactions. As an illustration figure 30 shows a comparison of the (γ, n) and (γ, p) cross sections [115] for Pd^{103}.

2. Energy Spectra

The evaporation of neutrons from heavy nuclei produces a spectrum that is predicted by the statistical model and may be approximated by an expression of the form

$$E_n e^{-E_n/T}$$

where E_n is the neutron energy and T the nuclear temperature. The evaporated neutrons proceed through many overlapping energy levels and have essentially isotropic angular distributions. Except for information concerning the nuclear temperature these distributions contain no information and are therefore uninteresting.

Direct emission results from most interactions in light nuclei and from a small fraction in heavy nuclei. These produce particle groups that come from the highly excited giant resonance states and populate the ground or excited states of the residual nucleus. The energies of these groups are:

$$\hbar\omega - T - E_h$$

where $\hbar\omega$ is the absorbed photon energy, T is the binding energy and E_h is the excitation energy of the hole.

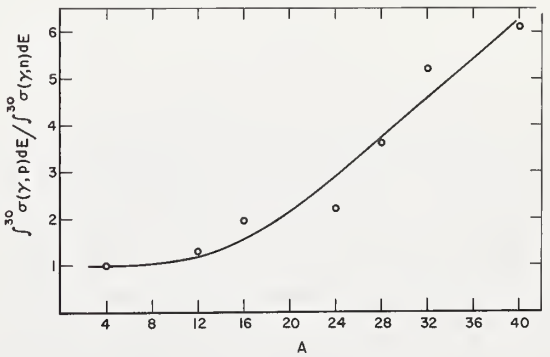

FIGURE 29. *The ratio* $\int^{30} \sigma(\gamma, \mathrm{p})\mathrm{dE} / \int^{30} \sigma(\gamma, \mathrm{n})\mathrm{dE}$ *up to* Ca^{40}.

These data come from table 8.

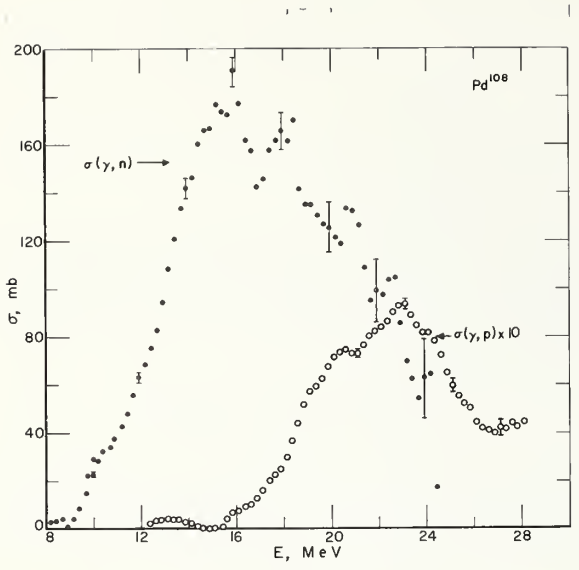

FIGURE 30. *A comparison* [115] *of the neutron producing cross sections of* Pd^{108} *with its* (γ, p) *cross section.*

3. Angular Distribution Formulae

The spins and parities of the final states as well as the composition of the excited states can be studied by investigating the angular distributions of the outgoing nucleons. The dependence of the angular distributions on various angular momentum parameters for transitions through isolated intermediate states of specified spin and parity has been exhaustively treated in the reviews [116, 117] on angular correlations. Here we will cite those formulae which may pertain to the photoeffect with particular emphasis on electric dipole transitions.

In angular correlations the transition is regarded as a two-step process through the intermediate state, I_k, each link being described by its own independent factor, A_ν, so that:

$$W(\theta) = \sum_\nu A_\nu(I_0 I_k) A_\nu(I_k I_f) P_\nu(\cos\theta) \quad (6.1)$$

When specialized to photonuclear reactions the quantity, $A_\nu(I_0 I_k)$, describes the transition from the initial state, I_0, to the state, I_k, through the absorption of a photon of multipolarity, L. In terms of the $3-j$ and $6-j$ symbols it is:

$$A_\nu(I_0 I_k) = (-1)^{I_0 - I_k + 2I_{k'} - 1} \hat{I}_k \hat{I}_{k'} \hat{L} \hat{L}' \hat{\nu} \begin{pmatrix} L & L' & \nu \\ -1 & 1 & 0 \end{pmatrix} \begin{Bmatrix} L & L' & \nu \\ I_{k'} & I_k & I_0 \end{Bmatrix} \Re_L^* \Re_{L'}. \quad (6.2)$$

where the primed symbols stand for interfering quantities and where I_k, for example, means $(2I_k+1)^{1/2}$. $\Re$ is the transition amplitude.

The decay of the state, I_k, through particle emission to form the final state, I_f, is more complicated since it involves the coupling of both the particle spin, s, and the orbital angular momentum, ℓ. There are two different representations that are commonly used to couple s, ℓ, and I_f to give I_k. These we will call the channel-spin representation and the j-representation (see fig. 31). In the channel spin representation s and I_f are coupled first to give the channel spin S, and then S and ℓ coupled to yield I_k. In the j-representation s and ℓ are coupled first to give j, the total angular momentum of the outgoing particle, and then j and I_f are coupled to yield I_k. In the channel spin formalism the transition between I_k and I_f is described by:

$$A_\nu(I_k I_f) = (-1)^{S - I_k} \hat{\ell} \hat{\ell}' \hat{I}_k \hat{I}_{k'} \hat{\nu} \begin{pmatrix} \ell & \ell' & \nu \\ 0 & 0 & 0 \end{pmatrix} \begin{Bmatrix} \ell & \ell' & \nu \\ I_{k'} & I_k & S \end{Bmatrix} \Re_{S\ell}^* \Re_{S\ell'} \quad (6.3)$$

and in the j-representation by:

$$A_\nu(I_k I_f) = (-1)^{I_f - I_k + 2I_{k'} + 2j - 1/2} \hat{I}_k \hat{I}_{k'} \hat{j} \hat{j}' \hat{\nu} \begin{pmatrix} j & j' & \nu \\ \frac{1}{2} & -\frac{1}{2} & 0 \end{pmatrix} \begin{Bmatrix} j & j' & \nu \\ I_{k'} & I_k & I_f \end{Bmatrix} \Re_j^* \Re_{j'} \quad (6.4)$$

The advantage of the channel-spin representation is that the distribution for each S is independent; there is no interference between the distributions corresponding to the two channel spins. The advantage of the j-representation is its relevance to calculations done in $j-j$ coupling, such as the particle-hole calculations of Brown or Gillet. These theories yield directly the amplitudes from which the angular distribution can be evaluated. If it is desirable, one can then obtain the weighting factors for the different channel spins by recoupling. For example, the amplitude associated with the channel spin, S, $\Re_S$, is just a linear combination of the two possible amplitudes in the j-representation.

$$\Re_S = \sum_j \Re_j (-1)^{-I_k - I_f - j - 2s} \hat{j} \hat{s} \begin{Bmatrix} I_k I_f j \\ s \ \ell \ S \end{Bmatrix} \quad (6.5)$$

It is worth noting that the complexity of the angular distribution formulae is limited by the condition that ν is less than or equal to the smallest of $2L$, 2ℓ, $2I_k$. It follows that reactions that proceed through intermediate states of spin zero or one-half of those that yield only s-wave particles have isotropic angular distributions.

For intermediate states of well-defined parity only even powers of ν occur in the sum. For electirc dipole transitions then there would be only terms involving

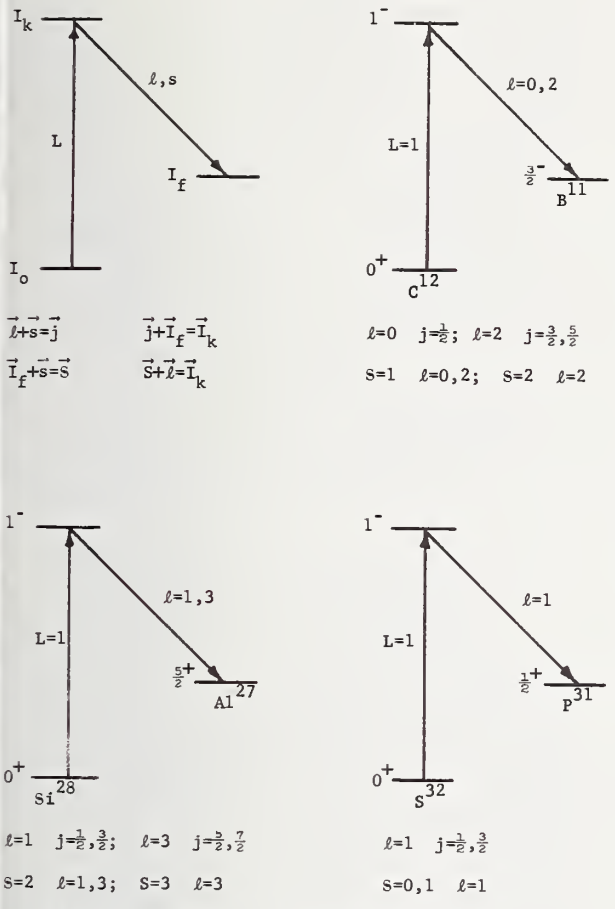

FIGURE 31. *The energy-level diagram for a simple* (γ, n) *or* (γ, p) *reaction.*

The coupling of the angular momenta in the channel spin and j-representations are shown. Electric dipole absorption by C^{12}, Si^{28}, and S^{32} followed by proton emission populating the ground states of B^{11}, Al^{27}, and P^{31} are illustrated, as specific examples.

P_0 and P_2. On the other hand, if the excited state results from two overlapping levels of opposite parity, terms odd in ν, such as P_1, appear. This effect is very important in photonuclear reactions where forward peaked angular distributions are common for excitation energies above the giant resonance. These are presumed to result from the interference between the states formed by the absorption of electric dipole and electric quadrupole radiation.

Tables 13 and 14 give some examples of simple angular distributions for particles of spin $\frac{1}{2}$ obtained using the two formulations. These are very unrealistic since they contain no interference terms.

Some time ago Courant [118] published the formulae for the angular distributions of nucleons emitted in so-called direct interactions following electric dipole absorption. The interaction was assumed to take place between the photon and a single nucleon, the rest of the nucleus being treated as a spectator. These distributions then depend only on the orbital angular momentum of the nucleon and are independent of the spins of the initial or final nuclear states. They are:

$$W(\theta)=\ell(\ell+1)+\tfrac{1}{2}(\ell+1)(\ell+2)\sin^2\theta \quad \text{for } \Delta\ell=+1$$

$$W(\theta)=\ell(\ell+1)+\tfrac{1}{2}(\ell-1)\sin^2\theta \quad \text{for } \Delta\ell=-1 \qquad (6.6)$$

where ℓ is the nucleon's orbital angular momentum before the interaction. Wilkinson [92, 93] has emphasized that the $\Delta\ell=+1$ transitions are much more likely to occur and the first of these two formulae has often been successfully compared with experiment. It is worth noting that this formula is identical to one of the two possibilities in the channel spin formalism. The channel spin S is $I_f\pm\frac{1}{2}$. The Courant formula corresponds to the choice $S=I_f-\frac{1}{2}$. These are labeled by an asterisk in table 13.

Tables 13 and 14 give some examples of simple angular distributions for outgoing particles of spin $\frac{1}{2}$. These are very unrealistic since they contain no interference terms. To include them consider electric dipole absorption by a spin-zero nucleus. Then in the channel spin representation we can write the amplitude $\Re_{\ell S}$ as $B_{\ell S}e^{i\delta_\ell}$ where δ_ℓ is the nuclear plus Coulomb phase shift and $\Delta_{\ell\ell'}=\delta_{\ell'}-\delta_\ell$. If we can have $\ell=0$, 2 and $S=1$, 2, 3 then

$$W(\theta)=3(B_{01}^2+B_{21}^2)+3[\sqrt{2}B_{21}B_{01}\cos\Delta_{02}+\tfrac{1}{2}(B_{22}^2-B_{21}^2)-\tfrac{1}{7}B_{23}^2]P_2(\cos\theta) \qquad (6.7)$$

For $\ell=1$, 3 and $S=0$, 1, 2, 3

$$W(\theta)=3[B_{10}^2+B_{11}^2+B_{12}^2+B_{32}^2+B_{33}^2]+3[-B_{10}^2+\tfrac{1}{2}B_{11}^2-\tfrac{1}{10}B_{12}^2-\tfrac{2}{5}B_{32}^2+\tfrac{3}{5}\sqrt{6}B_{12}B_{32}\cos\Delta_{13}]P_2(\cos\theta) \qquad (6.8)$$

Similarly, in the j-representation $\Re_j=B_{\ell j}e^{i\delta_\ell}$, the spins of the final states are specified

$$W(\theta,\tfrac{1}{2})=3[B_{01/2}^2+B_{23/2}^2]-3[\tfrac{1}{2}B_{23/2}^2+\sqrt{2}B_{01/2}B_{23/2}\cos\Delta_{02}]P_2(\cos\theta) \qquad (6.9)$$

$$W(\theta,\tfrac{3}{2})=3[B_{01/2}^2+B_{23/2}^2+B_{25/2}^2]+3[\tfrac{2}{5}B_{23/2}^2-\tfrac{2}{5}B_{25/2}^2-\tfrac{3}{5}B_{23/2}B_{25/2}+(1/\sqrt{5}B_{01/2}B_{23/2}-3/\sqrt{5}B_{01/2}B_{25/2})\cos\Delta_{02}]P_2(\cos\theta) \qquad (6.10)$$

The above expressions may be useful in understanding the angular distributions in the ground-state proton capture cross sections where the spins of initial and final states are known.

Transitions between discrete excited states and well separated final states are rare in photonuclear reactions. They do occur in the light elements where the level densities are low and they may also occur in some special cases for heavy elements. By and large, however, the giant resonance absorption is into a large number of overlapping excited states in the continuum. The decay takes place mainly by neutron emission populating a large number of final

TABLE 13. *Angular distributions in the channel spin formalism*

I_0	L	I_k	I_f	$S=s+I_f$	ℓ	$W(\theta)$	$W(\theta)$
0^+	$E1$	1^-	$1/2^+$	0	1	P_0-P_2	$3/2\sin^2\theta$*
			$1/2^-, 3/2^-$	1	0	$-1\sqrt{3}P_0$	Isotropic
			$1/2^-, 3/2^-$	1	2	$3[1-\frac{1}{2}P_2]$	$\frac{1}{2}(1+3/2\sin^2\theta)$*
			$1/2^+, 3/2^+$	1	1	$P_0+\frac{1}{2}P_2$	$3/2(1-\frac{1}{2}\sin^2\theta)$
			$3/2^-, 5/2^-$	2	1	$P_0-1/10\ P_2$	$9/10(1+1/6\sin^2\theta)$
			$3/2^-, 5/2^-$	2	2	$P_0+\frac{1}{2}P_2$	$3/2(1-\frac{1}{2}\sin^2\theta)$
			$3/2^+, 5/2^+$	2	3	$P_0-2/5\ P_2$	$3/5(1+\sin^2\theta)$*
			$5/2^-, 7/2^-$	3	2	$P_0-1/7\ P_2$	$6/7(1+\frac{1}{4}\sin^2\theta)$
	$M1$	1^+	$1/2^-$	0	1	P_0-P_2	$3/2\sin^2\theta$
			$1/2^-$	1	1	$P_0+\frac{1}{2}P_2$	$3/2(1-\frac{1}{2}\sin^2\theta)$
	$E2$	2^+	$1/2^-$	1	1	$5P_0-5/2\ P_2$	$15/2(1-\frac{1}{2}\sin^2\theta)$
			$1/2^-$	1	3	$5P_0+20/7(P_2-P_4)$	$5(1+2\sin^2\theta-5/2\sin^4\theta)$
$1/2^-$	$E1$	$1/2^-$	0^+	1/2	1	$-2P_0$	Isotropic
		$3/2^-$	0^+	1/2	1	$-4P_0+2P_2$	$-2(1+3/2\sin^2\theta)$
	$M1$	$1/2^+$	0^+	1/2	0	$-2P_0$	Isotropic
		$3/2^+$	0^+	1/2	2	$-4P_0+2P_2$	$-2(1+3/2\sin^2\theta)$
	$E2$	$3/2^+$	0^+	1/2	2	$-4P_0-2P_2$	$-6(1-\frac{1}{2}\sin^2\theta)$
		$5/2^+$	0^+	1/2	2	$-6P_0-24/7(P_2-P_4)$	$-6(1+2\sin^2\theta-5/2\sin^4\theta)$

states that are also overlapping. The angular distributions of these neutrons is then expected and observed to be isotropic.

The expression for the angular distribution resulting from plane polarized incident radiation has been given by Satchler [119]. For this we simply replace the $P_\nu(\cos\theta)$ in eq (6.1) by $\mathcal{P}_\nu(\cos\theta)$ where

$$\mathcal{P}_\nu(\cos\theta)=\mathcal{P}_\nu+\omega_{L'}f_\nu(LL')p_1P_\nu^2(\cos\theta)\cos 2\theta_1 \tag{6.11}$$

where $\omega_{L'}$ is ± 1 according to whether the transition is electric or magnetic, p_1 is the degree of polarization, P_ν^2 is the associated Legendre function, and

$$f(L,L')=\frac{-2L(L+1)}{(\nu-1)(\nu-2)[\nu(\nu+1)-2L(L+1)]} \tag{6.12}$$

The symbol θ_1 stands for the angle between the reaction plane and the electric vector.

If we include only electric dipole transitions and assume 100 percent plane polarization in the incident beam, then $\omega_{L'}=+1$, $p_1=1$, $f_2(1,\ 1)=-\frac{1}{2}$, $P\nu^0=P\nu^1=0$, $P\nu^2=3\sin^2\theta$, and

$$W(\theta)=A_0P_0+A_2[P_2-\tfrac{3}{2}\sin^2\theta\cos 2\theta_1]. \tag{6.13}$$

We wish to evaluate the intensities perpendicular to the beam direction, $\theta=\pi/2$, and at the azimuthal angles such that the electric vector is in the reaction plane $I^{\parallel}$, $\theta_1=0$; $\cos 2\theta_1=1$ and the electric vector perpendicular to the reaction plane, $I^{\perp}$, $\theta_1=\pi/2$; $\cos 2\theta_1=-1$. Recalling that $P_0(\cos\theta)=1$ and $P_2(\cos\theta)=\frac{1}{2}(3\cos^2\theta-1)$, we obtain

$$\begin{aligned} I(\pi/2)&=A_0P_0+A_2[P_2-\tfrac{3}{2}\sin^2\theta\cos 2\theta_1] \\ I^{\parallel}&=A_0-2A_2 \\ I^{\perp}&=A_0+A_2 \end{aligned} \tag{6.14}$$

In previously made measurements of photoneutron angular distributions the ratio A_2/A_0 varies from

TABLE 14. *Angular distributions in the* j*-representation for* $I=0^+$, $I_k=1^-$ and $L=1$

I_f	ℓ	j	$W(\theta)$	$W(\theta)$
1/2	1	1/2	$9P_0$	Isotropic
1/2	1	3/2	$3\sqrt{3}(P_0-\frac{1}{2}P_2)$	$3/2\sqrt{3}(1+3/2\sin^2\theta)$
3/2	2	3/2	$-3\sqrt{3}(P_0+2/5\ P_2)$	$-21/5\sqrt{3}(1-3/7\sin^2\theta)$
3/2	2	5/2	$3\sqrt{3}(P_0-2/5\ P_2)$	$9/5\sqrt{3}(1+\sin^2\theta)$
5/2	3	5/2	$3\sqrt{3}(P_0+16/35\ P_2)$	$153/35\sqrt{3}(1-8/17\sin^2\theta)$
5/2	3	7/2	$3\sqrt{3}(P_0-5/14\ P_2)$	$27/14\sqrt{3}(1+5/6\sin^2\theta)$

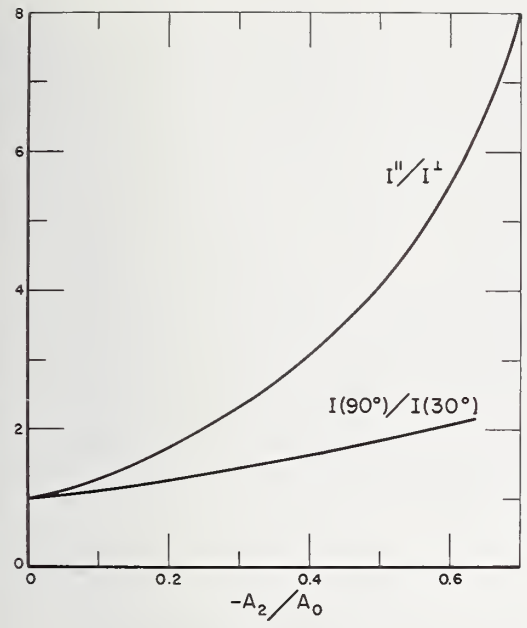

FIGURE 32. *The sensitivity of a measurement made with plane polarized photons compared with a normal angular distribution measurement as a function of the ratio* $-A_2/A_0$.

The symbol $I^{\parallel}$ represents the nucleon intensity in the photon polarization plane and $I^{\perp}$ that perpendicular to it.

-0.1 to -0.7 depending on the nucleus. Figure 32 shows a plot of $I^{\parallel}/I^{\perp}$ versus $-A_2/A_0$ over this range. For comparison is shown a plot of the ratio $I(\pi/2)/I(30°)$ as would be obtained in a simple distribution experiment. It is apparent that angular the measurement using polarized incident photons affords a more sensitive method of measuring $-A_2/A_0$.

4. Comparison With Experiments

It has already been pointed out that the electric dipole transition that dominates the giant resonance is always the one in which a nucleon, having the highest available angular momentum, makes a transition in which its angular momentum is increased by one more unit. The interactions that take place following photon absorption depend on the level density at the appropriate excitation energy as well as on the magnitudes of the Coulomb and angular momentum barriers. In the 1*s*-shell the level densities are so low that the nucleons emerge without interacting. In the 1*p*-shell the dominant transition in the absorption process is $1p_{3/2} \rightarrow 1d_{5/2}$. These particles survive the angular momentum and Coulomb barriers, though interactions with the excited $2p$–$2h$, $3p$–$3h$, etc. 1^- states produce occasional depressions in the cross section as we have seen in the case of O^{16}.

In the $2s$–$1d$ shell the giant resonance absorption cross section is qualitatively very different. It is fractured into a large number [37] of sharp peaks having widths of ≈ 70 keV. This striking feature is illustrated in figure 11 where the giant resonance shapes for C^{12} and Si^{28} are compared. The envelope of the fine structure consists of three or four peaks having widths of ≈ 1 MeV. These have been associated with the particle-hole transitions that form the entrance channel into the giant resonance. The excited nucleons are held in the nucleus by the angular momentum barrier for a time which is long enough for the initial $1p$–$1h$ state to mix with the many $2p$–$2h$ 1^- states existing at the giant resonance excitation energy. The width of the spikes in the cross section tells us that these complicated configurations last for a time $\approx \hbar/70$ keV. This phenomenon is also seen in the giant resonances [36, 38, 40] of Mg, S, and Ca.

This situation is further dramatized when we pass into the $2p1f$ shell. Here the dominant shell model transition is of the $f \rightarrow g$ type. These nucleons are confined within the nucleus where they mix with an even greater density of $2p$–$2h$, $3p$–$3h$, etc. states until finally the excitation energy is transferred to an *s*-wave neutron which is then evaporated. Figure 33 is included to illustrate this point. It shows the neutron yield produced by 30 MeV bremsstrahlung [120] divided by NZ/A as a function of Z. For nuclei up to Ca^{40} this quantity is almost constant. As soon as we enter the $2p1f$ shell the neutron yield makes a dramatic jump. This is a demonstration of the importance of the angular momentum barrier in keeping the nucleus together while the thermalization process occurs. The emission of *s*-wave neutrons then becomes dominant.

These ideas are supported by the angular distribution measurements. It has been found that, in general, the ground-state photoproton angular distributions are nearly constant functions of energy as though they were produced by a single excitation. For carbon and oxygen the distributions for outgoing ground-state protons are essentially those expected for outgoing *d*-wave particles; in both cases

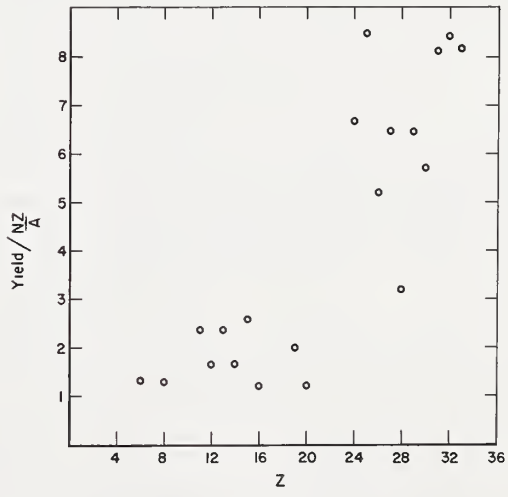

FIGURE 33. *The neutron yield divided by* NZ/A.

This quantity is essentially constant up to Ca^{40} after which it makes a dramatic jump. This is the point at which *s*-wave neutron emission becomes the dominant mode of decay for the giant resonance.

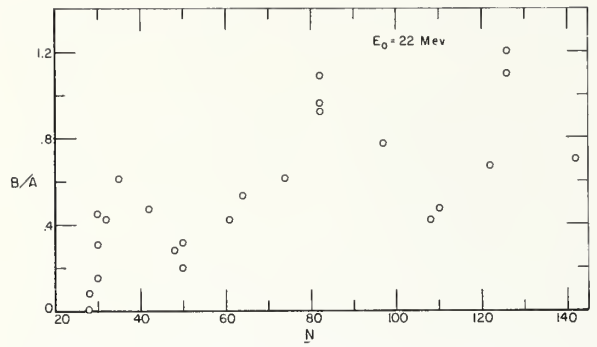

FIGURE 34. *The anisotropy,* B/A, *in the angular distributions [121] of the fast neutrons as a function of neutron number.*

some s-wave emission has to be mixed in. For these nuclei the excited nucleon emerges directly.

In the $2s$–$1d$ shell the ground-state (γ, p) cross section for Ne^{20} and S^{32} must emit p-wave particles in order to populate the $\frac{1}{2}^+$ ground state of F^{19} and P^{31}. These proceed almost entirely by p-wave emission in channel spin 0. Even though their dominant excitations would lead to f-wave emission, Mg^{24} and Si^{28} also emit p-wave particles in populating the ground states of Na^{23} and Al^{27}. Here the configuration mixing that fractures the cross section transfers the excitation energy to a p-wave proton which can leak out of the nucleus.

It is worthwhile pointing out that two of the minima [35] in the F^{19} (p, γ_0) Ne^{20} cross section occur at energies where the angular distribution coefficient, A_2/A_0, deviates from its constant value. This certainly suggests that at these energies more complicated configurations interact with the particle-hole state. Gillet, Melkanoff, and Raynal [111] have already shown that $2p2h$ states in the giant resonance of O^{16} can produce minima in the cross section by interference with the $1p1h$ excitation. The excursions of the angular distribution coefficient, A_2/A_0, may also be associated with this phenomenon.

For heavier nuclei about 10 percent of the photonucleons are emitted in direct interactions. Since the interaction takes place with the valence nucleons and those in the last filled shell, we might expect to see a correlation between the angular distributions of the more energetic nucleons and nuclear shell structure. On the basis of the Courant formula an outgoing nucleon with $\ell=1$ has an angular distribution proportional to $\sin^2\theta$ with no isotropic component. As ℓ increases the isotropic component becomes more and more important. When one considers that the angular momentum barrier inhibits the emission of nucleons having large ℓ, it is possible to understand the experimental results at least qualitatively.

Figure 34 shows the results of a survey published by Baker and McNeill [121]. They have irradiated many targets with 22 MeV bremsstrahlung and used silicon threshold detectors to measure the angular distributions of the outgoing neutrons. These detectors respond primarily to neutrons in the energy range 5–10 MeV. The ordinate, B/A, is the anisotropy, defined by the expression:

$$W(\theta)=A+B\sin^2\theta+C\cos\theta\sin^2\theta \quad (6.15)$$

The maximum in B/A for neutron number 35 certainly results from the filling of the low angular momentum $2p_{3/2}$ shell. The anisotropy decreases as higher angular momentum neutrons are added to the $1f_{5/2}$ and $1g_{9/2}$ shells. It increases once more with the filling of the $2d_{5/2}$, $2d_{3/2}$, and $2s_{1/2}$ shells. It then decreases once more as particles are added to the $1h_{11/2}$, $1h_{9/2}$, $2f_{7/2}$, and $2f_{5/2}$ shells. The final peak at neutron number 126 may be attributed to the filling of the $3p_{1/2}$ and $3p_{3/2}$ shells.

In order to discuss the asymmetry in the photonuclear angular distributions it is necessary to recall the effective charges that result from the relative motion of the outgoing nucleon with respect to the recoiling nucleus. For electric dipole absorption these are:

$$\begin{aligned} q_p &= N/A \\ q_n &= -Z/A \\ q_D &= (N-Z)/A \\ q_\alpha &= 2(N-Z)/A \end{aligned} \quad (6.17)$$

From these it follows incidentally that electric dipole absorption cannot result in the direct emission of deuterons or α particles from a self-conjugate nucleus. These heavier particles may, however, be evaporated from heavy nuclei and the observed numbers are consistent with the predictions of the statistical model.

For electric quadrupole absorption the effective charges are:

$$\begin{aligned} q_p &= 1-2/A+Z/A^2 \\ q_N &= Z/A^2 \\ q_D &= 1-2/A+2Z/A^2 \\ q_\alpha &= 2q_D \end{aligned} \quad (6.18)$$

It is important to note here that the effective charge for direct neutron emission is first of all very small and secondly, is opposite in sign to the effective charge associated with electric dipole absorption. The $E1$ and $E2$ effective charges for direct proton emission have the same sign. We would therefore expect that in the energy range above the giant resonance in heavy nuclei ($\approx$25 MeV), where both $E1$ and $E2$ participate, the photoproton angular distributions might be peaked forward of 90° and the photoneutron distributions peaked backward with a much smaller asymmetry. The experimental facts bear out this prediction only partially. The photoproton distributions are certainly peaked forward of 90° and the asymmetries observed in the photoneutron distributions are very much less pronounced but there is no doubt that they too are peaked forward of 90° [121, 122, 123]. Now for the first time Gorbunov [124] has found a backward

peaking of photoneutrons from He^4 following the absorption of photons having energies in the range 30–36 MeV. At higher energies the distribution is found to peak forward. This reversal presumably results from nucleon-nucleon correlations: it would be instructive to know if it occurs for other nuclei.

5. The Quasideuteron Effect

The dominant mode for the absorption of high energy x rays is through the quasideuteron mechanism. This becomes important for photon energies above the giant resonance and results from the interaction of the photon with a two-particle cluster rather than with a single nucleon. The interaction occurs with a neutron-proton pair since proton-proton and neutron-neutron pairs have no dipole moment, and hence the quasideuteron designation. The photon, having high energy and low momentum, picks out the high momentum components in the nuclear ground state, associated with the colliding neutron-proton pair, and disrupts this cluster so that both particles can emerge from the nucleus with the energy and angular correlation appropriate to the deuteron photodisintegration.

Levinger [125] pointed out that the quasideuteron inside the nucleus differed from a real deuteron in that the two particles must interact in a smaller volume. The ground-state wave function for the quasideuteron has effectively the same shape as that for the deuteron, the difference being that the interaction takes place in a much smaller volume so that the amplitude of the wave function must be correspondingly larger. He estimated the quasideuteron cross section to be

$$\sigma_{QD} = 6.4 \frac{NZ}{A} \sigma_D \qquad (6.19)$$

where NZ/A is the number of neutron-proton pairs in the nucleus.

Levinger also pointed out that one could expect the outgoing nucleons to reproduce the energy and angular distributions associated with the deuteron photodisintegration. Let us consider photon energies in the range 30–140 MeV, i.e., above the giant resonance but below the meson production threshold. Here the deuteron photodisintegration cross section consists mainly of an electric dipole contribution with an electric quadrupole component that increases with energy. The interference between the $E1$ and $E2$ components makes the proton angular distributions peak forward of 90° and the neutron distributions backward of 90° in the deuteron center of mass system. In the laboratory system both distributions peak forward of 90°; the backward peaking of the center-of-mass neutron distribution is more than compensated by the forward motion of the deuteron center of mass. The same is at least qualitatively true for the quasideuteron. It is never obvious, for instance, how to specify the quasideuteron binding energy, even if it is known that the residual nucleus is left in its ground state, for the neutrons and proton have a positive energy resulting from their motion inside the nucleus. The momentum associated with this motion also produces a smearing of energy spectra of the outgoing nucleons compared with those produced in the deuteron photodisintegration.

Insofar as the experiments (which are very difficult) have been performed they bear out most of the predicted features of the quasideuteron effect. In the first place the spectrum [126] of protons produced when a target was bombarded with high energy bremsstrahlung of maximum energy, E_0, varied approximately as E^{-2} with a very sharp break at $E_0/2$, decreasing very rapidly at higher energies. The E^{-2} dependence results from the fact that both bremsstrahlung spectrum and the deuteron photodisintegration cross section vary approximately as $1/E$ and the cut-off at $E_0/2$ occurs because the highest energy photon can only give half its energy to the proton. This result indicated very early that there was no other important source of high energy protons in the photoeffect.

The angular distribution [127] of neutrons in coincidence with protons of a specified energy has also been measured and shown to have the correlation dictated by the dynamics of the deuteron photodisintegration. The width of the angular distribution curves for complex nuclei have been found to be wider than those obtained with deuterium targets and this difference used to infer the internal energies of the nuclear particles.

For a long time the experiments implied that Levinger's estimate of the quasideuteron cross section magnitude was too large. New experiments, however, indicate that perhaps the constant in eq (6.19) is closer to 10 than 6.4. The newer experiments [128, 129] take into account all of the outgoing nucleons that do not populate the ground state of the residual nucleus.

VII. Isobaric Spin in Photonuclear Reactions

1. Introduction

Isobaric spin has some consequences for photonuclear reactions. If we express the electric dipole operator in terms of the isobaric spin operator t^z we have

$$D=e\sum_{i=1}^{Z}\mathbf{r}_i$$

$$=e\sum_{i=1}^{A}\mathbf{r}_i(\tfrac{1}{2}-t_i^z)$$

$$=e/2\sum_{i=1}^{A}\mathbf{r}_i-e\sum_{i=1}^{A}\mathbf{r}_i t_i^z \qquad (7.1)$$

where t^z has the eigenvalues $+\frac{1}{2}$ for neutrons and $-\frac{1}{2}$ for protons. The first term of the operator is associated with the center of mass motion and is responsible for Thomson scattering; the second term, $-e\sum_i^A \mathbf{r}_i t_i^z$, induces electric dipole transitions according to the selection rules $\Delta T=0\pm1$ for those nuclei having $T_z=(N-Z)/2\neq0$ in their ground states and $\Delta T=1$ for those having $T_z=0$. These selection rules can be violated in that the Coulomb interaction can mix excited states of different isobaric spin. If isobaric spin is a good quantum number and the selection rules are obeyed we should expect the electric dipole (γ, n) and (γ, p) cross sections for the self-conjugate nuclei to be identical in size and shape. In addition these nuclei would not emit deuterons or alpha particles in direct interactions following $E1$ absorption. In the following we cite various examples of violations of these rules. With that caution we will then consider the consequences of taking isobaric spin seriously.

2. Evidence for Isobaric Spin Impurities in the Giant Resonance

If we have perfect charge symmetry and electric dipole interactions in which the excited particle comes directly out of the nucleus, then the (γ, n) and (γ, p) cross sections should be identical in both magnitude and shape. The (γ, p) thresholds are, in general, lower than the (γ, n) thresholds by just such an amount as to compensate for the Coulomb barrier. For a given excitation energy, then, the outgoing protons do have slightly higher energies than the neutrons but only enough to make the (γ, p) cross sections $\approx$20 percent larger than the (γ, n) cross sections. Experimentally the ratio of the (γ, p) to the (γ, n) cross sections integrated over the giant resonance varies from 1 at helium to 6 at calcium. This is illustrated in figure 29 where $\int^{30}\sigma(\gamma, p)\,dE/\int^{30}\sigma(\gamma, n)\,dE$ is plotted for the self-conjugate nuclei. This is a gross indication of isotopic spin mixing in the giant resonance. Quantitatively the ratio of 6 for Ca^{40} corresponds to 40 percent contribution of the $T=0$ amplitude to the excited state—or a 15 percent contribution to the intensity.

C^{12} is an example of a nucleus for which the (γ, n) and (γ, p) cross sections [32, 130] are conspicuously different. These are compared in figure 35. Notice the huge dip in the (γ, n) cross section at exactly the energy where the (γ, p) cross section peaks. The corresponding cross sections for O^{16}, on the other hand, show no such obvious difference; the ground-state (γ, n) and (γ, p) cross sections are apparently identical.

In connection with the $2p2h$ excitation in O^{16} it has already been pointed out that the N^{14} (d, γ_0) O^{16} process does occur [112] with a rather sharp maximum at 22.7 MeV. Its angular distribution establishes it as an electric dipole phenomenon which must result from isobaric spin mixing.

The isobaric-spin forbidden reaction [131] Mg^{24} (α, γ_0) Si^{28} also takes place in electric dipole transitions. This result is also based on an unambiguous angular distribution measurement.

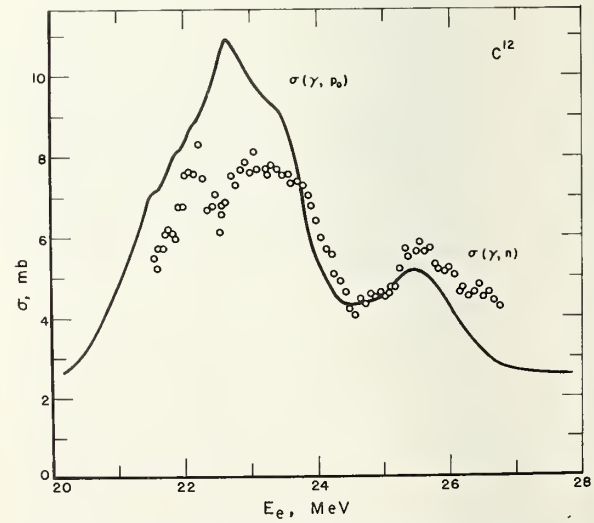

FIGURE 35. *A comparison of the* (γ, n) [130] *(open circle) and the* (γ, p) *cross sections* [32] *for* C^{12}.

3. Consequences of Isobaric Spin Purity

The ground states of the stable nuclei have their Z-component of isobaric spin $T_z=(N-Z)/2$, and $T=\pm T_z$. The dipole state has three isobaric spin components $T_k=T$, $T+1$, and $T-1$. Their relative strengths are given in part [132] by a geometrical factor:

$$(TT_z1\Delta T_z \mid T_kT_z+\Delta T_z)^2$$

Here $\Delta T_z=+1$ describes the electric dipole part of μ-capture on the target; $\Delta T_z=-1$ represents the electric dipole part of n, p reactions; and $\Delta T_z=0$ is the electric dipole giant resonance. The last then has two components $T_k=T$ and $T_k=T+1$. These have the relative geometrical intensities:

$$\frac{(TT10 \mid TT)^2}{(TT10 \mid T+1T)^2}=\frac{T/T+1}{1/T+1}=T=\frac{N-Z}{2} \quad (7.3)$$

This statement is consistent with the well-known fact that for the self-conjugate nuclei with $T=0$ the giant resonance consists only of $\Delta T=1$ transitions. If we consider only the geometrical factor, we find that for the nuclei having $T=\frac{1}{2}$, of which He^3 and C^{13} are examples, the $T+1$ giant resonance is the more important. The $T=1$ nucleus, Ni^{58}, would have $T=1$ and $T=2$ giant resonances of equal strength. As we progress through the periodic table T, or the neutron excess, increases and the $T+1$ giant resonance becomes less and less important. For Zr^{90} T is 5; for Pb^{208} it is 22. For Ca^{40} the $T+1$ resonance is everything; for Pb^{208} it must be less than 5 percent.

In figure 36 are illustrated the T and $T+1$ giant resonances for an arbitrary nucleus, (N, Z), having N neutrons and Z protons. The splitting of these two giant resonances is a few MeV; Lane's estimate [133] of $100(T+1)/A$ MeV would be ≈ 6 MeV for Zr^{90}. Also shown are the ground states of its neighbors, $(N-1, Z)$ and $(N, Z-1)$ having $T-\frac{1}{2}$ and $T+\frac{1}{2}$ respectively. Both giant resonances can emit protons to populate the ground state of the residual nucleus but only the lower can emit neutrons; neutron emission from the upper states involves $\Delta T=\frac{3}{2}$ which is forbidden. Neutron emission from the $T+1$ resonance can occur when the excitation energy exceeds the threshold for populating the first $T+\frac{1}{2}$ state in the residual nucleus, i.e. $Q_n+E_{ez}=Q_p+\Delta E_c$. The first $T+\frac{1}{2}$ state is the analogue of the ground state of the $(N, Z-1)$ system and separated from it by the Coulomb energy, $\Delta E_c=1.44\ Z/A^{1/3}-1.13$ MeV. This scheme is also illustrated for the specific nucleus, C^{13}.

One might think that we could test these ideas by looking for low energy neutrons as the excitation energy is increased across the threshold for populating the $T+\frac{1}{2}$ state. This situation, however, is muddied by the fact that either the $(\gamma, 2n)$ or (γ, pn) threshold usually occurs at this energy too.

Experimental evidence for the $T+1$ giant resonance is still paltry. The best example lies in the photodisintegration of C^{13}. Here the giant resonance [134], made up of the sum of the (γ, n) and (γ, p) cross sections, consists of a broad resonance centered near 23 MeV plus a smaller peak near 13 MeV. Presumably it contains both $T=\frac{1}{2}$ and $T=\frac{3}{2}$ components. The $T=\frac{1}{2}$ part of the N^{13} giant resonance has been excited [135] in the reaction C^{12} (p, γ_0) N^{13}. Its shape resembles very closely the lower energy part of the $C^{13}(\gamma, n)$ cross section (see fig. 37). It has been inferred [136] that the $T=\frac{1}{2}$ C^{13} giant resonance has this shape and that the remainder is the $T=\frac{3}{2}$ component.

Some evidence has also been cited in the photodisintegration of the Ni and Zr isotopes. Min [137] associates the large proton emission cross section of Ni^{58} at 19.5 MeV with the $T+1=2$ resonance, the lower $T=1$ resonance being at 17 MeV. The Zr isotopes have their main giant resonance at about 16 MeV, but on the falling side of the neutron production cross section there is a shoulder near 21 MeV that has been ascribed [50] to the $T+1$ giant resonance.

O'Connell [138] has derived a sum rule relating the strengths of the two giant resonances to the mean square radius of the excess neutrons and their correla-

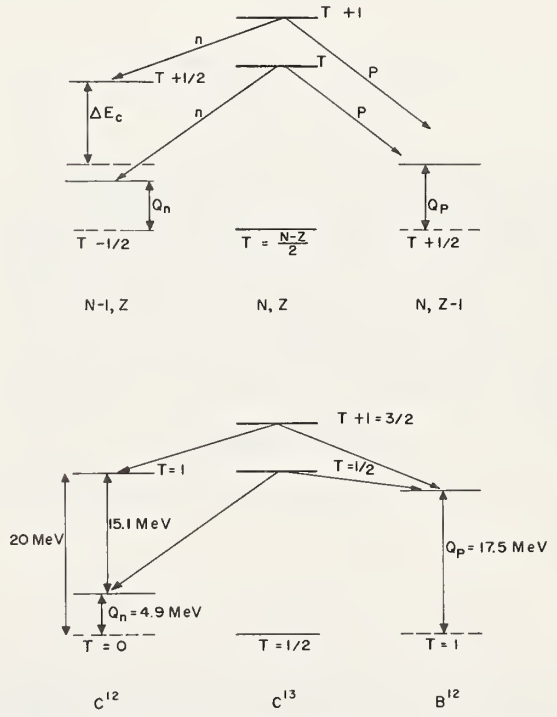

FIGURE 36. *An illustration of the* T *and* T+1 *giant resonances of the nucleus* (N, Z).

The ground states of the adjacent nuclei $(N-1, Z)$ and $(N, Z-1)$ having $T-\frac{1}{2}$ and $T+\frac{1}{2}$ are also shown. Both giant resonances can emit protons to populate the ground state of the $(N, Z-1)$ system whereas only the lower resonances can emit neutrons to populate the ground state of the $(N-1, Z)$ system. An excitation energy of $Q_p+\Delta E_c$ is required for neutrons from the $T+1$ giant resonance to populate the first $T+\frac{1}{2}$ state of the $(N-1, Z)$ system.

tions. This sum rule includes not only the geometrical factor already mentioned but also the dynamical factor discussed by MacFarlane [132] and Goulard and Fallieros [139]. The derivation of this sum rule assumes that isobaric spin is a good quantum number and uses the dipole operator in its long wavelength approximation. It is:

$$\frac{\pi^2e^2}{3\hbar c}\left[2T\langle R_V^2\rangle+T(2T-1)\langle R_T^2\rangle\right]$$
$$=\sigma_{-1}(T)-T\sigma_{-1}(T+1) \quad (7.4)$$

The notation $\sigma_{-1}(T)$ stands for $\int \sigma(T)/E\, dE$, often called the bremsstrahlung weighted cross section but is, in fact, proportional to the sum of the squares of the transition matrix elements, $\sum_k D_k^2(T)$, populating the giant resonance having isobaric spin, T:

$$\sigma_{-1}(T)=\frac{4\pi^2}{\hbar c}\sum_k D_k^2(T) \quad (7.5)$$

The quantities, R_V and R_T, are called respectively the isovector radius and the isotensor radius. They are defined in terms of the reduced matrix elements of their respective operators.

The isovector radius depends on the mean square neutron and proton radii:

$$2T_z\langle R_V^2\rangle=\left\langle TT_z\left|\sum_{i=1}^{A} r_i^2\tau_i^z\right|TT_z\right\rangle$$
$$=N\langle R_n^2\rangle-Z\langle R_p^2\rangle \quad (7.6)$$

(O'Connell's operator, τ_i^z has the eigenvalues ± 1.) If we assume that the neutron and proton radii are approximately the same, then the mean square isovector radius is just proportional to the number of excess neutrons, $2T$, times their mean square radius. For making numerical estimates we assume that the mean square radius of the excess neutrons is the same as the measured mean square charge radius. Then

$$2T_z\langle R_V^2\rangle=2T\langle R_{\rm ch}^2\rangle \quad (7.7)$$

The isotensor radius, R_T, is defined by the relationship:

$$[3T_z^2-T(T+1)]\langle R_T^2\rangle$$
$$=\langle TT_z|\sum_{j<i}(\mathbf{r}_j\cdot\mathbf{r}_i)(3\tau_j^z\tau_i^z-\boldsymbol{\tau}_j\cdot\boldsymbol{\tau}_i)|TT_z\rangle \quad (7.8)$$

The mean square isotensor radius, $\langle R_T\rangle$, then depends on the correlation between pairs of nucleons, i and j. The factor, $(\mathbf{r}_i\cdot\mathbf{r}_j)$, represents their spatial correlation function. The weighting factor, $(3\tau_j^z\tau_i^z-\boldsymbol{\tau}_j\cdot\boldsymbol{\tau}_i)$, has the value zero for a neutron–proton pair with $t=0$. For $t=1$ pairs it is 2 for neutron–neutron pairs 2 for proton–proton pairs, and -4 for neutron–proton pairs. In other words, this factor yields zero for the $T=0$ core of the nucleus. The isotensor radius then measures the correlation between pairs of excess neutrons.

To examine the consequences of this sum rule, set the term involving $\langle R_T^2\rangle$ equal to zero. This can happen for a nucleus with $T=\frac{1}{2}$ or if there are no correlations between pairs of excess neutrons, i.e., in a literal independent particle model. Then

$$\frac{2\pi^2e^2}{3\hbar c}T\langle R_{\rm ch}^2\rangle=\sigma_{-1}(T)-T\sigma_{-1}(T+1) \quad (7.9)$$

Combining eq (7.9) with

$$\sigma_{-1}=\sigma_{-1}(T)+\sigma_{-1}(T+1) \quad (7.10)$$

we have

$$\frac{\sigma_{-1}(T+1)}{\sigma_{-1}}=\frac{1}{T+1}\left[1-\frac{2\pi^2e^2}{3\hbar c}\frac{T\langle R_{\rm ch}^2\rangle}{\sigma_{-1}}\right]$$
$$=\frac{1}{T+1}\left[1-\frac{0.48T\langle R_{\rm ch}^2\rangle}{\sigma_{-1}}\right] \quad (7.11)$$

Here we recognize the factor, $1/(T+1)$, as the geometrical factor that determines the importance of the $(T+1)$ giant resonance. The term in the square bracket is the dynamical factor that remains.

For a harmonic oscillator

$$\sigma_{-1}=\int\frac{\sigma}{E}\,dE=\frac{1}{E}\int\sigma\,dE$$
$$=\frac{60}{42A^{-1/3}}\frac{NZ}{A}=0.36A^{4/3}\text{ mb} \quad (7.12)$$

for $N=Z=A/2$. If we take $\langle R^2{}_{\rm ch}\rangle=A^{2/3}$ fm^2, then

$$\frac{\sigma_{-1}(T+1)}{\sigma_{-1}}=\frac{1}{T+1}\left[1-\frac{4T}{3A^{2/3}}\right] \quad (7.13)$$

This is essentially the result Goulard and Fallieros [139] obtained in the harmonic oscillator model. It is imperative to point out that the harmonic oscillator model certainly does not apply to the real world since no giant resonance peaks at $42A^{-1/3}$ MeV. In fact, the data imply that the coefficient in eq (7.12) is 0.16 rather than 0.36 (see fig. 2). This would make the dynamical factor even more important in decreasing the size of the $T+1$ giant resonance. Using $\sigma_{-1}=0.16A^{4/3}$ mb and the em pirical dependence [140] of A on T

$$T=0.2A^2/(A+200),$$

we find that the strength of the $T+1$ giant resonance becomes zero at $A\sim 110$.

For $A>110$ it transpires that σ_{-1} is much too large to be consistent with the nuclear radius. The correlations between the excess neutrons, represented in eq (7.4) by $\langle R_T^2\rangle$, must therefore play an important role. This term in the sum rule has to be appreciable and negative.

An investigation of the properties of $\langle R_T^2\rangle$ shows, indeed, that it is negative [141]. Furthermore, it stems from the anticorrelated pairs of excess neutrons occupying orbits of opposite parity. The sum rule then states that even if $\sigma_{-1}(T+1)$ vanishes for large A, there must also be large anticorrelations of the excess neutrons moving in shells of opposite

parity in order to make the experimentally observed bremsstrahlung weighted cross sections, $\int \sigma/E\, dE$, consistent with the nuclear radii. Having established that the correlation term exists, we are no longer confined by the harmonic oscillator result that $\sigma_{-1}(T+1)$ is zero for $A>110$; it can be small but finite.

Pb [208] represents an extreme case. In this nucleus there are no $\Delta T=1$ electric dipole transitions and the entire giant resonance has the isobaric spin of the ground state [142]. The sum rule may then be written as

$$\frac{\pi^2 e^2}{3\hbar c}\left[2T\langle R_V^2\rangle + T(2T-1)\langle R_T^2\rangle\right] = \sigma_{-1}(T) = \sigma_{-1} \tag{7.14}$$

Using the experimental result $\sigma_{-1}=202$ mb and the charge radius of 5.5 fm for R_V, we obtain

$$\frac{\pi^2 e^2}{3\hbar c}\, T(2T-1)\langle R_T^2\rangle = -116 \text{ mb}.$$

This quantity is a measure of the correlations between the excess neutrons.

The sum rule may also be applied to the $T=\frac{1}{2}$ nuclei for which the correlation term vanishes because of the $(2T-1)$ factor multiplying it;

$$\frac{2\pi^2 e^2}{3\hbar c}\left[N\langle R_n^2\rangle - Z\langle R_p^2\rangle\right] = 2\sigma_{-1}(T) - \sigma_{-1}(T+1). \tag{7.15}$$

We recognize the Cabibbo–Radicati [143] sum rule in its nonrelativistic form. Omitted is a term containing magnetic moments that stems from the usually neglected spin-flip parts of the electric dipole operator. This rule has already been combined [144, 145] with a formula due to Foldy [2] and applied to the three-nucleon system. Foldy gives the bremsstrahlung-weighted cross section for nuclei having symmetric ground states, i.e., those in the 1s shell, in terms of their mean square matter radii, R^2:

$$\sigma_{-1} = \sigma_{-1}(T) + \sigma_{-1}(T+1) = \frac{4\pi^2}{3}\frac{e^2}{\hbar c}\frac{NZ}{A-1}R^2$$

The resulting relationship is:

$$\frac{2\pi^2}{3}\frac{e^2}{\hbar c}R^2 = \sigma_{-1}(T) = \sigma_{-1}(T+1)$$

Experimentally He^3 has two break-up modes:

$$He^3 \rightarrow d+p$$

$$He^3 \rightarrow n+p+p$$

The first can have only $T=\frac{1}{2}$; whereas the second can have both $T=\frac{3}{2}$ and $\frac{1}{2}$. However their measured values are substantially the same:

$$\sigma_{-1}(2) = 1.34 \pm 0.05 \text{ mb}$$

$$\sigma_{-1}(3) = 1.42 \pm 0.07 \text{ mb}$$

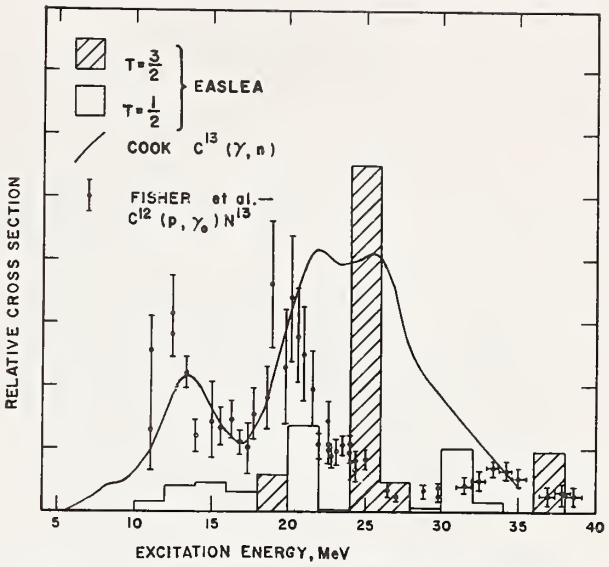

FIGURE 37. *A comparison of the results of the calculation of Easlea [146] with the measured* C^{13} (γ, n) *and* C^{12} (p, γ_0)N^{13} *cross sections [134, 136].*

Both $T=\frac{1}{2}$ and $T=3/2$ states were populated in the former; while only $T=\frac{1}{2}$ states were formed in the latter.

If equal, we are led to the conclusion that the three-body break-up mode is to be associated with $T=\frac{3}{2}$.

The sum rule can also be applied to C^{13} which has $T=\frac{1}{2}$. The giant resonance should therefore consist of $T=\frac{1}{2}$ and $T=\frac{3}{2}$ parts. Cook [134] has synthesized the total cross section for C^{13} by summing his measured (γ, n) and (σ, p) cross sections. The calculation of Easlea [146] as well as the $C^{12}(p, \gamma_0)N^{13}$ experiment of Fisher et al. [135] can be used as a guide to decide on a dividing line between the $T=\frac{1}{2}$ and $T=\frac{3}{2}$ strength. Figure 37 shows the data from the (p, γ_0) experiment which populates only $T=\frac{1}{2}$ states along with the (γ, n) cross section that populates both $T=\frac{1}{2}$ and $T=\frac{3}{2}$ states. The energy, 22.5 MeV, was then taken as the boundary between the two giant resonances and the integrals evaluated from the total cross section which is not shown.
These were

$$\sigma_{-1}(\tfrac{1}{2}) = 3.3 \text{ mb} \quad \text{and} \quad \sigma_{-1}(\tfrac{3}{2}) = 4.3 \text{ mb}$$

$$\sigma_{-1}(\tfrac{1}{2}) - \tfrac{1}{2}\sigma_{-1}(\tfrac{3}{2}) = 1.15 \text{ mb}$$

Using the charge radius as the radius of the valence neutron $R_V=2.36$ fm, the left hand side of the equation becomes 1.34 mb. These two numbers are certainly in satisfactory agreement.

These notes are based on lectures given under the auspices of a Sir Thomas Lyle Fellowship at the School of Physics of the University of Melbourne. The author thanks Professor Brian Spicer for his hospitality during that visit.

References

[1] Levinger, J. S., and Bethe, H. A., Phys. Rev. 78, 115 (1950).
[2] Foldy, L. L., Phys. Rev. 107, 1303 (1957).
[3] Levinger, J. S., Nuclear Photodisintegration. Oxford University Press (1960).
[4] Fano, U., Nat. Bur. Stand. (U.S.), Tech. Note 83, 27 pages (Nov. 1960).
[5] Maric, Z., and Möbius, P., Nuclear Physics 10, 135 (1959).
[6] Reibel, K., and Mann, A. K., Phys. Rev. 118, 701 (1960).
[7] Wolff, M. M., and Stephens, W. E., Phys. Rev. 108, 1644 (1957).
[8] Carroll, E. E., and Stephens, W. E., Phys. Rev. 118, 1256 (1960).
[9] Shin, Y. M., and Stephens, W. E., Phys. Rev. 136, 660 (1964).
[10] Kellogg, E. M., and Stephens, W. E., Phys. Rev. 149, 798 (1966).
[11] Welsh, R. E., and Donahue, D. J., Phys. Rev. 121, 880 (1961).
[12] Green, L., and Donahue, D. J., Phys. Rev. 135, B701 (1964).
[13] Hurst, R. R., and Donahue, D. J., Nucl. Phys. A91, 365 (1967).
[14] Ben-David, G., and Huebschmann, B., Physics Letters 3, 87 (1962).
[15] Ben-David, G., Avad, B., Balderman, J., and Schlesinger, Y., Phys. Rev. 146, B852 (1966).
[16] Knowles, J. W., AECL 2535 (1966).
[17] Kuehne, H. W., Axel, P., and Sutton, D. C., Phys. Rev. 163, 1278 (1967).
[18] Shiff, L. I., Phys. Rev. 83, 252 (1951).
[19] O'Connell, J., Tipler, P., and Axel, P., Phys. Rev. 126, 228 (1962).
[20] Axel, P., Min, K., Stein, N., and Sutton, D. C., Phys. Rev. Letters 10, 299 (1963).
[21] Kuchnir, F. T., Axel, P., Crieger, L., Drake, D. M., Hanson, A. O., and Sutton, D. C., Phys. Rev. 163, 1278 (1967).
[22] Schuhl, C., and Tzara, C., Nucl. Instr. and Meth. 10, 217 (1961).
[23] Jupiter, C. P., Hansen, N. E., Shafer, R. E., and Fultz, S. C., Phys. Rev. 121, 866 (1961).
[24] Ziegler, B., Wyckoff, J. M., and Koch, H. W., Nucl. Instr. and Meth. 24, 301 (1963).
[25] Wyckoff, J. M., Ziegler, B., Koch, H. W., and Uhlig, R., Phys. Rev. 137, B576 (1965).
[26] Fuller, E. G., and Hayward, E., Phys. Rev. 101, 692 (1956). The scattering cross sections given here were incorrectly evaluated and should be multiplied by 0.866.
[27] Penfold, A. S., and Leiss, J. E., Analysis of Photo Cross Sections (Physics Research Laboratory, University of Illinois, Champaign, Illinois, 1958).
[28] Fuller, E. G., and Weiss, M. S., Phys. Rev. 112, 560 (1958).
[29] Gemmell, D. S., and Jones, G. A., Nuclear Physics 33, 102 (1962).
[30] Tanner, N. W., Thomas, G. C., and Earle, E. D., Nuclear Physics 52, 29 (1964).
[31] Gove, H. E., Litherland, A. E., and Batchelor, R., Nuclear Physics 26, 480 (1961).
[32] Allas, R. G., Hanna, S. S., Meyer-Schützmeister, L., Singh, P. P., and Segel, R. E., Nuclear Physics 58, 122 (1964).
[33] Fisher, P. S., Measday, D. F., Nikolaev, F. A., Kalmykov, A., and Clegg, A. B., Nuclear Physics 45, 113 (1963).
[34] Tanner, N. W., Thomas, G. C., and Earle, E. D., Nuclear Physics 52, 45 (1964).
[35] Segel, R. E., Vagar, Z., Meyer-Schützmeister, L., Singh, P. P., and Allas, R. G., Nuclear Physics, A93, 31 (1967).
[36] Bearse, R. C., Meyer-Schützmeister, L., and Segel, R. E., Nuclear Physics, A116, 682 (1968).
[37] Singh, P. P., Segel, R. E., Meyer-Schützmeister, L., Hanna, S. S., and Allas, R. G., Nuclear Physics 65, 577 (1965).
[38] Dearnaley, G., Gemmell, D. S., Hooton, B. W., and Jones, G. A., Nuclear Physics, 64, 177 (1965).
[39] Kimura, M., Shoda, K., Mutsuro, N., Sugawara, M., Abe, K., Kageyama, K., Mishina, M., Ono, A., Ishizuka, I., Mori, S., Kawamura, N., Nakagawa, I., and Tanaka, E., J. Phys. Soc. Japan 18, 477 (1963).
[40] Hafele, J. C., Bingham, F. W., and Allen, J. S., Phys. Rev. 135, B365 (1964).
[41] Firk, F. W. K., Nuclear Physics 52, 437 (1964).
[42] Baglin, J. E. E., private communication.
[43] Fultz, S. C., Bramblett, R. L., Caldwell, J. T., Hansen, N. E., and Jupiter, C. P., Phys. Rev. 128, 2345 (1962).
[44] Bramblett, R. L., Caldwell, J. T., Auchampaugh, G. F., and Fultz, S. C., Phys. Rev. 129, 2723 (1963).
[45] Fultz, S. C., Bramblett, R. L., Caldwell, J. T., and Harvey, R. R., Phys. Rev. 133, B1149 (1964).
[46] Bowman, C. D., Auchampaugh, G. F., and Fultz, S. C., Phys. Rev. 133B, 676 (1964).
[47] Fultz, S. C., Bramblett, R. L., Caldwell, J. T., and Kerr, N. A., Phys. Rev. 127, 1273 (1962).
[48] Harvey, R. R., Caldwell, J. T., Bramblett, R. L., and Fultz, S. C., Phys. Rev. 136, B126 (1964).
[49] Bramblett, R. L., Caldwell, J. T., Berman, B. L., Harvey, R. R., and Fultz, S. C., Phys. Rev. 148, B1198 (1966).
[50] Berman, B. L., Caldwell, J. T., Harvey, R. R., Kelly, M. A., Bramblett, R. L., and Fultz, S. C., Phys. Rev. 162, 951 (1967).
[51] Berman, B. L., Bramblett, R. L., Caldwell, J. T., Davis, H. S., Kelly, M. A., and Fultz, S. C., Phys. Rev. 177, 1745 (1969).
[52] Berman, B. L., Kelly, M. A., Bramblett, R. L., Caldwell, J. T., Davis, H. S., and Fultz, S. C., Phys. Rev. 185, 1576 (1969).
[53] Danos, M., Photonuclear Physics, University of Maryland Technical Report 221 (1961).
[54] Danos, M., Nuclear Physics 5, 23 (1958).
[55] Fuller, E. G., and Hayward, E., Nuclear Reactions II, edited by P. M. Endt and P. B. Smith (North-Holland Publishing Company, Amsterdam, 1962).
[56] Ambler, E., Fuller, E. G., and Marshak, H., Phys. Rev. 138B, 117 (1965).
[57] Bogdankevich, O. V., Goryachev, B. I., Zapevalov, V. A., Zhur. Eksptl. i. Teoret. Fiz. 42, 1502 (1962); Soviet Phys. JETP 15, 1044 (1962).
[58] Fuller, E. G., and Hayward, Evans, Nuclear Physics 30, 613 (1962).
[59] Parsons, R. W., and Katz, L., Can. J. Phys. 37, 809 (1959).
[60] Spicer, B. M., Thies, H. H., Baglin, J. E., and Allum, F. R., Austral. J. Phys. 11, 298 (1958).
[61] Bergère, R., Beil, H., and Veyssière, A., Nuclear Physics, A121, 463 (1968).

[62] Semenko, S. F., Phys. Letters 10, 182 (1964); 13, 157 (1964).
[63] Semenko, S. F., J. Nucl. Phys. (U.S.S.R.) 1, 414 (1965).
[64] Le Tourneux, J., Mat. Fys. Medd. Dan. Vid. Selsk. 34, Nr. 11 (1965).
[65] Le Tourneux, J., Phys. Letters 13, 325 (1964).
[66] Danos, M., and Greiner, W., Phys. Rev. 134, B284 (1964).
[67] Huber, M. G., Weber, H. J., Danos, M., and Greiner, W., Phys. Rev. Letters 15, 529 (1965).
[68] Arenhövel, H., and Greiner, W., Phys. Letters 18, 136 (1965); Arenhövel, H., Danos, M., and Greiner, W., Phys. Rev. 157, 1109 (1967).
[69] Weber, H. J., Huber, M. G., and Greiner, W., Z. Physik 192, 182 (1966).
[70] Huber, M. G., Weber, H. J., and Greiner, W., Z. Physik 192, 223 (1966).
[71] Huber, M. G., Weber, H. J., Danos, M., and Greiner, W., Phys. Rev. 155, 1073 (1967).
[72] Arenhövel, H., and Weber, H. J., Nuclear Physics A91, 145 (1967).
[73] Arenhövel, H., and Greiner, W., Nuclear Physics 86, 193 (1966).
[74] Cannington, P. H., Stewart, R. J. J., Hogg, G. R., Lokan, K. H., and Sargood, D. G., Nuclear Physics 72, 23 (1965).
[75] Fano, U., and Racah, G., Irreducible Tensorial Sets, Academic Press, New York p. 84 (1959).
[76] Shimizu, S., Isomuzi, Y., Nakayama, Y., Physics Letters 25B, 124 (1967).
[77] Arenhövel, H., and Hayward, E., Phys. Rev. 165, 1170 (1968).
[78] Ligensa, R., Greiner, W., and Danos, M., Phys. Rev. Letters 16, B535 (1966).
[79] Fast, R. W., Flournoy, P. A., Tickle, R. S., and Whitehead, W. D., Phys. Rev. 118, 535 (1960).
[80] Gregory, A. G., Sherwood, T. R., and Titterton, E. W., Nuclear Physics 32, 543 (1962).
[81] Min, K., and Whitehead, W. D., Phys. Rev. 137, B301 (1965).
[82] Bolen, L. N., and Whitehead, W. D., Phys. Rev. Letters 9, 458 (1962).
[83] Morrison, R. C., Stewart, J. R., and O'Connell, J. S., Phys. Rev. Letters 15, 367 (1965).
[84] Dolbilkin, B. S., Korin, V. I., and Nikolaev, F. A., ZhETF Pis'ma 1, No. 5 (1965); JETP Letters 1, 148 (1965).
[85] Ishkanov, B. S., Kapitonov, I. M., Shevchenko, V. G., and Yur'ev, B. A., Physics Letters 9, 162 (1964).
[86] Dolbilkin, B. S., Korin, V. I., Lazareva, L. E., Nikolaev, F. A., and Zapevalov, V. A., Nuclear Physics 72, 137 (1965).
[87] Bolen, L. N., and Whitehead, W. D., Phys. Rev. 132, 2251 (1963).
[88] Johansson, S. A. E., Phys. Rev. 97, 1186 (1955).
[89] Bolen, L. N., and Whitehead, W. D., Phys. Rev. 132, 2251 (1963).
[90] Dolbilkin, B. S., Korin, V. I., Lazareva, L. E., and Nikolaev, F. A., Phys. Letters 17, 49 (1965).
[91] Min, K., Bolen, L. N., and Whitehead, W. D., Phys. Rev. 132, 749 (1963).
[92] Wilkinson, D. H., Proc. Conf. Nuclear and Meson Phys., Glasgow, 1954, (Pergamon Press, London, 1955) p. 161.
[93] Wilkinson, D. H., Physica 22, 1039 (1956).
[94] Glendenning, N. K., Phys. Rev. 114, 1297 (1959).
[95] Mayer, M. G., and Jensen, J. H. D., Elementary Theory of Nuclear Shell Structure, p. 236, John Wiley, New York (1955).
[96] Wilkinson, D. H., Phil. Mag. 3, 567 (1958).
[97] Elliott, J. P., and Flowers, B. H., Proc. Roy. Soc. (London) Ser. A242, 57 (1957).
[98] Gillet, V., and Vinh Mau, N., Physics Letters 1, 25 (1962).
[99] Sawicki, J., and Soda, T., Nuclear Physics 28, 270 (1961).
[100] Brown, G. F., Castillejo, L., and Evans, J. A., Nuclear Physics 22, 1 (1961).
[101] Gillet, V., Thesis, Univ. of Paris (1962).
[102] Raynal, J. M., Melkanoff, M. A., and Sawada. T., Nuclear Physics, A101, 369 (1967).
[103] Buck, B., and Hill, A. D., Nuclear Physics A95, 271 (1967).
[104] Wahsweiler, W. G., Danos, M., and Greiner, W., Phys. Rev. 170, 893 (1968).
[105] Kluge, G., Zeits. f. Physik 197, 288 (1966).
[106] Maison, J. M., Langevin, M., and Loiseaux, J. M., Phys. Letters 19, 308 (1965).
[107] Caldwell, J. T., Bramblett, R. L., Berman, B. L., Harvey, R. R., and Fultz, S. C., Phys. Rev. Letters, 15, 976 (1965).
[108] Yergin, P. F., Augustson, R. H., Kaushal, N. N., Medicus, H. A., Moyer, W. R., and Winhold, E. J., Phys. Rev. Letters 12, 733 (1964).
[109] Owens, R. O., and Baglin, J. E. E., Phys. Rev. Letters 19, 308 (1965).
[110] Caldwell, J. T., Thesis, University of California (1967).
[111] Gillet, V., Melkanoff, M. A., and Raynal, J., Nuclear Physics, A97, 631 (1967).
[112] Suffert, M., Nuclear Physics 75, 226 (1965).
[113] Suffert, M., and Feldman, W., Phys. Letters 24B, 579 (1967).
[114] Warburton, E. K., Olness, J. W., and Alburger, D. E., Phys. Rev. 140, B1202 (1965).
[115] Deague, T., private communication.
[116] Goldfarb, L. J. B., Nuclear Reactions I, edited by P. M. Endt and M. Demeur (North-Holland Publishing Company, Amsterdam, 1959).
[117] Biedenharn, L. C., Nuclear Spectroscopy, Part B, edited by F. Ajzenberg-Selove (The Academic Press, New York, 1960).
[118] Courant, E. D., Phys. Rev. 82, 703 (1951).
[119] Satchler, G. R., Proc. Phys. Soc. 68A, 1041 (1955).
[120] Costa, S., Ferrero, F., Ferroni, S., Minetti, B., Molino, C., Malvano, R., Phys. Letters 6, 226 (1963).
[121] Baker, R. G., and McNeill, K. G., Can. J. Phys. 39, 1138 (1961).
[122] Borello, O., Ferrero, F., Malvano, R., and Molinari, A., Nuclear Physics 31, 53 (1962).
[123] Reinhardt, G. C., and Whitehead, W. D., Nuclear Physics 30, 201 (1962).
[124] Gorbunov, A. N., Phys. Letters 27B, 436 (1968).
[125] Levinger, J. S., Phys. Rev. 84, 43 (1951).
[126] Feld, B. T., Godbole, R. D., Odion, A., Scherb, F., Stein, P. C., and Wattenberg, A., Phys. Rev. 94, 1000 (1954).
[127] Barton, M. Q., and Smith, J. H., Phys. Rev. 110, 1143 (1958).
[128] Garvey, J., Patrick, B. H., Rutherglen, J. G., and Smith, I. L., Nuclear Physics 70, 241 (1965).
[129] Smith, I. L., Garvey, J., Rutherglen, J. G., and Brookes, G. R., Nuclear Physics B1, 483 (1967).
[130] Lochstet, W. A., and Stephens, W. E., Bull. Am. Phys. Soc. 10, 94 (1965).
[131] Meyer-Schutzmeister, L., Vager, Z., Segel, R. E., and Singh, P. P., Nuclear Physics 108, 180 (1968).
[132] MacFarlane, M. H., Isobaric Spin in Nuclear Physics, edited by John D. Fox and Donald Robson, Academic Press (1966).
[133] Lane, A. M., Nuclear Physics 35, 676 (1962).
[134] Cook, B. C., Phys. Rev. 106, 300 (1957).
[135] Fisher, P. S., Measday, D. F., Nicolaev, F. A., Kalmykov, A., and Clegg, A. B., Nuclear Physics 45, 113 (1963).
[136] Measday, D. F., Clegg, A. B., and Fisher, P. S., Nuclear Physics 61, 269 (1965).
[137] Min, K., Phys. Rev. 182, 1359 (1969).
[138] O'Connell, J. S., Phys. Rev. Letters 22, 1314 (1969).
[139] Goulard, B., and Fallieros, S., Can. J. Phys. 45, 3221 (1967).
[140] Green, A. E. S., and Edwards, D., Phys. Rev. 91, 46 (1953).
[141] O'Connell, J. S., private communication.
[142] Morinaga, H., Zeits. f. Physik 188, 182 (1965).
[143] Cabibbo, N., and Radicati, L. A., Phys. Letters 19, 697 (1966).
[144] Barton, G., Nuclear Physics A104, 289 (1967).
[145] Gerimosov, S. B., JEPT Letters 5, 337 (1967).
[146] Easlea, B. R., Phys. Letters 1, 163 (1962).

... PRINTING OFFICE: 1970 O—382-848

U.S. DEPARTMENT OF COMMERCE
WASHINGTON, D.C. 20230

OFFICIAL BUSINESS

POSTAGE AND FEES PAID
U.S. DEPARTMENT OF COMMERCE